Technical Memorandum No. 33-94

Investigation of the DSIF 85-Foot Antenna Structural Deflections Caused by Deadload and Thermal Inputs

Floyd W. Stoller

JET PROPULSION LABORATORY
CALIFORNIA INSTITUTE OF TECHNOLOGY
PASADENA, CALIFORNIA

August 7, 1962

Technical Memorandum No. 33-94

Investigation of the DSIF 85-Foot Antenna Structural Deflections Caused by Deadload and Thermal Inputs

Floyd W. Stoller

JET PROPULSION LABORATORY
CALIFORNIA INSTITUTE OF TECHNOLOGY
PASADENA, CALIFORNIA

August 7, 1962

NATIONAL AERONAUTICS AND SPACE ADMINISTRATION
CONTRACT NO. NAS 7-100

Technical Memorandum No. 33-94

Investigation of the DSIF 85-Foot Antenna Structural Deflections Caused by Deadload and Thermal Inputs

Floyd W. Stoller

JET PROPULSION LABORATORY
CALIFORNIA INSTITUTE OF TECHNOLOGY
PASADENA, CALIFORNIA

August 7, 1962

CONTENTS

CONTENTS (Cont'd)

FIGURES

FIGURES (Cont'd)

FIGURES (Cont'd)

FIGURES (Cont'd)

FIGURES (Cont'd)

FIGURES (Cont'd)

FIGURES (Cont'd)

ABSTRACT

24029

In the Spring of 1962, an investigation was made of the tracking discrepancies found in the data of the Australian and South African Deep Space Instrumentation Facility (DSIF) stations. Test equipment in development was employed to determine the sources of these errors. Measurements were made on the 85-ft antenna at the DSIF Station No. 5 (South Africa) of the quadripod, dish structure, and pedestal deflections due to deadload and thermal inputs.

The Report includes discussions of the problem, the test program, data-processing procedures and reduction mechanization, and data reduction. Auxiliary investigations are described, the test results analyzed, and recommendations, both current and future, are made to correct or eliminate tracking errors.

Author

I. INTRODUCTION

Analysis of the *Ranger* 3 (RA-3) tracking data disclosed larger than expected tracking errors in the Australian and South African station data. Further inspection of the RA-3 data seemed to indicate that a large part of these errors might be due to deflections of the quadripod, dish structure, and pedestal caused by deadload and/or thermal effects.

While it had always been apparent that the pointing data of the DSIF antennas contained systematic errors in addition to those correctable by optical startracking, the specific contribution of each had not been resolved as a data-reduction insertion for the following reasons:

1. The accuracy of the existing theoretical data had not been affirmed empirically and appeared to be in question.
2. The deflection effects of wind and Sun were not predictable ahead of time, but required resolution from real-time data.
3. The instrumentation for measuring and recording these deflections, in real time with some satisfactory reference point, was still in the development stage.

With the advent of the RA-3 tracking discrepancies, it was decided to employ the equipment in development to determine the sources of these errors.

In order to simulate the specific conditions of joint fixity, deadload positions, and incident thermal energy peculiar to the stations in question, it was decided that the investigations would have to be carried out at one of these stations as soon as possible.

The experimental equipment, test procedures, and data-reduction methods are explained in some detail prior to presentation of the reduced data.

II. PROBLEM

As the tracking data from RA-3, with all the existing startrack calibration data removed, still showed unresolved error slopes, the problem was to decide what the possible sources of these errors were and how they could be measured.

A. Possible Sources of Error

1. Environmental

Environmental conditions during the RA-3 track differed from those of the "pre-track" startracks in the following areas:

a. Time of track—transition from night to day, with the associated change in thermal inputs to various parts of the antenna

b. Wind load—direction and velocity

2. Structural

Errors not detected during boresight operations or startrack calibrations appear as shifts of the RF axes and are due to deflections of the structure, as follows:

a. Deflections of the quadripod caused by thermal or deadload effects

b. Deflections of the dish structure caused by thermal or deadload effects

c. Deflections of the feed mount caused by thermal or deadload effects

d. Errors in the mechanical pointing axes caused by thermal effects on the pedestal structure

B. Theoretical Data

Very few theoretical data are available for the areas in question and the accuracy of those available is in question. Also, such modifying effects as the degree of joint fixity, incident solar energy, and deadload positions for a specific track are peculiar to each station and would strongly affect the direct application of theoretical calculations.

Figures 1 and 2 supply the theoretical data available and indicate pictorially the conditions of loading (data are for deadload only).

C. Empirical Data

It was concluded that the major sources of error, with the exception of the real-time wind loads, could reasonably be simulated or reproduced and the effects instrumented and measured.

III. PROPOSED TEST PROGRAM

The test program proposed to detect and measure the effects described in Section II consisted of the following:

1. Set up a startracking program utilizing stars with values of DEC, HA, and GMT similar to those experienced during RA-3 track.

2. Carry out this program of simulated RA-3 targets both for the RA-3 track period and at nighttime only.

3. Instrument the dish structure, quadripod, and feed mount for deflection measurements—both deadload and thermal.

4. Instrument and mechanize the test procedures to measure the effects of deadloads and thermals on the pointing ability of the antenna mount (exclusive of dish, quadripod, and feed-mount effects.)

5. Undertake the test program as soon as possible, with selected test days, in order to achieve as close an approximation to the RA-3 track environmental conditions as possible.

IV. TEST PROGRAM

The actual test program and its mechanization followed the general outline of Section III; it is described below.

A. Simulated RA-3 Targets

Two stars were utilized as simulated RA-3 targets—one to simulate the actual RA-3 track and its transition from night into day, and one to simulate the RA-3 track pattern at night only.

It was ascertained that the two stars which readily filled the time and coordinate requirements, as well as being sufficiently bright for daytime tracking, were Antares (SHA = 113.230 deg, DEC = 333.652 deg) for the transition target and Beta Corvi (SHA = 171.898 deg, DEC = 333.812 deg) for the nighttime target.

B. Environmental Conditions

Checks with the National Weather Bureau at Pretoria affirmed that the test-period environmental conditions would be reasonably compatible with those in existence during the RA-3 track period, and provided days were selected to avoid overcast or rain on which the average wind velocity did not exceed 20 mph. The validity of the data was to be strengthened by running redundant tests. This was done both to achieve good average values for each area investigated and to determine whether small variations in environmental conditions created significant errors.

C. Equipment

The following facilities and equipment were used during the test program:

1. The Station 5 (Johannesburg) antenna and hydromechanical building were used as the basic test vehicle and operations headquarters, respectively (see Fig. 3).

2. Six "Pandux" surface-temperature thermometers, with a measuring range of 0°F to 300°F and an accuracy of ±1°F, were used to measure the surface temperature of the quadripod and pedestal legs during the deflection-vs.-temperature tests.

   Figure 4 shows the "Pandux" container, thermometer unit, magnetic clamp, silicon contact grease can, and aluminum dome or transducer shield. The transducers yield false readings as a result of direct heating of the bi-metal coil by the Sun and, therefore, may not indicate the true surface temperature of the structural member being monitored. For this reason, the aluminum dome pictured in Fig. 4 was developed. Sketch 1 illustrates the problem and the solution developed. Energy *A* heats the plate; heat from the plate, energy *C*, activates the bi-metal indicator spring to record the surface temperature of the plate; the silvered surface of the transducer is supposed to prevent direct heating of the bi-metal spring by energy *A*. However, if the Sun's energy is incident, as is energy *B*, the silvered top affords no protection, and false readings are evidenced. As seen in Sketch 1, the aluminum dome covers the transducer, avoiding direct heating. The dome has vent holes to prevent the dome from acting as an oven.

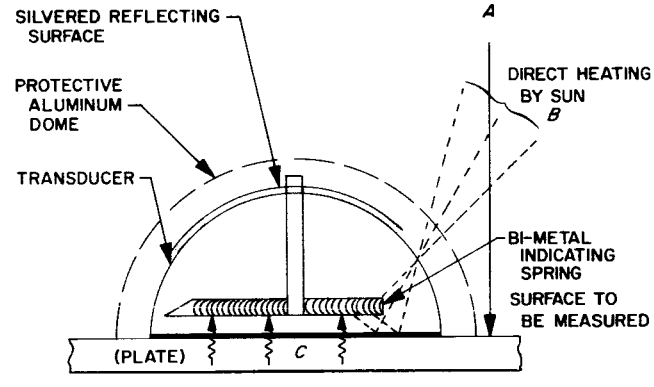

Sketch 1

3. The quadripod imaging fixture is an auxiliary lens attachment which fits on the zoomar lenses of either the boresight or TV cameras and images a target located at the focal point or focal plane of the quadripod (see Fig. 5). It enables the boresight camera to monitor the focal-point position at any specific time. This focal-point position, relative to the boxgirder, is time-correlated with the angle data of the antenna.

   The boxgirder network contains the optical package, which, in turn, contains the boresight camera and zoomar lens on which the quadripod imaging

fixture is mounted. The stability of the optical package, relative to the boxgirder structure, has been determined on a preliminary basis; however, one of the required tests was reaffirmation of this stability.

The fixture has a system resolution of 0.003 in. approaching 0.001, depending on the film reader used.

The accuracy of the system is dependent on the stability of the optical axes of the specific lens on which it is mounted. When used in association with the current DSIF Tracking Aid system, the fixture measures translations normal to the dish axes with an accuracy of approximately 0.008 in.; rotation about the dish axes with an accuracy of approximately 30 sec of arc; and rotation about the axes normal to the dish axes with the same accuracy.

Figures 6 and 7 show the fixture mounted on the boresight camera lens and the reference target on the ground plane of the feed, respectively. The reference target may be secured either to the feed ground plane or to the center of the feed. The crosshairs on the target are aligned with the crosshairs of the boresight camera at the zenith position. The target, when secured to the ground plane of the feed, is positioned for alignment with the two quadripod legs straddling the DEC axis.

4. The extensometer or chaining fixture, to which four survey tapes are attached, is located at the focal point. It is so designed that projections of the tapes intersect at the local point through the connection clamps at the applied angle.

   The other ends of the tapes connect to selected points on the boxgirder or dish-structure edges through tension scales and turnbuckles. The tension on the tapes is always set to 30 lb prior to reading the change in tape length. The chaining-fixture assembly has a resolution of $\frac{1}{50}$ in. and an accuracy of about $\frac{1}{16}$ in.

   Figures 8 and 9 show the chaining-fixture attachment at the focal point. Figures 10 and 11 show the chaining-tape passage through the dish and the attachment via tension scales and turnbuckles to the corners of the boxgirder, respectively.

5. Dial indicators were used at various points to resolve local deflections or structure movements (see Fig. 12). These indicators have a resolution of 0.001 in. and an accuracy of 0.002 in.

D. Measurements

The following measurements were made on the various portions of the antenna to determine the possible sources of the tracking errors:

1. Simulated RA-3 tracks—transition
2. Simulated RA-3 tracks—nighttime
3. Chaining—focal point to boxgirder
4. Chaining—focal point to dish edges
5. Feed movement relative to quadripod tip
6. Temperature effects—zenith with Sun transit
7. Temperature effects—collimation-tower lock-on with Sun transit

The following are descriptions of each of the measurements and the procedures and equipment used.

1. Simulated RA-3 Tracks—Transition

In this measurement, the star Antares was tracked through the same DEC and HA ranges and with the same relationship to GMT and Sun position as RA-3.

While Antares was being tracked via normal startrack procedures, the focal point (F.P.) was monitored by the quadripod imaging fixture and any deflections were recorded by the boresight camera.

2. Simulated RA-3 Track—Nighttime

The procedure used here was the same as in the transition track, the only difference being that the test was made entirely at night. The purpose of this track was to obtain simulated RA-3 deflection and startrack data free of the transition-track thermal effects.

3. Chaining—Focal Point to Boxgirder

In this measurement, survey chains were run from the F.P. to the corners of the boxgirder to measure movement of the F.P. relative to the corners of the boxgirder.

While this chaining measurement was being carried out, the F.P. was monitored for translation by the quadripod imaging fixture.

The purpose of this test was to validate the data acquired by the quadripod imaging fixture and to detect any peculiar motions of the F.P. not detected by the quadripod imaging fixture.

Figure 13 shows an over-all picture of the survey chains running from the focal point to the boxgirder.

Figures 14 and 15 present closeups of the survey chains and show the manner in which they were secured to the F.P. and to the boxgirder corners.

4. Chaining—Focal Point to Dish-Structure Edges

In this measurement, the survey chains were run from the F.P. to the dish-structure edges in proximity to the planes through the quadripod legs (see Figs. 16 and 17). The procedure was to maintain the DEC wheel at a fixed position while moving the polar wheel to various positions, recording the change in chain length at each position. At the same time, the F.P. was being monitored by the quadripod imaging fixture.

Variations in chain length, at various static positions, were read by personnel via the "cherry picker" (see Fig. 18). The readings were taken in this fashion for two reasons: (1) so as not to load the structure in the areas of chain attachment and (2) because in many cases it would have been impossible, or extremely dangerous, to do otherwise.

The purpose of this measurement was to determine to what degree the F.P. tracked the dish-structure deflections, whether the dish structure deforms astigmatically, and to detect any unsymmetrical deformations of the dish edges relative to the F.P.

5. Feed Movement Relative to the Quadripod Tip

Measurements of the F.P. movement relative to the local supporting quadripod structure were made by securing dial indicators to the quadripod legs in the proximity of the feed and indexing them to the ground plane of the feed assembly (see Fig. 19). During this test, the antenna was moved to various DEC and HA positions, and the movement of the F.P. relative to the local quadripod structure was measured.

6. Temperature Effects on the Quadripod—Zenith Position

These measurements were made by positioning the dish so that it pointed to zenith and allowing the Sun to transit the structure. For the test period, two of the quadripod legs and one of the pedestal legs were instrumented for temperature measurements. The transducers on the quadripod legs were placed 90 deg apart (Figs. 20 and 21) and the transducers on the pedestal legs 180 deg apart (Figs. 22 and 23). The positioning of the transducers was a compromise in which the most desirable data regions were instrumented within the limits imposed by the number of transducers available. During this test, the transducers were read periodically, and the movement of the F. P. (as determined by the quadripod imaging fixture) was recorded.

7. Temperature Effects on the Quadripod—Collimation-Tower Position

These measurements and the associated procedures are similar to those discussed in Section IVD-6, except that the dish was pointed at the collimation tower rather than to zenith.

Two sets of measurements were made, on different days, to determine the effects, if any, of slightly different environmental conditions.

V. DATA-PROCESSING PROCEDURES AND REDUCTION MECHANIZATIONS

The following is a brief description of the data-reduction procedures, film reading procedures, and computer programs.

A. Types of Data

The data were recorded in one of three ways: by film, by TTY printout and tape, or by tab or hand logging.

B. Data-Reduction Procedures

Figure 24 presents the general data-reduction flow diagram.

1. Simulated RA-3 and Nighttime Tests and Multiple DEC Position Tests

The 35-mm films for RA-3 tests No. 1, 3, 4, and 6, along with the nighttime test and a zenith calibration test, were read on a Coleman comparator. The readouts were punched on IBM cards using an IBM 523 summary punch. Every film frame was read for each test run. The crosshair and the center of the target were read along with the film-frame lower left corner when it was visible. The light-bulb filaments of the target were read relative to their reticles, and a constant correction factor was incorporated where the reticles of the target were not visible.

Readings were taken of the four reticles or crosses on the target to obtain a constant conversion factor in inches/count. The distance between the crosses was known to be 3 in. Since the pictures were taken at an angle, different conversion factors were used for the HA and DEC directions.

The zenith film readings were converted and averaged to obtain a calibration to which the RA-3 and nighttime tests were referenced.

The RA-3 and nighttime tests, along with the multiple DEC position test, were then converted, referenced to the crosshair and zenith calibration films, and correlated with tape time with the IBM 1620 computer. The RA-3 tests were then referenced to the nighttime test through a computer program. These final outputs, tape time, HA and DEC in degrees, and ΔHA, ΔDEC, ΔC_x, and ΔC_y in inches, were plotted for presentation.

The multiple DEC position test follows the same procedure as the RA-3 tests except for the referencing to the nighttime test.

2. Chaining Deflection Test—Focal Point to Boxgirder Corner and Focal Point to Dish Edges

Every frame of the associated film data was read with the same procedures as the RA-3 and nighttime tests. The zenith run was converted, and reference calibrations were obtained. The data runs were then converted, referenced to the crosshair and zenith calibration run, and correlated with the tape time. Averages were taken of ΔHA and ΔDEC in inches, where HA and DEC in degrees remained the same.

The tabulated data were keypunched and run through a computer program to obtain tape time, HA and DEC in degrees, and ΔHA and ΔDEC in inches.

The final film outputs, tape time, HA and DEC in degrees, and ΔHA and ΔDEC in inches, along with the final tabulated data, were then plotted for presentation.

3. Quad Deflection vs. Temperature—Sun Transit; Zenith and Collimation Tower

The film data were read and reduced in the same manner as the RA-3 and nighttime tests.

The tabulated temperature data were associated with time and plotted along with ΔHA and ΔDEC in inches to show the relationship of temperature and F.P. deflection across the legs. Temperature gradients were developed across the legs, associated with time, and then plotted for final presentation.

C. Film Data

The following information shows the polarities and orientation of the film when reducing the quadripod imaging fixture data.

1. The film is positioned so that its orientation, as seen by the film reader, is that shown in Fig. 25. Figure 26 presents a closeup of a specific film frame.

2. The film is read out with the following polarities and orientation relative to the film readers axes:

Film reader		*Physical reality*
$-x$	=	$-$HA
$+x$	=	$+$HA
$-y$	=	$-$DEC
$+y$	=	$+$DEC

Zero references are made to both the center of the crosshairs (*A*) and the lower left corner of the film frame (*B*).

D. Significance of Data Polarities

Sketch 2 illustrates the relationship of the data polarities with physical reality. The top two figures portray the quadripod imaging fixture and the bottom four the chaining fixture.

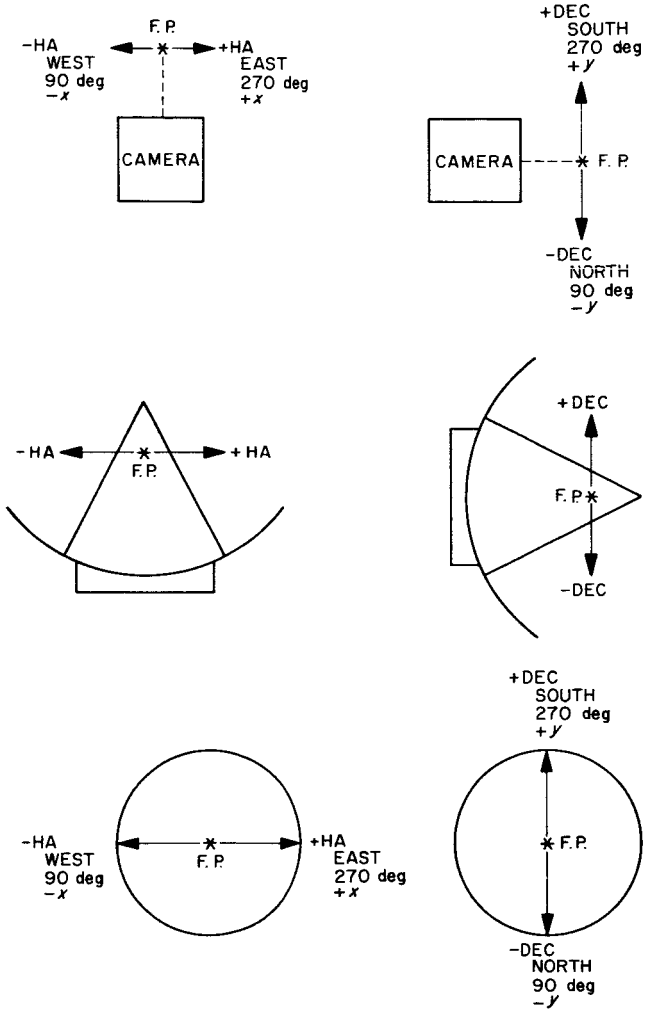

Sketch 2

E. Computer Program

The various computer programs (IBM 1620) used in the reduction of the test data are shown below.

1. The following program was used for the conversion of film data on all RA-3, nighttime, multiple DEC position, chaining deflection, quad deflection, and collimation-tower tests. The first card read by the program gave the zenith calibrations.

```
ZX5 = THE DELTA DISTANCE,IN INCHES,BETWEEN THE CROSSHAIR AND THE CENTER OF THE
      TARGET AS READ ON THE ZENITH RUN,IN THE X DIRECTION.
ZY5 = THE SAME AS ZX5,BUT IN THE Y DIRECTION.
ZX2 = THE DELTA DISTANCE,IN INCHES,BETWEEN THE CROSSHAIR AND THE LOWER LEFT
      FILM FRAME CORNER AS READ ON THE ZENITH RUN,IN THE X DIRECTION.
ZY2 = THE SAME AS ZX2,BUT IN THE Y DIRECTION.
ZX3 = THE DELTA DISTANCE,IN INCHES,BETWEEN THE TARGET CENTER AND THE LOWER
      LEFT FILM FRAME CORNER AS READ ON THE ZENITH RUN,IN THE X DIRECTION.
ZY3 = THE SAME AS ZX3,BUT IN THE Y DIRECTION.
  A = CONVERSION FACTOR,IN INCHES/COUNT,FOR THE X DIRECTION.
  B = THE SAME AS A,BUT IN THE Y DIRECTION.
 X1 = THE READINGS,IN COUNTS,OF THE LOWER LEFT FILM FRAME CORNER,
      IN THE X DIRECTION.
 Y1 = THE SAME AS X1,BUT IN THE Y DIRECTION.
 X2 = THE READINGS,IN COUNTS,OF THE CROSSHAIR,IN THE X DIRECTION.
 Y2 = THE SAME AS X2,BUT IN THE Y DIRECTION.
 X3 = THE READINGS,IN COUNTS,OF THE TARGET CENTER,IN THE X DIRECTION.
 Y3 = THE SAME AS X3,BUT IN THE Y DIRECTION.
HA2 = THE CROSSHAIR DEVIATION,IN INCHES,AS REFERENCED TO THE ZENITH LOWER
      LEFT FILM FRAME CORNER,IN THE X DIRECTION.
DEC2 =THE SAME AS HA2,BUT IN THE Y DIRECTION.
HA3 = THE DELTA DISTANCE,IN INCHES,BETWEEN THE CROSSHAIR AND THE TARGET CENTER
      AS REFERENCED TO THIS SAME DELTA DISTANCE OF THE ZENITH RUN,
      IN THE X DIRECTION.
DEC3 =THE SAME AS HA3,BUT IN THE Y DIRECTION.

THE SYMBOLS X4,Y4,X5, AND Y5 ARE THE SAME AS X2,Y2,X3, AND Y3 RESPECTIVELY,
BUT UNDER THE CONDITION WHERE THE FILM FRAME CORNER WAS NOT VISIBLE. OR UNDER
THE CONDITION WHERE ONLY THE LIGHT BULB FILIMENT WAS VISIBLE.
```

```
08300 C  JPL SIMULATED RA-3 FILM DATA RUN
08300 C  FIRST DATA CARD GIVES NEW ZENITH CALIBRATIONS
08300    33 FORMAT(48HFIRST DATA CARD MUST CONTAIN ZENITH CALIBRATIONS)
08420     1 FORMAT(3X,I3,I6,I4,F8.0,F10.0,I9)
08480     2 FORMAT(49HFOR READOUTS 4 AND 0, TURN SW 3 ON ALL OTHERS OFF)
08602    30 FORMAT(46HIF INPUT USES READ OUTS 1,2,AND 3,TURN SW 4 ON)
08718    31 FORMAT(23HPUSH START TO READ DATA)
08788    32 FORMAT(46HIF INPUT USES READ OUTS 4 AND 5, TURN SW 4 OFF//)
08914       PRINT 30
08938       PRINT 32
08962       PRINT 2
08986       PRINT 33
09010       PRINT 31
09034       PAUSE
09046    34 FORMAT(8F10.6)
09104       READ 34,ZX5,ZY5,ZX2,ZY2,ZX3,ZY3,A,B
09212       IF(SENSE SWITCH 3)300,99
09232    99 IF(SENSE SWITCH 4)3,40
09252     3 CONTINUE
09252    98 M=0
```

```
09276          DO 10 I=1,3,1
09288          READ 1,NO,NFF,NRO,X,Y,MFC
09372          M=M+NRO
09408          IF(NRO-1)5,4,5
09476        4 X1=X
09500          Y1=Y
09524          GO TO 10
09532        5 IF(NRO-2)7,6,7
09600        6 X2=X
09624          Y2=Y
09648          GO TO 10
09656        7 IF(NRO-3)10,8,10
09724        8 X3=X
09748          Y3=Y
09772       10 CONTINUE
09808          IF(M-6)11,12,11
09876       11 PRINT 13,MFC,NO
09912          PUNCH 13,MFC,NO
09948       13 FORMAT(19HCARD MISSING FR NO ,I4,4X,7HRUN NO ,I3)
10056          PAUSE
10068          GO TO 98
10076       12 CONTINUE
10076          X3=X2-X3
10112          Y3=Y2-Y3
10148          X2=X2-X1
10184          Y2=Y2-Y1
10220          X2=X2*A
10256          Y2=Y2*B
10292          X3=X3*A
10328          Y3=Y3*B
10364          HA2=X2-ZX2
10400          HA3=ZX5-X3
10436          DEC2=Y2-ZX2
10472          DEC3=ZY5-Y3
10508       20 FORMAT(I4,4F9.3)
10550          PUNCH 20,MFC,HA2,DEC2,HA3,DEC3
10622          GO TO 98
10630       40 CONTINUE
10630       41 MM=0
10654          DO 50 I=1,2,1
10666          READ 1,NO,NFF,NRO,X,Y,MFC
10750          MM=MM+NRO
10786          IF(NRO-4)43,42,43
10854       42 X4=X
10878          Y4=Y
10902          GO TO 50
10910       43 IF(NRO-5)50,44,50
10978       44 X5=X
11002          Y5=Y
11026       50 CONTINUE
11062          IF(MM-9)51,52,51
11130       51 PRINT 13,MFC,NO
11166          PUNCH 13,MFC,NO
11202          PAUSE
11214          GO TO 41
11222       52 CONTINUE
11222          X5=X4-X5
11258          Y5=Y4-Y5
11294          X5=X5*A
11330          Y5=Y5*B
11366          HA3=ZX5-X5
11402          DEC3=ZY5-Y5
11438          PUNCH 53,MFC,HA3,DEC3
11486       53 FORMAT(I4,2F12.3)
11518          GO TO 41
11526      202 FORMAT(33HREADOUT NUMBERS MUST BE   4 AND 0)
```

```
11616    300 PRINT 202
T1640    298 DO 210 I=1,2,1
T1652        READ 1,NO,NFF,NRO,X,Y,MFC
T1736        IF(NRO)206,205,206
T1792    205 X5=X+5.0
T1828        Y5=Y+1.0
T1864        GO TO 210
T1872    206 IF(NRO-4)210,207,210
T1940    207 X4=X
T1964        Y4=Y
T1988    210 CONTINUE
T2024        X5=X4-X5
T2060        Y5=Y4-Y5
T2096        X5=X5*A
T2132        Y5=Y5*B
T2168        HA3=ZX5-X5
T2204        DEC3=ZY5-Y5
T2240    218 FORMAT(I4,2F12.3)
T2272        PUNCH 218,MFC,HA3,DEC3
T2320        GO TO 298
T2328        END

PROG SW 1 ONFOR SYMBOL TABLE, PUSH START
SW 1 OFF TO IGNORE SUBROUTINES, PUSH START
1620 FORTRAN SUBR. REVISED  6/7/62
PROCESSING COMPLETE
```

2. The following program was used to calculate the HA and DEC deflection from the given tabulated data for the chaining deflection test, F. P. to box-girder corners. The first card read gave the zenith calibrations, which are calculated and used in the program after statement No. 98.

```
W1,W2,W3, = THE TABULATED READINGS IN FEET,INCHES, AND 50S OF AN INCH
            RESPECTIVELY,FOR THE WEST.
E1,E2,E3, = THE SAME AS W1,W2, AND W3,BUT FOR THE EAST.
AN1,AN2,AN3 = THE SAME AS W1,W2, AND W3,BUT FOR THE NORTH.
S1,S2,S3 = THE SAME AS W1,W2, AND W3,BUT FOR THE SOUTH.
T1,T2,T3 = THE TABULATED TIME IN HOURS,MINUTES,AND SECONDS RESPECTIVELY.
HA = THE TABULATED HOUR ANGLE IN DEGREES.
DEC = THE TABULATED DECLINATION ANGLE IN DEGREES.
A = THE CONSTANT USED TO CONVERT FEET TO INCHES.
B = THE CONSTANT USED TO CONVERT 50S OF AN INCH TO INCHES.
BB = THE GIVEN CONSTANT WHICH IS IN INCHES AND SQUARED.
AZW = THE CONPUTED VALUE OF A AT ZENITH FOR THE WEST.
AZE = THE SAME AS AZW,BUT FOR THE EAST.
AZN = THE SAME AS AZW,BUT FOR THE NORTH.
AZS = THE SAME AS AZW,BUT FOR THE SOUTH.
HA1 = THE COMPUTED DEFLECTION FOR HA IN INCHES.
DEC1 = THE COMPUTED DEFLECTION FOR DEC IN INCHES.
```

```
08300 C  JPL CHAINING DEFLECTION TEST F.P. TO BOXGIRDER CORNER - TAB DATA
08300      1 FORMAT(38HFIRST CARD MUST BE ZENITH CALIBRATIONS)
08400      2 FORMAT(23HPUSH START TO READ DATA)
08470        PRINT 1
08494        PRINT 2
08518        PAUSE
08530      3 FORMAT(3F3.0,F8.0,2F3.0,F8.0,2F3.0,F8.0,2F3.0,1X,3I3,2F7.2)
08642        READ 3,W1,W2,W3,E1,E2,E3,AN1,AN2,AN3,S1,S2,S3,T1,T2,T3,HA,DEC
08858        A=12.0
08882        W1=W1*A
08918        E1=E1*A
08954        AN1=AN1*A
08990        S1=S1*A
09026        B=50.0
09050        W3=W3/B
09086        E3=E3/B
09122        AN3=AN3/B
09158        S3=S3/B
09194        W1=W1+W2+W3
09242        E1=E1+E2+E3
09290        AN1=AN1+AN2+AN3
09338        S1=S1+S2+S3
09386        BB=238534.56
09410        AZW=(W1**2.0)-BB
09458        AZW=SQRTF(AZW)
09482        AZE=(E1**2.0)-BB
09530        AZE=SQRTF(AZE)
09554        AZN=(AN1**2.0)-BB
09602        AZN=SQRTF(AZN)
09626        AZS=(S1**2.0)-BB
09674        AZS=SQRTF(AZS)
09698        PUNCH 5
```

```
09722      5 FORMAT(20X,24HCHAINING DEFLECTION TEST)
09842        PUNCH 6
09866      6 FORMAT(20X,35HF.P. TO BOXGIRDER CORNER - TAB DATA/)
T0012        PUNCH 7
T0036      7 FORMAT(6X9HTAPE TIME,9X2HHA,11X3HDEC,8X8HDELTA HA,3X9HDELTA DEC)
T0260        PUNCH 8
T0284      8 FORMAT(7X7HH  M  S,8X7HDEGREES,7X7HDEGREES,6X6HINCHES,6X6HINCHES)
T0506        DEC1=0.0
T0530        HA1=0.0
T0554      9 FORMAT(5X,3I3,2F14.2,2F12.3)
T0624     98 PUNCH 9,T1,T2,T3,HA,DEC,HA1,DEC1
T0720        READ 3,W1,W2,W3,E1,E2,E3,AN1,AN2,AN3,S1,S2,S3,T1,T2,T3,HA,DEC
T0936        W1=W1*A
T0972        E1=E1*A
T1008        AN1=AN1*A
T1044        S1=S1*A
T1080        W3=W3/B
T1116        E3=E3/B
T1152        AN3=AN3/B
T1188        S3=S3/B
T1224        W1=W1+W2+W3
T1272        E1=E1+E2+E3
T1320        AN1=AN1+AN2+AN3
T1368        S1=S1+S2+S3
T1416        W1 =(W1**2.0)-BB
T1464        W1=SQRTF(W1)
T1488        E1 =(E1**2.0)-BB
T1536        E1=SQRTF(E1)
T1560        AN1=(AN1**2.0)-BB
T1608        AN1=SQRTF(AN1)
T1632        S1 =(S1**2.0)-BB
T1680        S1=SQRTF(S1)
T1704        AE=AZE-E1
T1740        AW=W1-AZW
T1776        AS=AZS-S1
T1812        AN=AN1-AZN
T1848        HA1=(AE+AW)/2.0
T1896        DEC1=(AN+AS)/2.0
T1944        GO TO 98
T1952        END

PROG SW 1 ONFOR SYMBOL TABLE, PUSH START
SW 1 OFF TO IGNORE SUBROUTINES, PUSH START
```

3. The following program was used to calculate the HA and DEC deflection from the given tabulated data for the chaining deflection test, F. P. to dish edges.

```
W1,W2 = THE TABULATED READINGS IN FEET AND INCHES RESPECTIVELY FOR THE WEST.
E1,E2 = THE SAME AS W1 AND W2, BUT FOR THE EAST.
AN1,AN2 = THE SAME AS W1 AND W2, BUT FOR THE NORTH.
S1,S2 = THE SAME AS W1 AND W2, BUT FOR THE SOUTH.
T1,T2,T3 = THE TABULATED TIME IN HOURS,MINUTES,AND SECONDS RESPECTIVELY.
HA = THE TABULATED HOUR ANGLE IN DEGREES.
DEC = THE TABULATED DECLINATION ANGLE IN DEGREES.
Z = THE CONSTANT USED TO CONVERT FEET TO INCHES.
A = THE CALCULATED VALUE AT ZENITH IN INCHES AND SQUARED.
BW = THE COMPUTED CHANGE IN B FOR THE WEST.
BE = THE SAME AS BW BUT FOR THE EAST.
BN = THE SAME AS BW BUT FOR THE NORTH.
BS = THE SAME AS BW BUT FOR THE SOUTH.
DBW = THE COMPUTED DELTA CHANGE IN B FOR THE WEST.
DBE = THE SAME AS DBW BUT FOR THE EAST.
DBN = THE SAME AS DBW BUT FOR THE NORTH.
DBS = THE SAME AS DBW BUT FOR THE SOUTH.
DDEC = THE COMPUTED DELTA DEFLECTION FOR DEC IN INCHES.
DHA =  THE COMPUTED DELTA DEFLECTION FOR HA IN INCHES.
```

```
08300 C  JPL CHAINING DEFLECTION TEST F.P. TO DISH EDGES - TAB DATA
08300      3 FORMAT(46HHEADER CARDS MUST BE PLACED IN FRONT OF OUTPUT)
08416      4 FORMAT(23HPUSH START TO READ DATA)
08486        PRINT 3
08510        PRINT 4
08534        PAUSE
08546      1 FORMAT(F3.0,F4.2,F6.0,F4.2,F6.0,F4.2,F6.0,F4.2,3X,3I3,2F10.3)
08642      2 READ1,W1,W2,E1,E2,AN1,AN2,S1,S2,T1,T2,T3,HA,DEC
08810        Z=12.0
08834        W1=W1*Z
08870        E1=E1*Z
08906        AN1=AN1*Z
08942        S1=S1*Z
08978        W1=W1+W2
09014        E1=E1+E2
09050        AN1=AN1+AN2
09086        S1=S1+S2
09122        A=76295.279
09146        BW =(W1**2.0)-A
09194        BW =SQRTF(BW)
09218        BE =(E1**2.0)-A
09266        BE =SQRTF(BE)
09290        BN =(AN1**2.0)-A
09338        BN =SQRTF(BN)
09362        BS =(S1**2.0)-A
09410        BS=SQRTF(BS)
09434        BZ=510.0
09458        DBW=BW-BZ
09494        DBE=BZ-BE
```

```
09530          DBN=BN-BZ
09566          DBS=BZ-BS
09602          DDEC=(DBN+DBS)/2.0
09650          DHA=(DBW+DBE)/2.0
09698        5 FORMAT(3I3,2F10.3,6F8.3)
09770          PUNCH 5,T1,T2,T3,HA,DEC,DHA,DDEC,DBN,DBS,DBW,DBE
09914          GO TO 2
09922          END

PROG SW 1 ONFOR SYMBOL TABLE, PUSH START
SW 1 OFF TO IGNORE SUBROUTINES, PUSH START
```

VI. REDUCED DATA

The following graphs (Figs. 27–135) present the reduced data from the tests outlined in Section IVD-1 through -7. A short description will precede each data grouping.

A. Simulated RA-3 Tracks—Transition

Figures 27–34 present the ΔHA and ΔDEC errors (translation normal to the dish axes in inches) as measured by the quadripod imaging fixture and correlated with local hour-angle position, GMT, and the approximate time at which the Sun's energy fell on the structure.

The zero reference position is taken when the dish is looking at local zenith.

B. Simulated RA-3 Tracks—Nighttime Only

Figures 35 and 36 present the ΔHA and ΔDEC errors (translation normal to the dish axes in inches) as measured by the quadripod imaging fixture and correlated with local hour-angle position and GMT.

The zero reference position is taken when the dish is looking at local zenith.

C. Simulated RA-3 Transition Data Referenced to Simulated RA-3 Nighttime Data

Figures 37–44 present the ΔHA and ΔDEC errors (in inches) of the simulated RA-3 nighttime track subtracted from the ΔHA and ΔDEC errors (in inches) of the simulated RA-3 transition tracks, as follows:

$$\text{Diff. } \Delta\text{HA, in.} = \Delta\text{HA}_{\text{transition}} - \Delta\text{HA}_{\text{nighttime}}, \text{ in.}$$

$$\text{Diff. } \Delta\text{DEC, in.} = \Delta\text{DEC}_{\text{transition}} - \Delta\text{DEC}_{\text{nighttime}}, \text{ in}$$

The above data are then plotted against hour-angle position, the correlated time of day (GMT) of the specific transition track, and the approximate time at which the Sun fell on the structure for a specific transition track.

D. Simulated RA-3 Tracks—Startrack Reductions

Figures 45–49 present the normal ΔHA and ΔDEC errors (in degrees), associated with the standard DSIF startrack reduction, as follows:

$$\Delta\text{HA, deg} = \text{observed} - \text{ephemeris, deg}$$

$$\Delta\text{DEC, deg} = \text{observed} - \text{ephemeris, deg}$$

These deltas are plotted against hour-angle position, time of day (GMT), and the approximate time the Sun fell on the structure.

E. Simulated RA-3 Startrack Data Comparisons

Figures 50–53 present the ΔHA and ΔDEC errors (in degrees) of the nighttime startrack subtracted from the similar error data for the specific transition startrack, as follows:

$$\text{Diff. } \Delta\text{HA, deg} = \Delta\text{HA}_{\text{transition}} - \Delta\text{HA}_{\text{nighttime}}, \text{ deg}$$

$$\text{Diff. } \Delta\text{DEC, deg} = \Delta\text{DEC}_{\text{transition}} - \Delta\text{DEC}_{\text{nighttime}}, \text{ deg}$$

The difference deltas are plotted against hour-angle position, time of day (GMT), and the approximate time the Sun fell on the structure for a specific track.

F. Temperature Effects on Quadripod—at Zenith

Figures 54–56 present the ΔHA and ΔDEC errors (translation normal to the dish axes in inches) of the focal point as measured by the quadripod imaging fixture and related to the time of day and temperature measurements of the quadripod and pedestal legs.

In this test, the dish remains positioned to local zenith and the Sun is allowed to transit the structure.

G. Temperature Effects on Quadripod—Collimation Tower

Figures 57–62 present the ΔHA and ΔDEC errors (translation normal to the dish axes in inches) of the focal point as measured by the quadripod imaging fixture and related to the time of day and temperature measurements of the quadripod and pedestal legs.

In this test, the dish remains positioned on the collimation tower and the Sun is allowed to transit the structure.

H. Comparison of Film Reference Points

Figures 63–70 present a comparison of the two film zero points—point *A*, or the crosshair center, and point *B*, or the lower left corner of the film frame, as follows:

$$\Delta C_x, \text{ in.} = B_x \text{ zero} - A_x \text{ zero, in.}$$

$$\Delta C_y, \text{ in.} = B_y \text{ zero} - A_y \text{ zero, in.}$$

The deltas are plotted against local hour-angle position and GMT for a specific simulated RA-3 track.

I. Chaining—Focal Point to Boxgirder Corners

Figures 71–92 present the ΔHA and ΔDEC errors (translation normal to the dish axes in inches) of the focal point, as determined by chaining from the F. P. to the boxgirder angel-wings or corners. Coincident with the chaining process, the F. P. is monitored for translation by the quadripod imaging fixture.

The data are plotted against local hour-angle position for various DEC angle settings.

J. Chaining—Focal Point to Dish-Structure Edges

Figures 93–103 present the ΔHA and ΔDEC errors (translation normal to the dish axes in inches) of the focal point, as determined by chaining from the F. P. to the dish-structure edges. Coincident with the chaining process, the F. P. is monitored for translation by the quadripod imaging fixture.

The data are plotted against local hour-angle position for various DEC angle settings.

K. Feed Movement Relative to Quadripod Tip

Figures 104 and 105 present the ΔHA and ΔDEC errors (translation normal to the dish axes in inches) of the F. P., on the feed, relative to the adjacent quadripod legs.

The data are plotted against local hour-angle position for various DEC angle positions.

VII. AUXILIARY INVESTIGATIONS

The following auxiliary investigations were undertaken in support of the prime test program:

1. *Quadripod leg attachments:* The quadripod leg-attachment points in the backup structure were inspected for possible deterioration or fixity peculiarities; none were in evidence.

2. *A-Frame stiffeners:* The A-frame stiffeners on each quadripod leg were inspected for structure deterioration or other peculiarities; none were in evidence.

3. *Quadripod leg stiffeners and spoilers:* The quadripod leg stiffeners and spoilers were inspected for structural deterioration or other peculiarities. All of the legs evidenced fracture lines in the welding. Whether or not the damage was of a significant level or a progressive nature was not resolved.

4. *RF and TV Pointing Axes—Temperature Effects:* On previous visits to Station 5, the station personnel were requested to make tests of the thermal effects on the RF and TV pointing axes, using continuous boresights on the collimation tower with the sun in transit.

   The test procedure was to take an RF and TV boresight reading on the collimation tower, recording the angle readouts in time correlation over a period of several days at approximately 10-min intervals (Figs. 106 through 118).

   As these measurements were carried out prior to the start of the deflection tests, the quadripod imaging fixture was not available; therefore, no associated focal-point movement data are given.

5. *Quadripod Deflections due to Deadload—Multiple or Calibration Runs:* With the quadripod imaging fixture monitoring the focal point, full hour-angle sweeps were made, with a specific DEC wheel position for each sweep. These data were correlated with the regular HA and DEC angle readout data (Figs. 119 through 135). The former data were used both to supply a calibration series for the antenna and to determine whether such a calibration series is a reasonable substitute for real-time data.

VIII. TEST RESULTS AND ANALYSIS

A. Test Results

1. Simulated RA-3 tracks—transition (all data are peak-to-peak values)

Test No.	LHA traverse, deg	ΔHA, in.	ΔDEC, in.	Adj. ΔHA, deg	Adj. ΔDEC, deg
1[a]	322 – 78 = 116	0.60	0.14	0.083	0.021
3[a]	307 – 80 = 133	0.56	0.20	0.067	0.021
4[a]	297 – 85 = 148	0.68	0.20	0.074	0.021
6	285 – 80 = 155	0.74	0.20	0.076	0.021
$\overline{\text{Adj. ΔHA}}$ = 0.075 deg, $\overline{\text{adj. ΔDEC}}$ = 0.021 deg					
[a]Adjusted for HA traverse of 155 deg.					

2. Simulated RA-3 track—nightime only (all data are peak-to-peak values)

Test No.	LHA traverse, deg	ΔHA, in.	ΔDEC, in.	Adj. ΔHA, deg	Adj. ΔDEC, deg
1[a]	310 – 85 = 135	0.68	0.16	0.080	0.019
[a]Adjusted for HA traverse of 155 deg.					

3. Simulated RA-3 startracks—transition minus nighttime (all data are peak-to-peak values)

Test No.	LHA traverse, deg	ΔHA, in.	ΔDEC, in.	Adj. ΔHA, deg	Adj. ΔDEC, deg
1[a]	322 – 78 = 116	0.35	0.05	0.046	0.005
3[a]	307 – 80 = 133	0.40	0.05	0.047	0.005
4[a]	297 – 85 = 148	0.40	0.00	0.043	0.005
6	285 – 80 = 155	—	—	—	—
$\overline{\text{Adj. ΔHA}}$ = 0.045 deg, $\overline{\text{adj. ΔDEC}}$ = 0.005 deg					
[a]Adjusted for HA traverse of 155 deg.					

4. Chaining—F. P. to boxgirder corner (all data are peak-to-peak values)

Data type	DEC position, deg	LHA traverse, deg	ΔHA, in.	ΔDEC, in.	ΔHA, deg	ΔDEC, deg
Film[a] (imager)	280	270 – 90	0.77	0.16	0.079	0.016
	334	270 – 90	0.76	0.26	0.078	0.027
	019	270 – 90	0.78	0.17	0.080	0.017
	048	270 – 90	0.73	0.24	0.075	0.025
Tab[b] (chaining)	280	270 – 90	0.88	0.24	0.090	0.025
	334	270 – 90	0.83	0.34	0.085	0.035
	019	270 – 90	0.94	0.14	0.096	0.014
	048	270 – 90	0.86	0.20	0.088	0.020
Tab minus film	Diff. $\overline{\Delta HA}$ = 0.089 – 0.078 = 0.011 deg					
	Diff. $\overline{\Delta DEC}$ = 0.024 – 0.021 = 0.003 deg					
[a]$\overline{\Delta HA}$ = 0.078 deg $\overline{\Delta DEC}$ = 0.021 deg. [b]$\overline{\Delta HA}$ = 0.089 deg $\overline{\Delta DEC}$ = 0.024 deg.						

5. Chaining—F. P. to dish-structure edges (all data are peak-to-peak values)

   a. Film data (full HA traverse)

   ΔHA (DEC at 334 deg) = 0.77 in. = 0.078 deg

   ΔDEC (DEC at 334 deg) = 0.185 in. = 0.019 deg

   b. Tab data (full HA traverse)

   ΔHA (DEC at 334 deg) = 0.42 in. = 0.043 deg

   ΔDEC (DEC at 334 deg) = 0.02 in. = 0.002 deg

   c. Tab data minus film data

   Diff. ΔHA = 0.078 – 0.043 = 0.035 deg

   Diff. ΔDEC = 0.019 – 0.002 = 0.017 deg

6. Feed F. P. movement relative to local quadripod supports (all data are peak-to-peak values)

   ΔHA (full HA traverse – DEC at 334 deg) = 0.200 in. = 0.020 deg

   ΔDEC (full HA traverse – DEC at 334 deg) = 0.01 in. = 0.001 deg

7. Quadripod deflections due to temperature inputs (film data) (all data are maximum values)

   ΔHA–Zenith position = 0.10 in. = 0.010 deg

   Collimation-tower position = 0.07 in. = 0.007 deg (cloudy day)

   Collimation-tower position = 0.11 in. = 0.011 deg

   ΔDEC–Zenith position = 0.04 in. = 0.004 deg

   Collimation-tower position = 0.07 in. = 0.007 deg (cloudy day)

   Collimation-tower position = 0.06 in. = 0.006 deg

8. Crosshair or optical axis movement

   No apparent movement of crosshairs (or optical axes) on film data.

9. Dish astigmatism (all data are maximum values)

HA position, deg	DEC position, deg	West edge	East edge	North edge	South edge
000	290	48 ft. 4 in.	48 ft. 4 in.	48 ft. 4.06 in.	48 ft. 3.94 in.
000	334	48 ft. 4 in.	48 ft. 4 in.	48 ft. 4 in.	48 ft. 4 in.
000	064	48 ft. 4 in.	48 ft. 3.92 in.	48 ft. 3.92 in.	48 ft. 4.10 in.
270	334	48 ft. 4.18 in.	48 ft. 3.92 in.	48 ft. 3.92 in.	48 ft. 3.92 in.
000	334	48 ft. 4 in.	48 ft. 4 in.	48 ft. 4 in.	48 ft. 4 in.
090	334	48 ft. 3.8 in.	48 ft. 3.94 in.	48 ft. 3.94 in.	48 ft. 3.96 in.

10. RF and TV axis boresight shifts (all data are maximum values)
    a. Nighttime:
    $\Delta HA = 0$ deg, $\Delta DEC = 0$ deg
    b. Daytime:
    $\Delta HA = 0.040$ deg, $\Delta DEC = 0.005$ deg
11. Quadripod deadload deflections — multiple DEC position calibration runs (Figs. 119 through 135) (all data are peak-to-peak values)
    a. ΔHA (for full HA traverse—any DEC) $\simeq 0.079$ deg
    b. ΔDEC (for full HA traverse), depends on DEC position; can be as high as 0.045 deg

B. Analysis

The test data imply that the RF pointing errors not resolved during startracks are caused by six general structural areas:

1. Shifting of the RF axes caused by quadripod F. P. deflections due to deadload.
2. Shifting of the RF axes caused by quadripod F. P. deflections due to thermals.
3. Shifting of the RF axes caused by quadripod F. P. deflections due to local deflections of the feed mount.
4. Shifting of the RF axes caused by dish-structure deflections due to deadload.
5. Shifting of the RF axes caused by dish-structure deflections due to thermals.
6. Shifting of the RF optical axes due to thermals on the base structure.

Figures 136 and 137 show the possible relationship of the various error sources to each other. (ΔAX is the shift in RF axes, ΔF. P., Δdish, and ΔTB the physical movements causing ΔAX; and $\Delta\theta$ and $\Delta\phi$ are the readout angle changes resulting from ΔAX.) The possible polarity combinations follow:

HA

B-1 $\equiv$ positive $(+\ \Delta\theta)$

B-2 $\equiv$ positive $(+\ \Delta\theta)$ if antenna leads Sun and input is directly into legs; can be negative if energy is reflected from dish into opposite legs

$\equiv$ negative $(-\ \Delta\theta)$ if antenna lags Sun and input is directly into legs; can be positive if energy is reflected from dish into opposite legs

B-3 $\equiv$ positive $(+\ \Delta\theta)$

B-4 $\equiv$ negative $(-\ \Delta\theta)$

B-5 $\equiv$ negative $(-\ \Delta\theta)$ if antenna leads Sun

$\equiv$ positive $(+\ \Delta\theta)$ if antenna lags Sun

B-6 $\equiv$ negative $(-\ \Delta\theta)$ if antenna leads Sun

$\equiv$ positive $(+\ \Delta\theta)$ if antenna lags Sun

$\equiv$?

DEC

B-1 $\equiv$ positive $(+\ \Delta\phi)$

B-2 $\equiv$ positive $(+\ \Delta\phi)$ if input is directly into legs

$\equiv$ negative $(-\ \Delta\phi)$ if input is reflected from dish into opposite legs

B-3 $\equiv$ positive $(+\ \Delta\phi)$

B-4 $\equiv$ negative $(-\ \Delta\phi)$

B-5 $\equiv$ negative $(-\ \Delta\phi)$ for both lead and lag Sun

B-6 $\equiv$ negative $(-\ \Delta\phi)$ for both lead and lag Sun

$\equiv$?

The following combination of errors may have existed during RA-3:

$$\begin{aligned} HA &= [(B\text{-}1 + B\text{-}3) + B\text{-}6] - [B\text{-}2 + B\text{-}4 + B\text{-}5] \\ &= [0.075\ \text{deg} + 0.045\ \text{deg}] \\ &\quad - [0.007\ \text{deg} + 0.035\ \text{deg} + 0] \\ &= 0.120\ \text{deg} - 0.042\ \text{deg} \\ &= 0.078\ \text{deg} \end{aligned}$$

$$\begin{aligned} DEC &= [(B\text{-}1 + B\text{-}2) + B\text{-}3] - [B\text{-}4 + B\text{-}5 + B\text{-}6] \\ &= [0.021\ \text{deg} + 0.015\ \text{deg}] \\ &\quad - [0.017\ \text{deg} + 0 + 0.005\ \text{deg}] \\ &= 0.026\ \text{deg} - 0.022\ \text{deg} \\ &= 0.004\ \text{deg} \end{aligned}$$

IX. CONCLUSIONS

Based on the information presented in Sections I through VIII, the following general conclusions were drawn:

1. Movement of the F.P. resulting from quadripod deadload deflections can cause peak-to-peak RF tracking errors as large as 0.1 deg in HA and 0.03 deg in DEC.

2. The errors in 1 above are offset by the dish deadload deflections by as much as 0.04 deg in HA and 0.001 deg in DEC (peak to peak).

3. Stiffening of the quadripod structure can create a condition in which the dish deadload deflections cancel the effects of quadripod deadload deflections.

4. As part of the quadripod deadload deflection is due to local deflections in the feed mount, stiffening the feed mount will help to approach the condition of 3 above. Local feed mount deflections account for as much as 0.03 deg in HA and 0.005 deg in DEC (peak to peak) of the quadripod deadload deflections.

5. Thermal inputs (solar) into the quadripod structure may create maximum RF pointing errors as large as 0.02 deg, but errors are generally 0.01 or less.

6. RF pointing errors specifically due to thermal effects on the dish structure have not been resolved.

7. RF and optical-axis maximum pointing errors due to thermal effects on the base structure may be as large as 0.05 deg in HA and 0.01 deg in DEC.

8. The optical package is sufficiently stable, referenced to the boxgirder corners, to validate the use of the quadripod imaging fixture as a calibrating device.

9. The optical axes of the boresight camera lens contribute no significant errors to the data.

10. As indicated in Section VIID, unless taken under identical conditions or at night only, RF–TV boresight data may incorporate maximum errors as large as 0.04 deg in HA and 0.005 deg in DEC.

11. The theoretical deadload deflection data for the quadripod are less than the empirical data by a factor of about two. This disagreement may be due to the deletion of certain areas from the calculations, such as the local deflection of the feed mount, variations in joint fixity, etc.

12. The dish evidences slight astigmatism (within the limitations of the measuring system) when moving from zenith to the horizon, as follows:

    to the East – an increase in east–west diameter of 0.01 in. and a decrease in north–south diameter of 0.16 in.

    to the West – no apparent change in east–west diameter and a decrease in north–south diameter of 0.10 in.

    to the North – an increase in north–south diameter of 0.02 in. and no change in east–west diameter.

    Because of the resolution and accuracy of the chaining equipment used, the above conclusions are questionable; however, they are included because they imply sense of direction of the mechanical activity.

13. The variations in F.P. movement due to thermal inputs, wind-loading, and joint fixity afford conditions of nonrepeatability as high as ± 0.01 deg to the F.P. deflections. For this reason, it appears that real-time deflection measurements will be required to give a high degree of accuracy to the data corrections.

14. The DEC axis position does not appear to affect the ΔHA error of the F.P. position appreciably.

15. Variations in sky conditions (cloudy, uncloudy) can affect thermal deflections by as much as 0.01 deg.

X. RECOMMENDATIONS

A. Current

1. As evidenced in Section VIIIA-1, the deadload deflections of the quadripod (adjusted) have an uncertainty of as much as ± 0.01 deg. This would seem to imply that if highly accurate correction data are desired, the quadripod deflection data must be real-time data for any specific track. Therefore, each station should be equipped with its own fixture and personnel instructed in its use. If high accuracy for the correction data is not a stringent requirement, a single calibration series for each antenna would suffice.

2. As shown by the data, thermal effects are significant and cannot be ignored for accurate correction data; also, they are peculiar to each track and require real-time or simulated real-time resolution. Therefore, a procedure for detecting thermally induced tracking errors would require both a simulated track and real-time monitoring of the F.P. A more promising solution which is currently under investigation is to protect the antenna from thermal distortion by special painting.

B. Future

1. Investigate existing quadripod configurations to determine whether a configuration change would afford quadripod and dish-structure deflections which offset each other.

2. Carry out further investigations of the thermal effects on antenna RF pointing and tracking capabilities with a view toward pinpointing the critical areas.

3. Continue investigations into the possible reduction or elimination of thermal effects on the DSIF antennas.

4. Apply the results of investigations 1, 2, and 3 above to an actual DSIF antenna for empirical confirmation.

It is significant to note that the results of this study indicate that the systematic errors remaining after straightforward calibration techniques may be reduced to about 0.02 deg peak if the temperature distortions can be made negligible by suitable techniques.

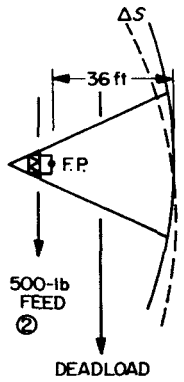

ΔT	① = 0.011 in. ② = 0.020 in.	DEFLECTION OF FOCAL POINT DUE TO TRANSLATION
ΔR	① = 0.250 in. ② = 0.046 in.	DEFLECTION OF FOCAL POINT DUE TO ROTATION OF QUAD LEGS
ΔS	= 0.278 in.	DEFLECTION OF FOCAL POINT DUE TO MOVEMENT OF SUPPORTING STRUCTURES
$\Delta\Sigma$	= 0.605 in.	DEFLECTION OF FOCAL POINT DUE TO ALL CAUSES

Fig. 1. Quadripod deflections; old polar-mount quad. without A-frames

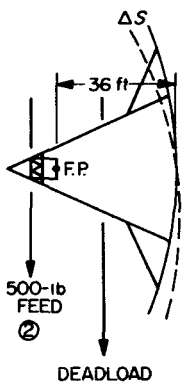

ΔT	① = 0.010 in. ② = 0.015 in.	DEFLECTION OF FOCAL POINT DUE TO TRANSLATION
ΔR	① = 0.026 in. ② = 0.023 in.	DEFLECTION OF FOCAL POINT DUE TO ROTATION OF QUAD LEGS
ΔS	= 0.260 in.	DEFLECTION OF FOCAL POINT DUE TO MOVEMENT OF SUPPORTING STRUCTURES
$\Delta\Sigma$	= 0.352 in.	DEFLECTION OF FOCAL POINT DUE TO ALL CAUSES

Fig. 2. Quadripod deflections; old polar-mount quad. with A-frames

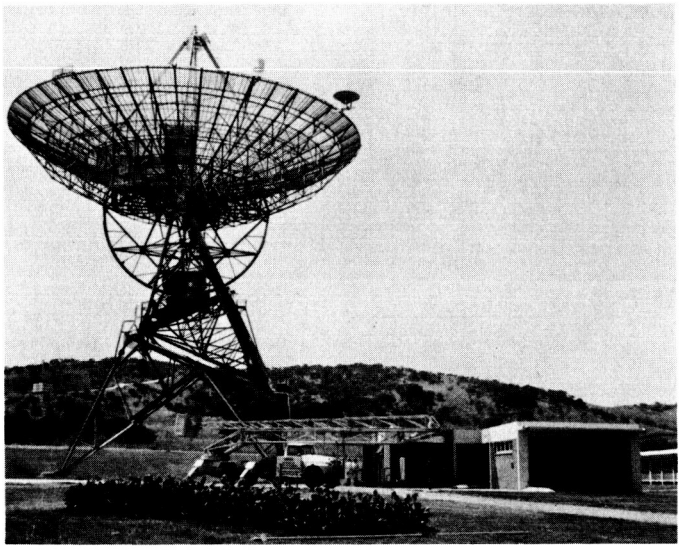

Fig. 3. DSIF antenna at Station 5

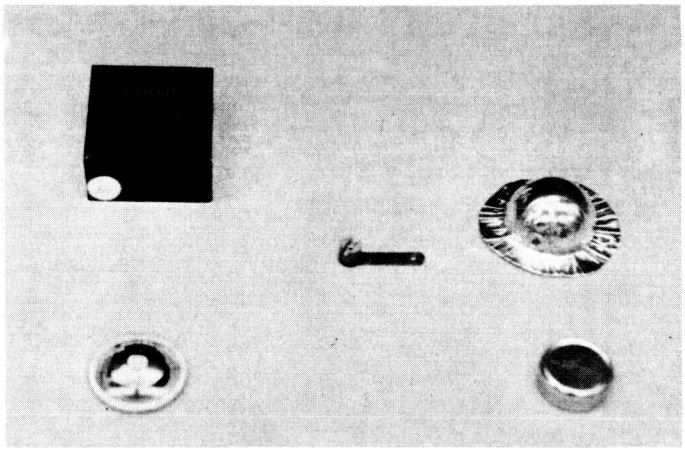

Fig. 4. "Pandux" surface-temperature transducer

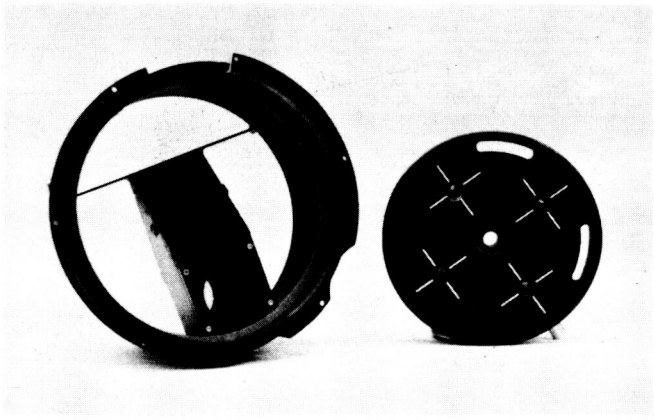

Fig. 5. Quadripod imaging fixture and reference target

Fig. 6. Quadripod imaging fixture mounted on boresight camera lens

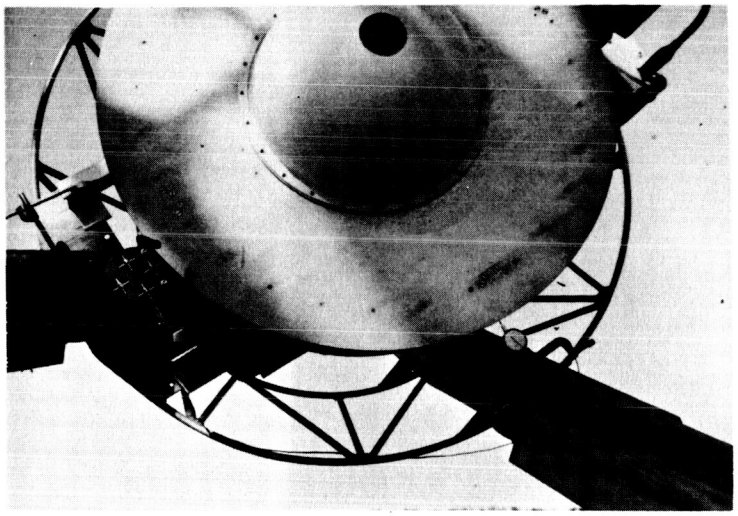

Fig. 7. Reference target mounted on feed ground plane

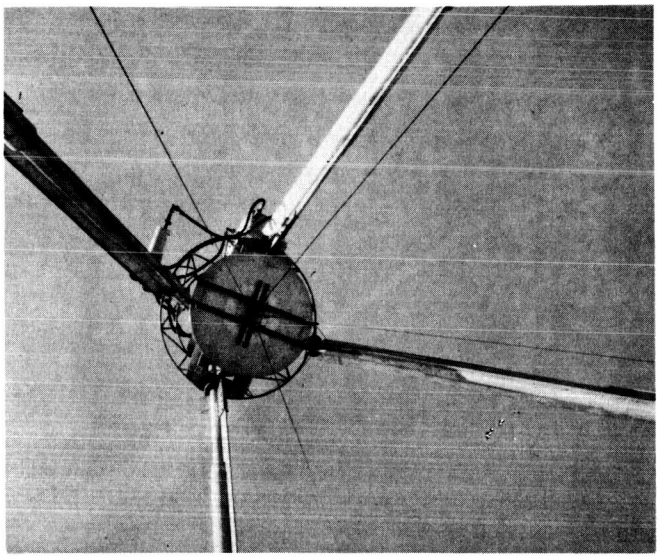

Fig. 8. Chaining fixture at focal point; horizon view with reference target

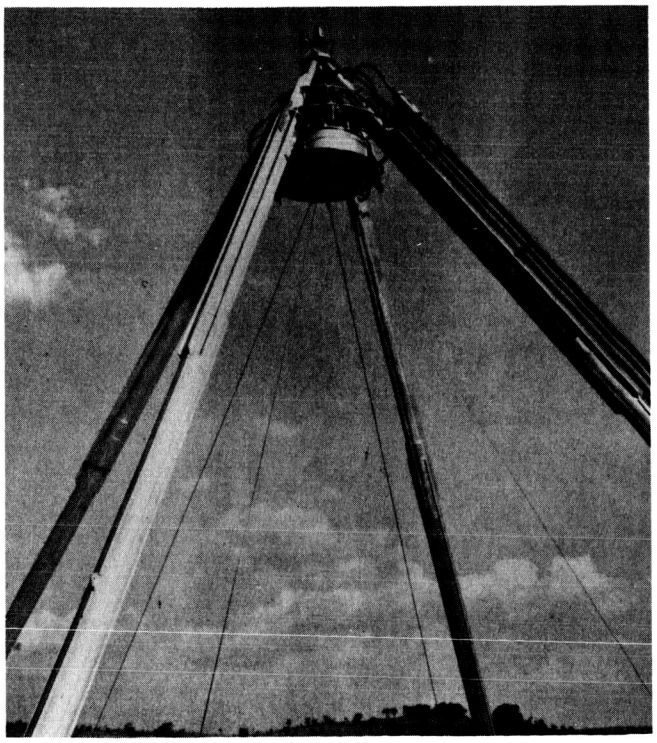

Fig. 9. Chaining fixture showing surveying tapes; zenith view

Fig. 10. Chaining tapes; path through dish surface

Fig. 11. Clamp, tension scale, and turnbuckle connecting chaining tape to boxgirder corner

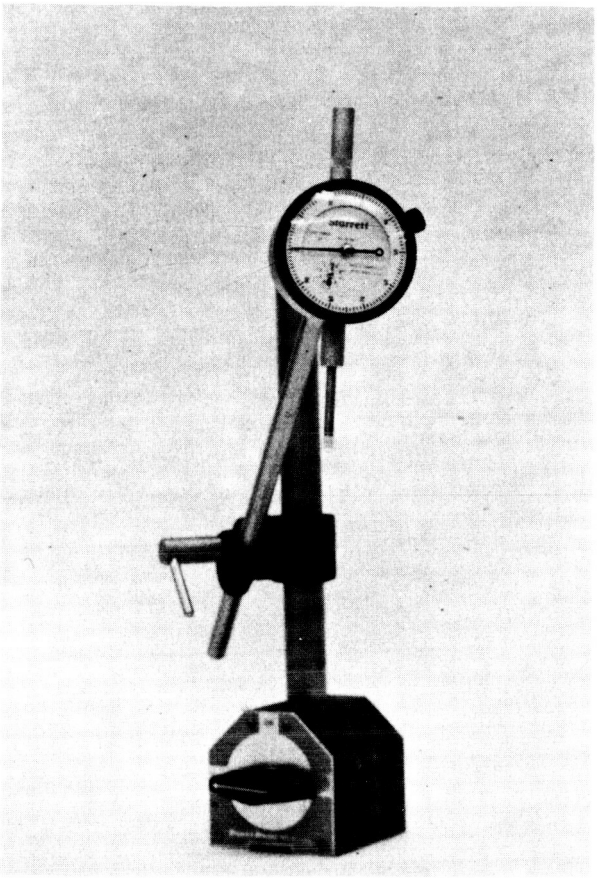

Fig. 12. Dial indicator and adjustable mount

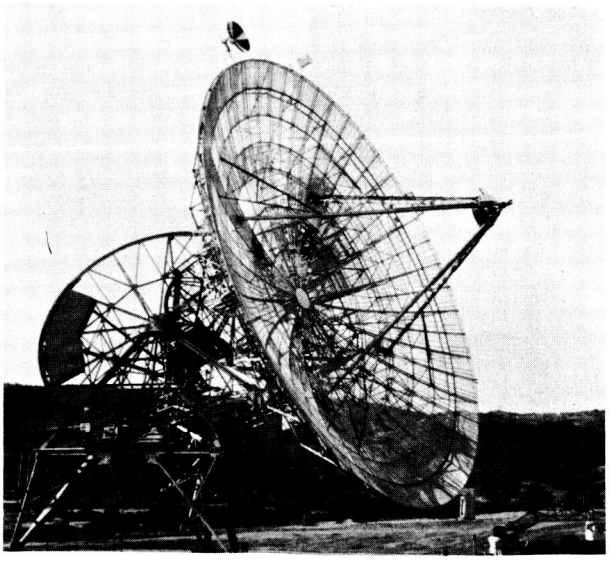

Fig. 13. Over-all view of chains through dish to boxgirder corners

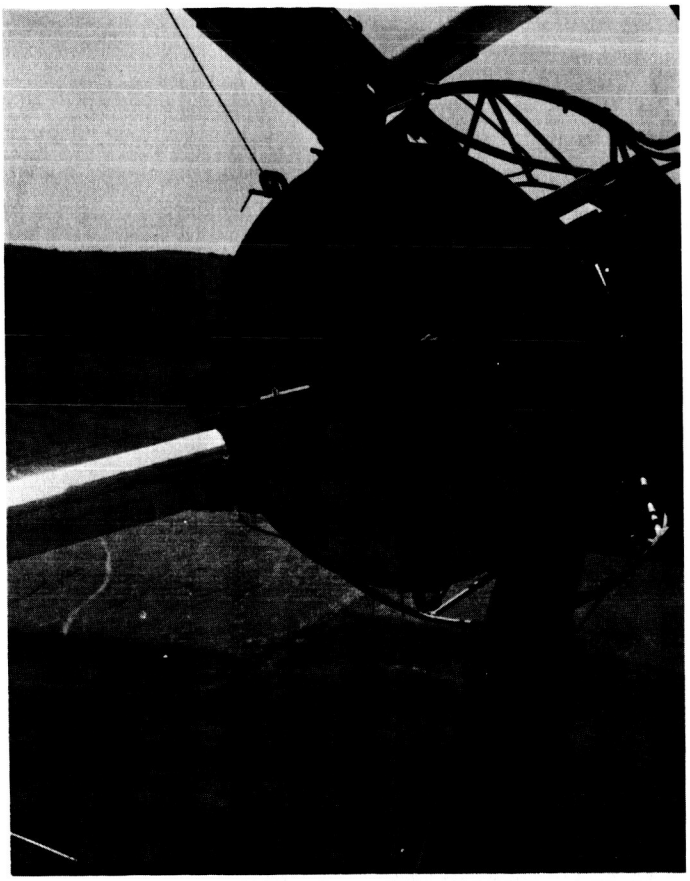

Fig. 14. Closeup of chaining fixture and chaining-tape attachment

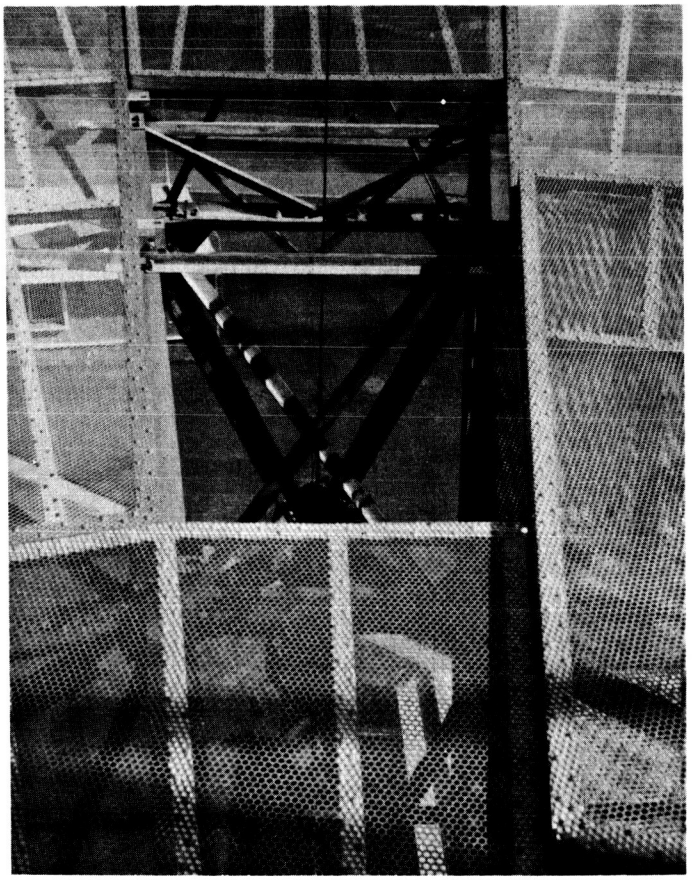

Fig. 15. Closeup of chain passage through dish surface and attachment to boxgirder corners

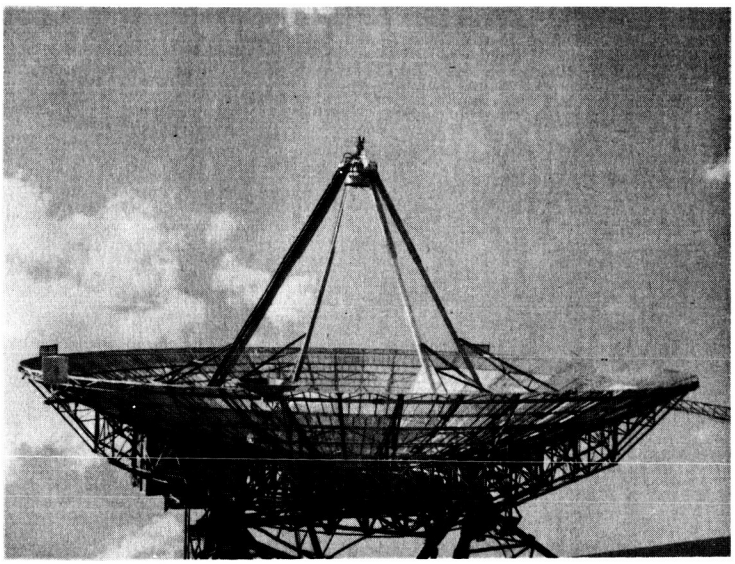

Fig. 16. Over-all view of chaining tapes running from focal point to dish edges

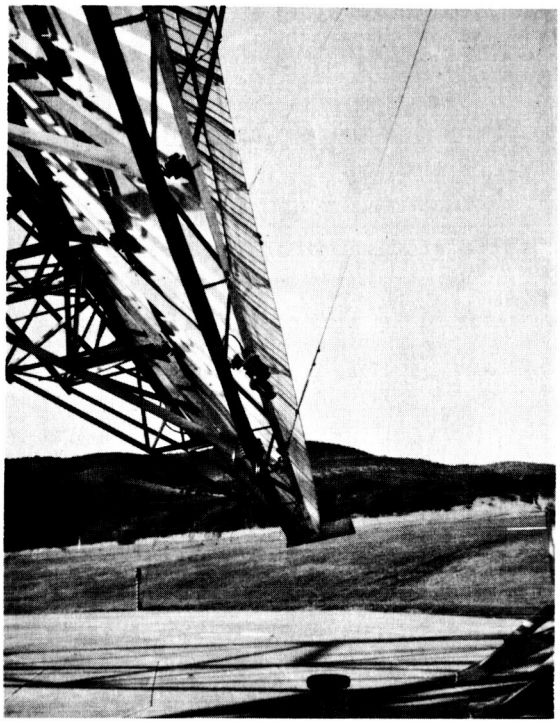

Fig. 17. Closeup of chaining tape attachment to edge of dish structure

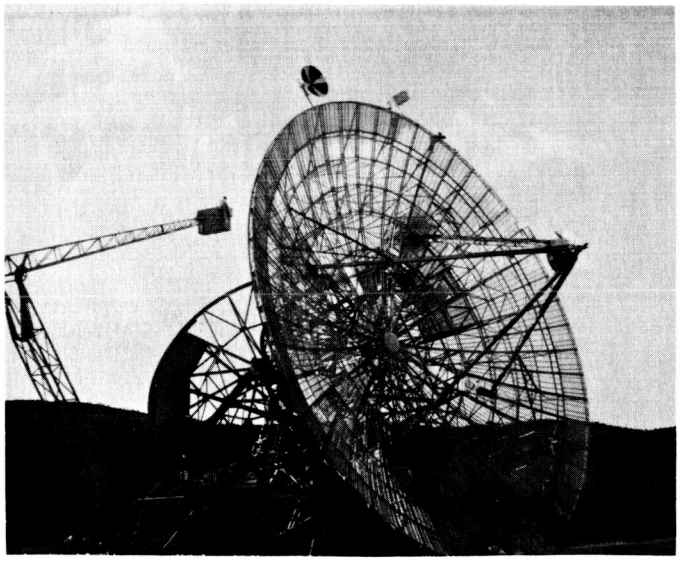

Fig. 18. Method used to read chaining tapes without loading dish structure locally

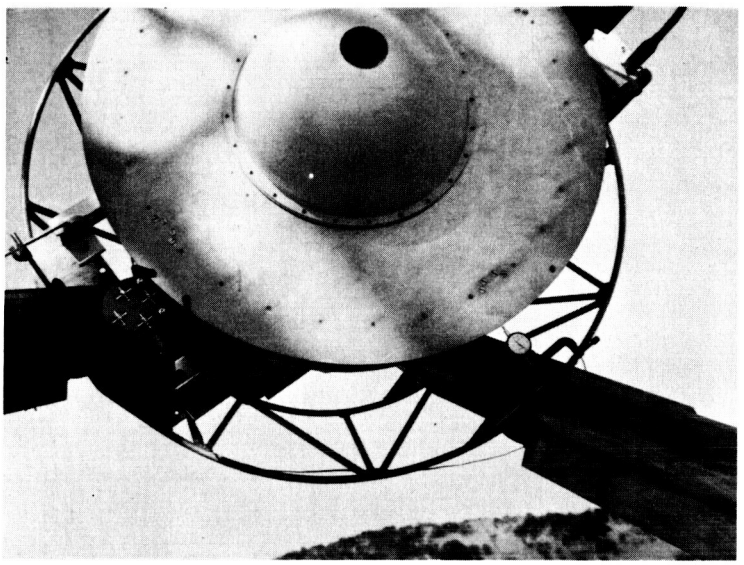

Fig. 19. Mounting of dial indicators on quadripod structure

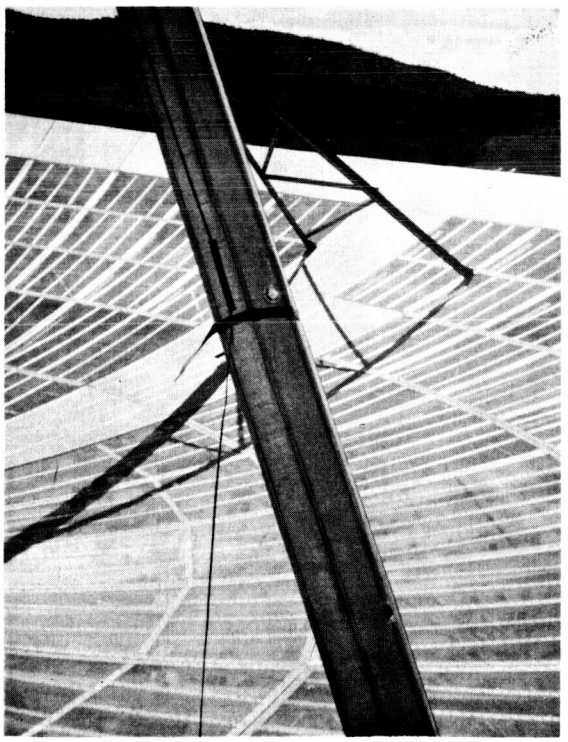

Fig. 20. Mounting of "Pandux" transducer on top of quadripod leg

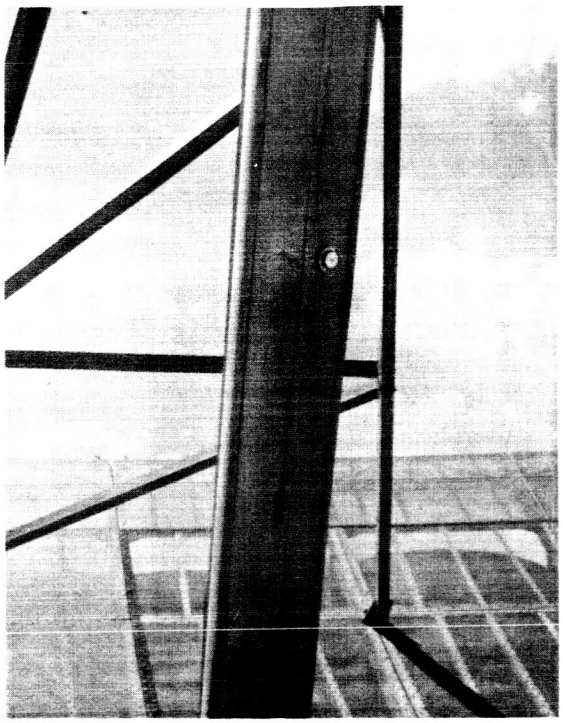

Fig. 21. Mounting of "Pandux" transducer on side of quadripod leg

Fig. 22. Closeup of "Pandux" transducer mounted on pedestal leg

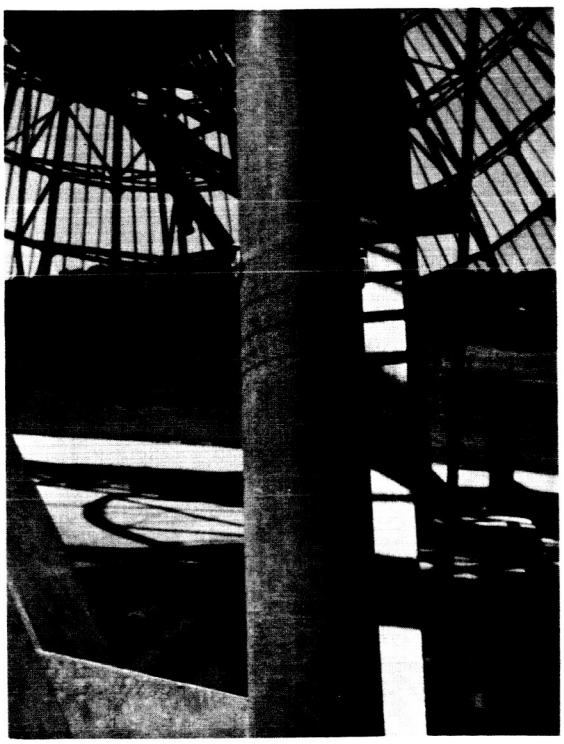

Fig. 23. Side view of "Pandux" transducer mounted on pedestal leg showing differential mounting

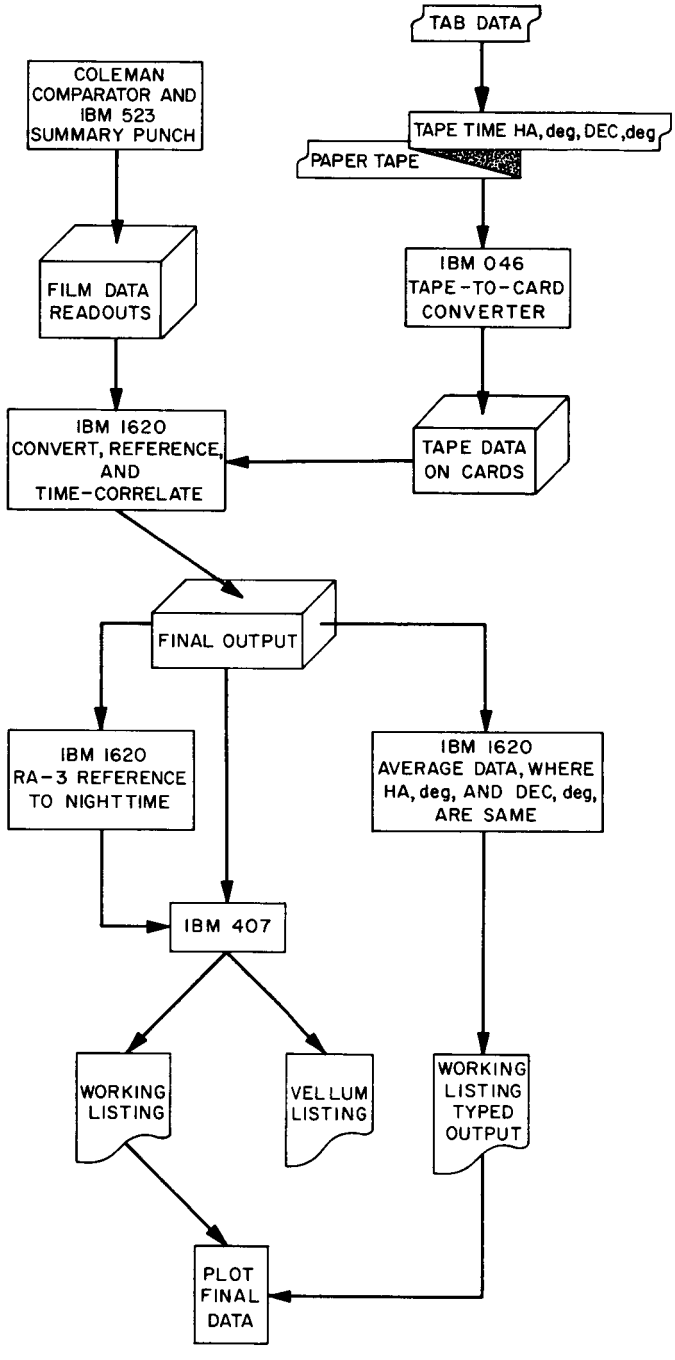

Fig. 24. General data-reduction procedure

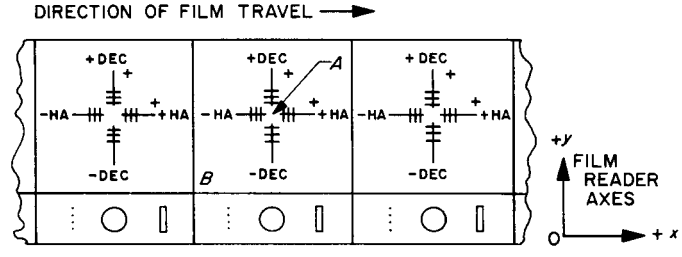

Fig. 25. Typical filmstrip from quadripod imaging fixture

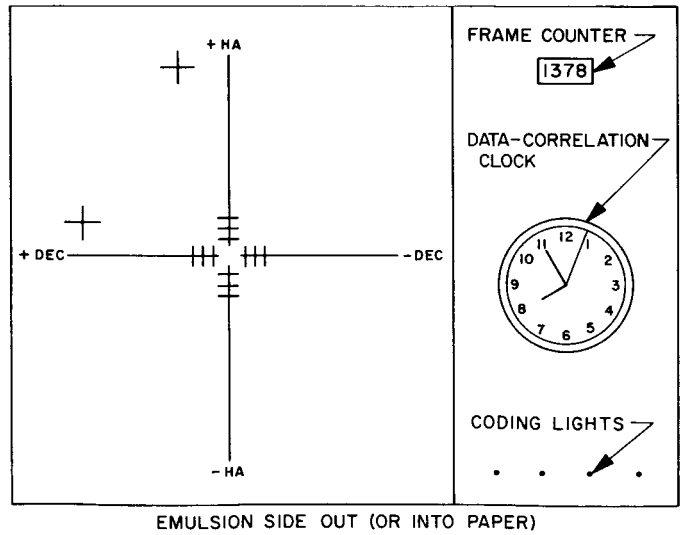

Fig. 26. Typical film frame

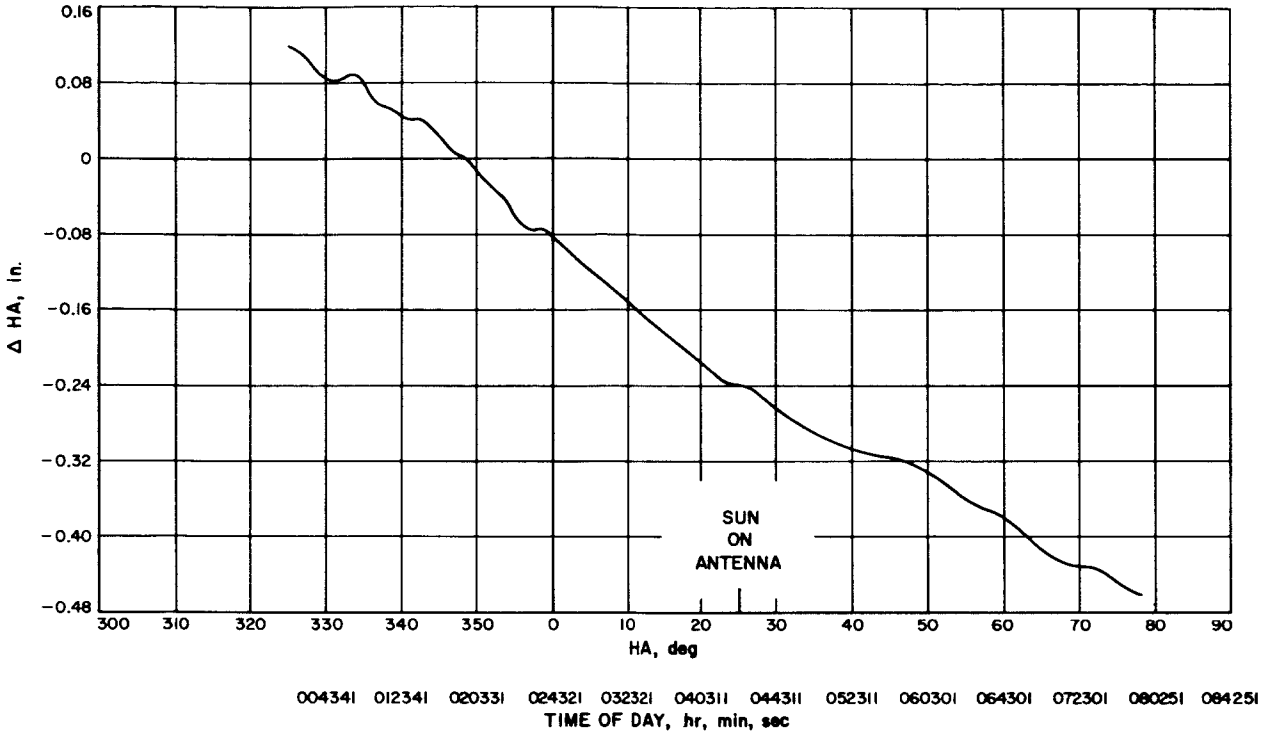

Fig. 27. ΔHA simulated RA-3 test No. 1, 15-16 March 1962

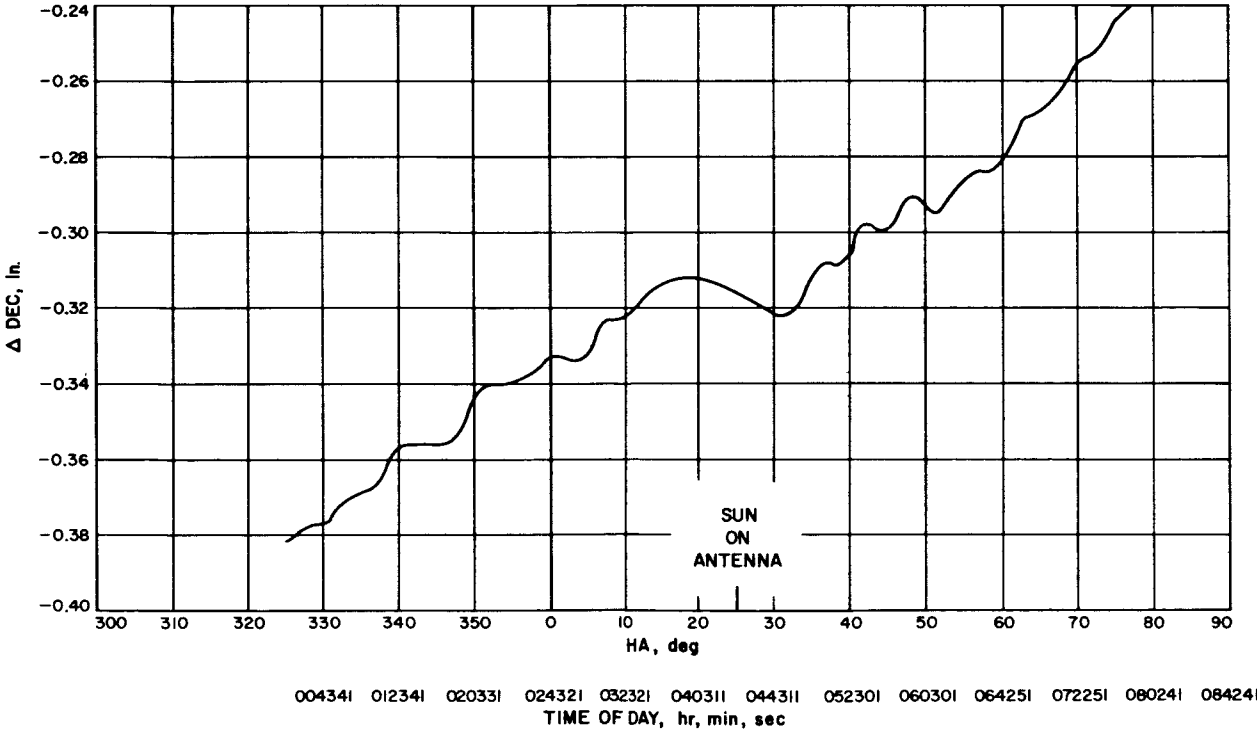

Fig. 28. ΔDEC simulated RA-3 test No. 1, 15-16 March 1962

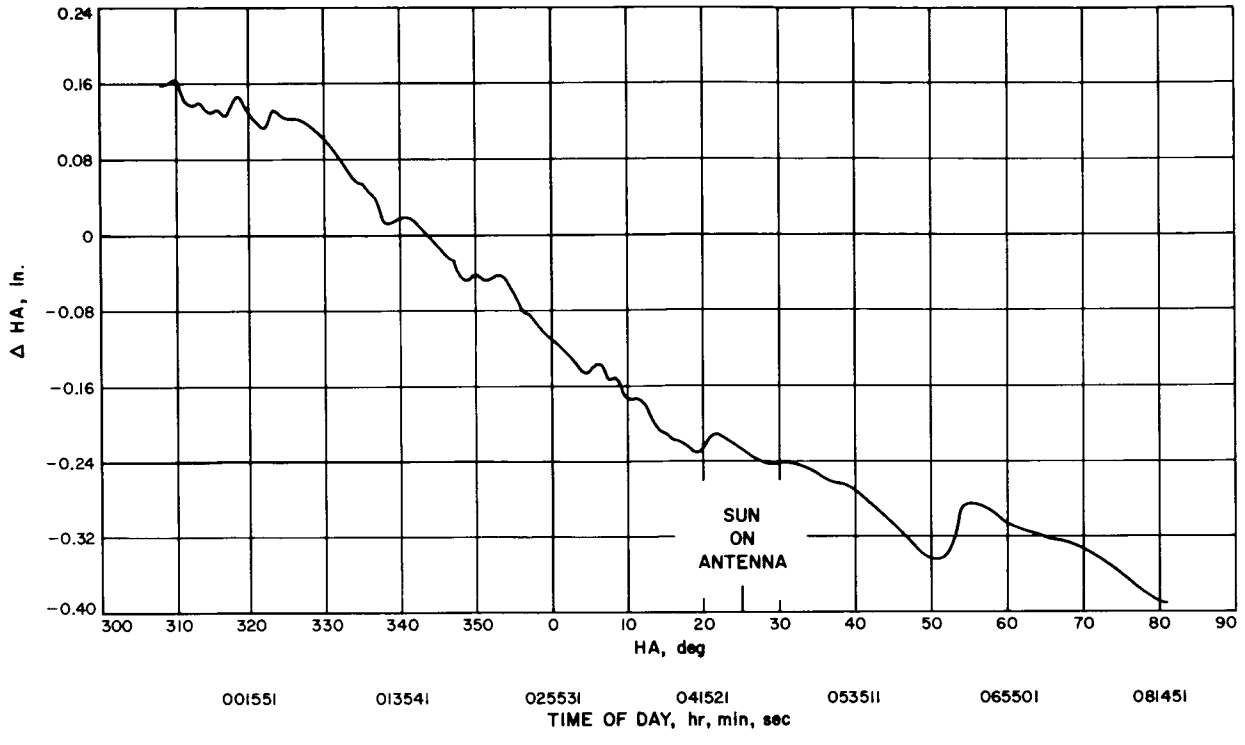

Fig. 29. ΔHA simulated RA-3 test No. 3, 17-18 March 1962

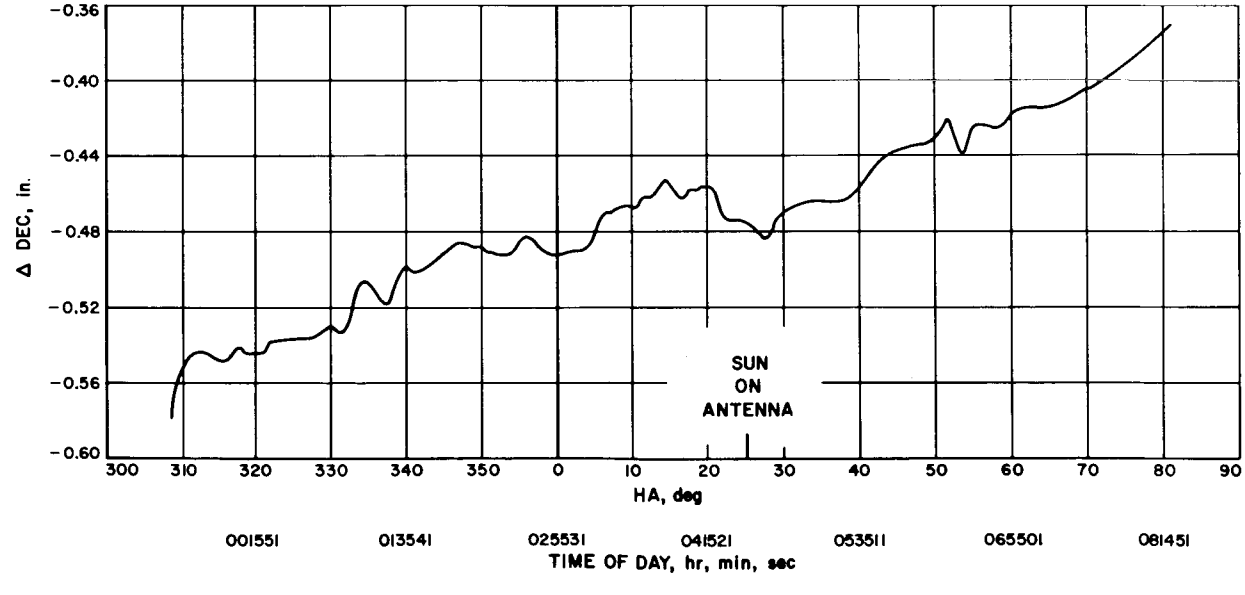

Fig. 30. ΔDEC simulated RA-3 test No. 3, 17-18 March 1962

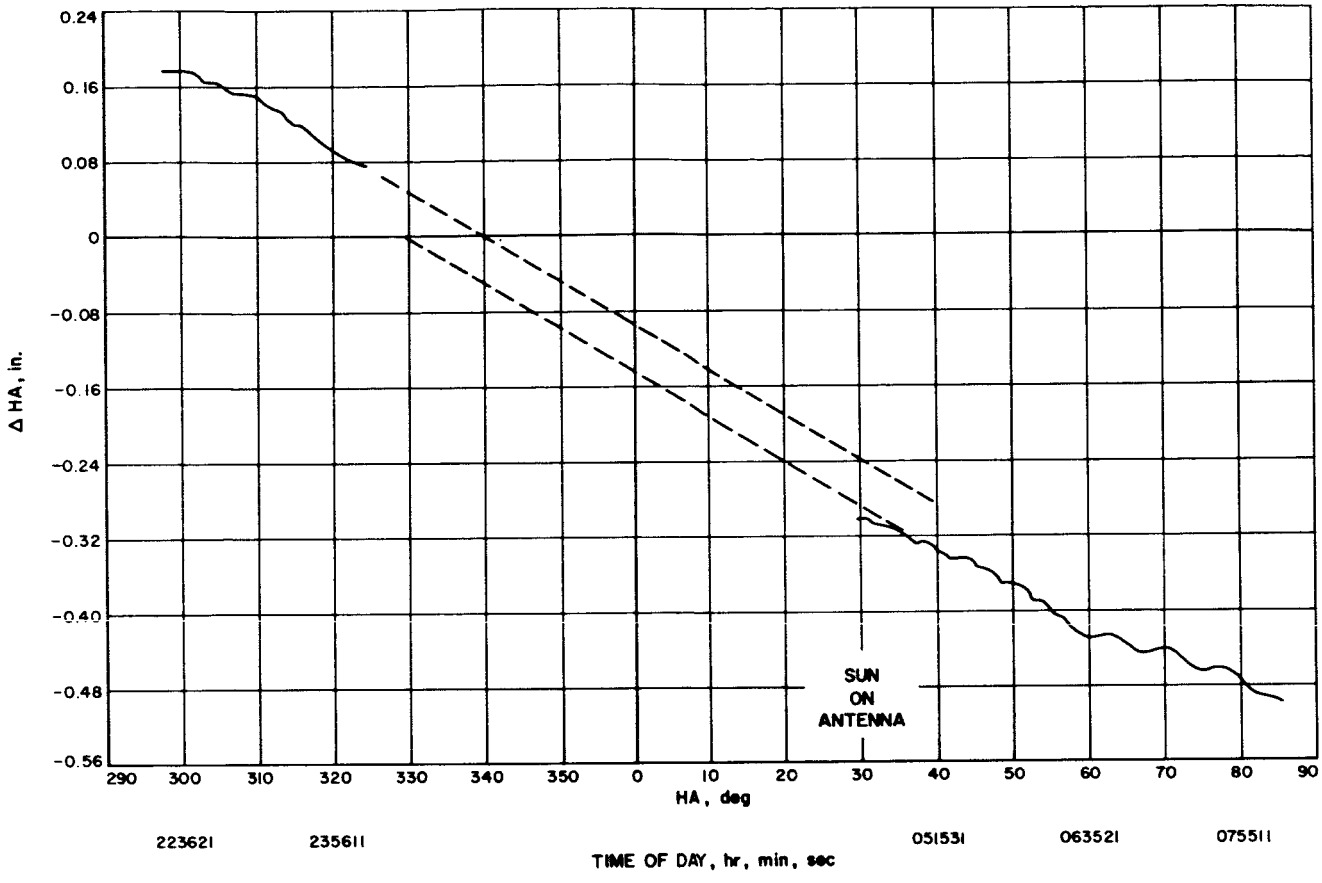

Fig. 31. ΔHA simulated RA-3 test No. 4, 22-23 March 1962

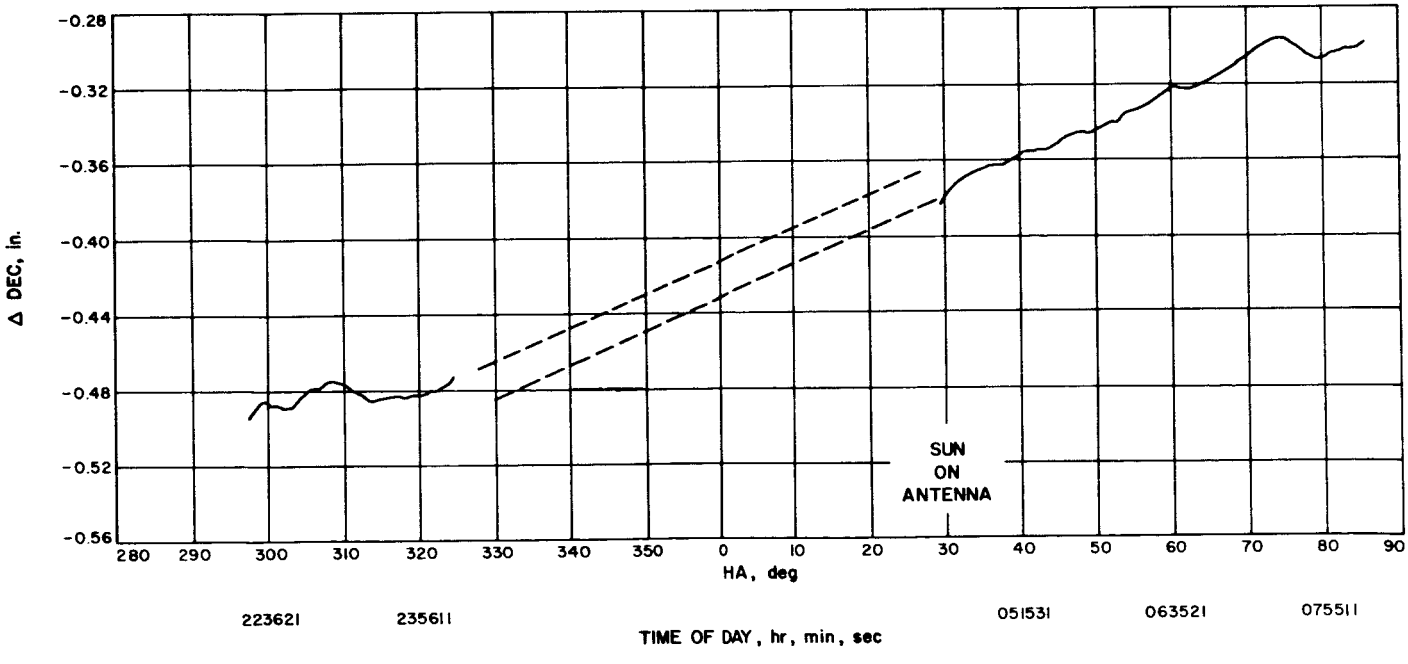

Fig. 32. ΔDEC simulated RA-3 test No. 4, 22-23 March 1962

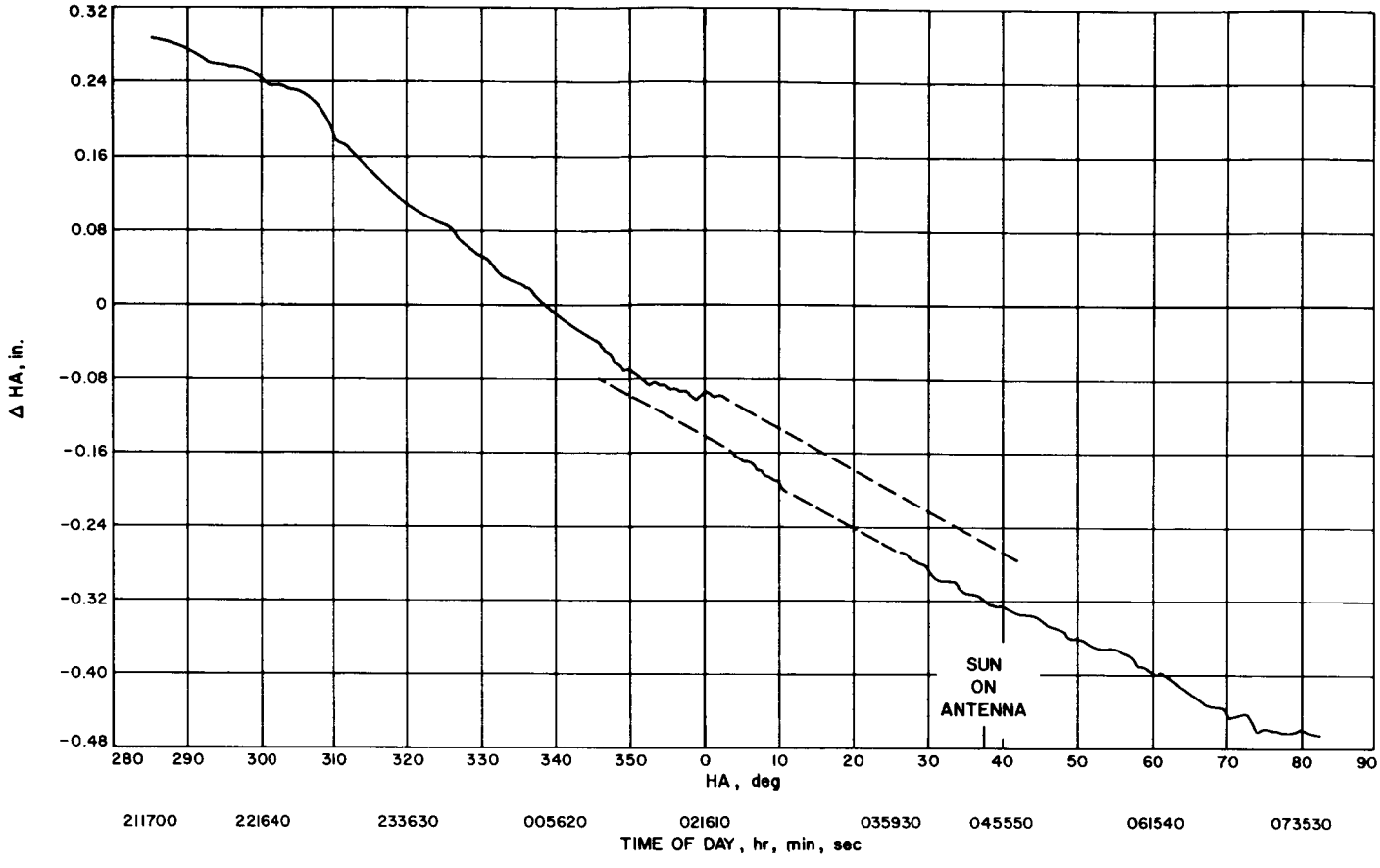

Fig. 33. ΔHA simulated RA-3 test No. 6, 27-28 March 1962

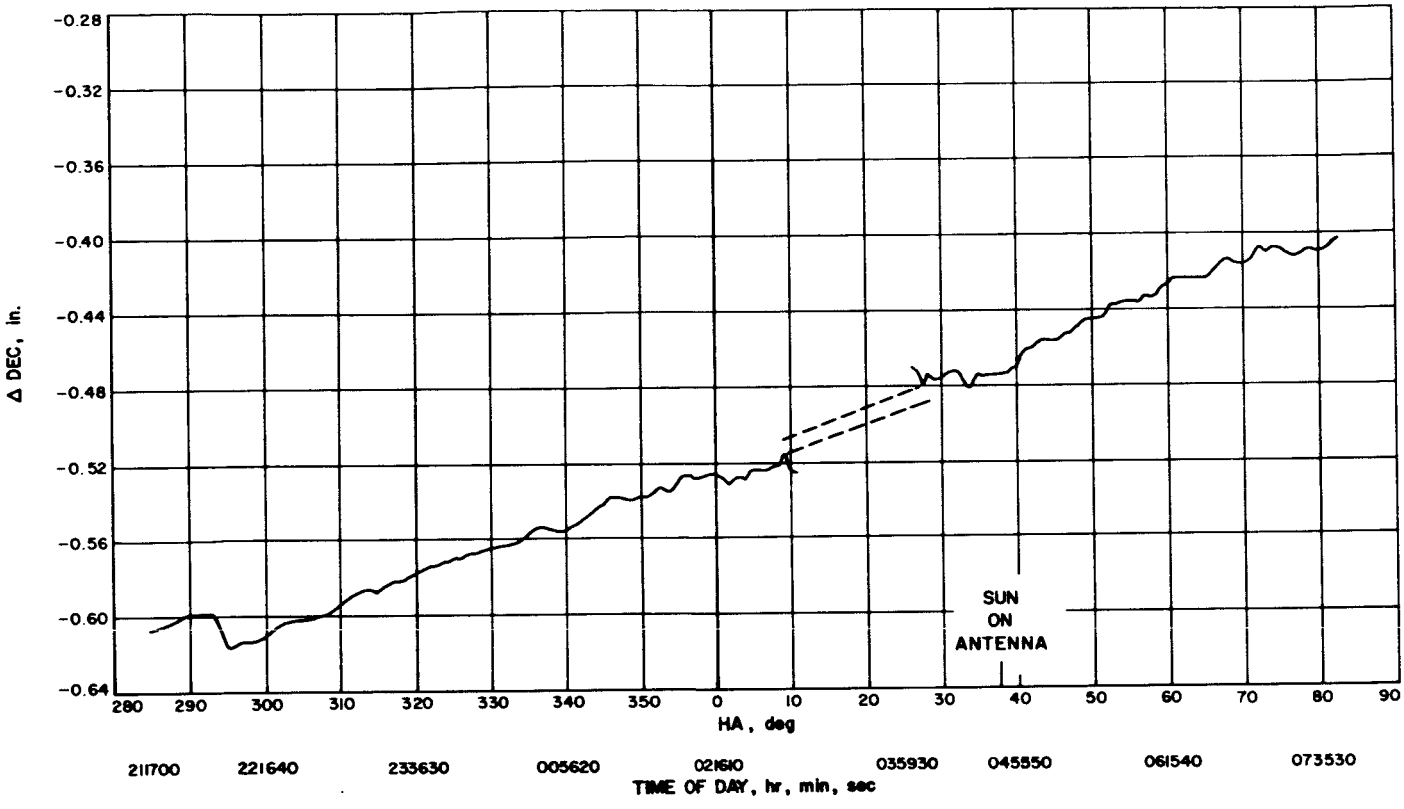

Fig. 34. ΔDEC simulated RA-3 test No. 6, 27-28 March 1962

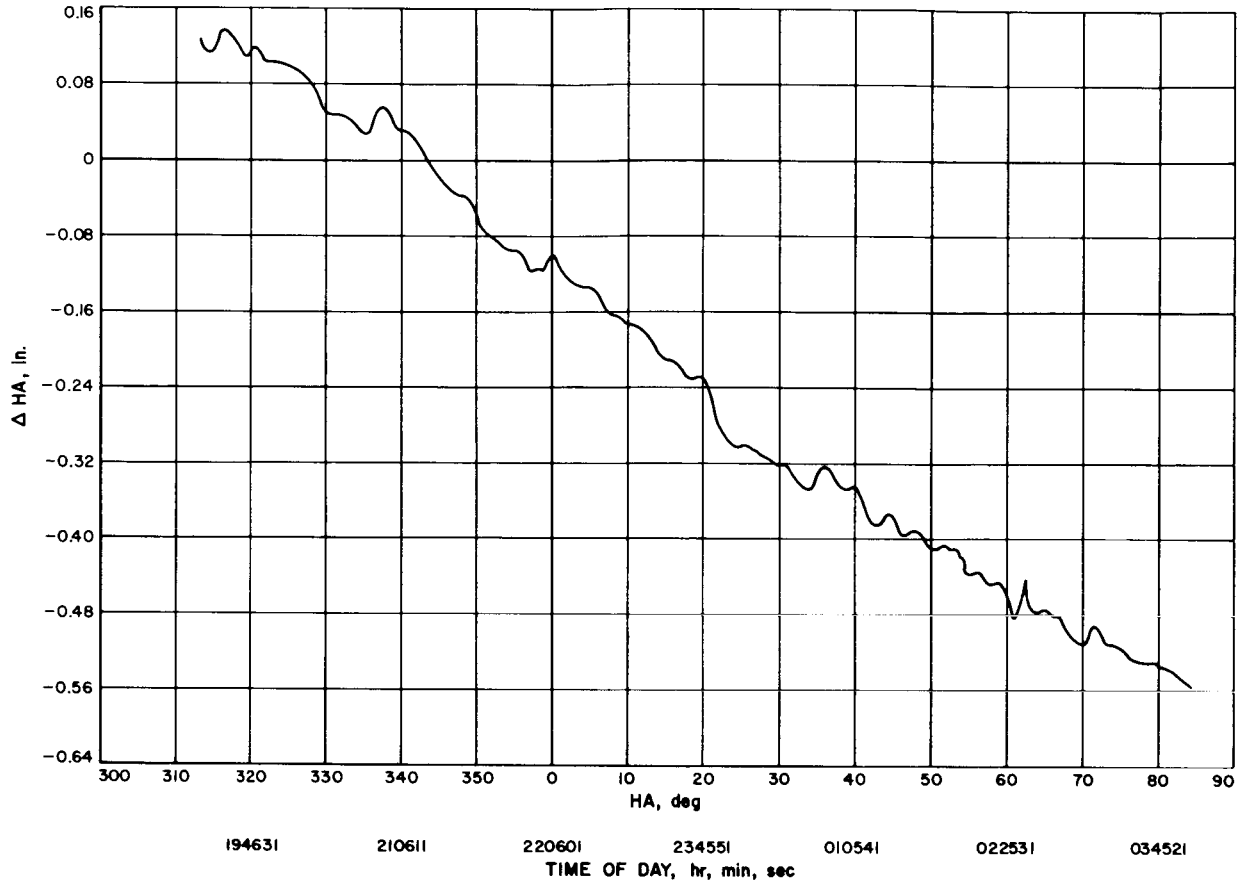

Fig. 35. ΔHA simulated RA-3 test, nighttime only, 26-27 March 1962

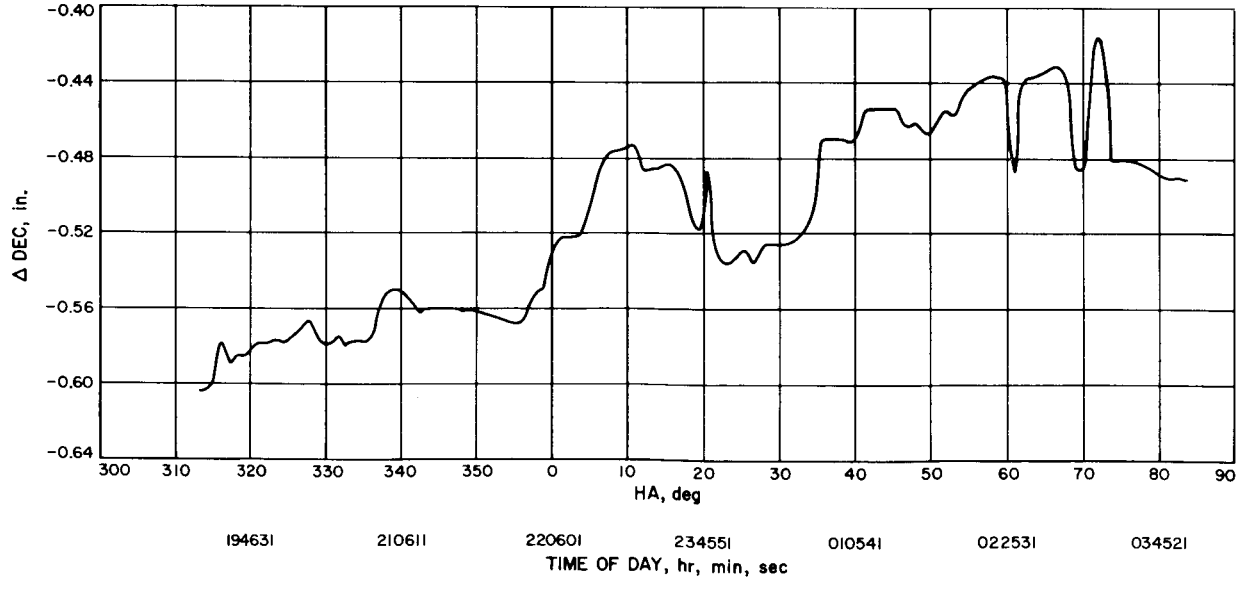

Fig. 36. ΔDEC simulated RA-3 test, nighttime only, 26-27 March 1962

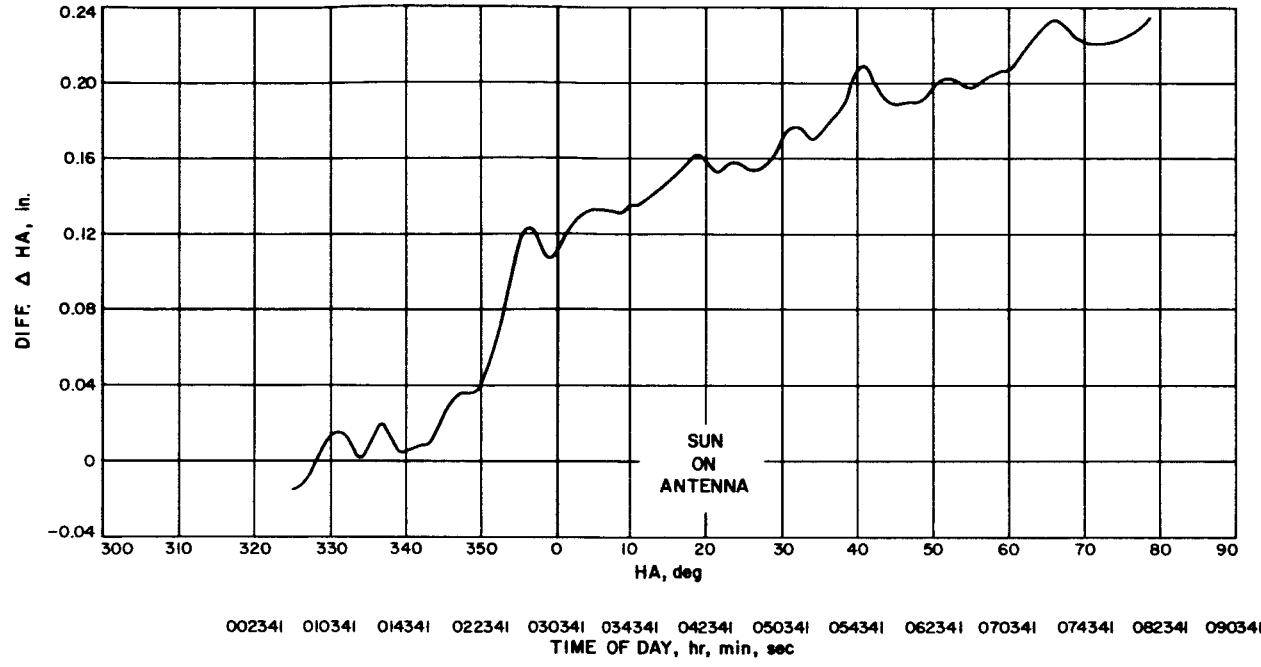

Fig. 37. ΔHA simulated RA-3 test No. 1, data referenced to nighttime only test, 15-16 March and 26-27 March 1962

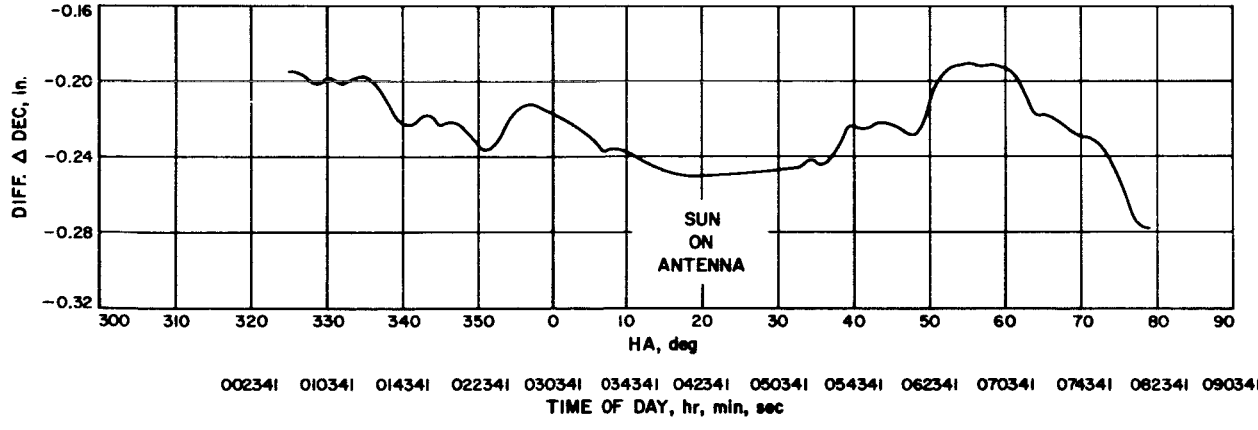

Fig. 38. ΔDEC simulated RA-3 test No. 1, data referenced to nighttime only test, 15-16 March and 26-27 March 1962

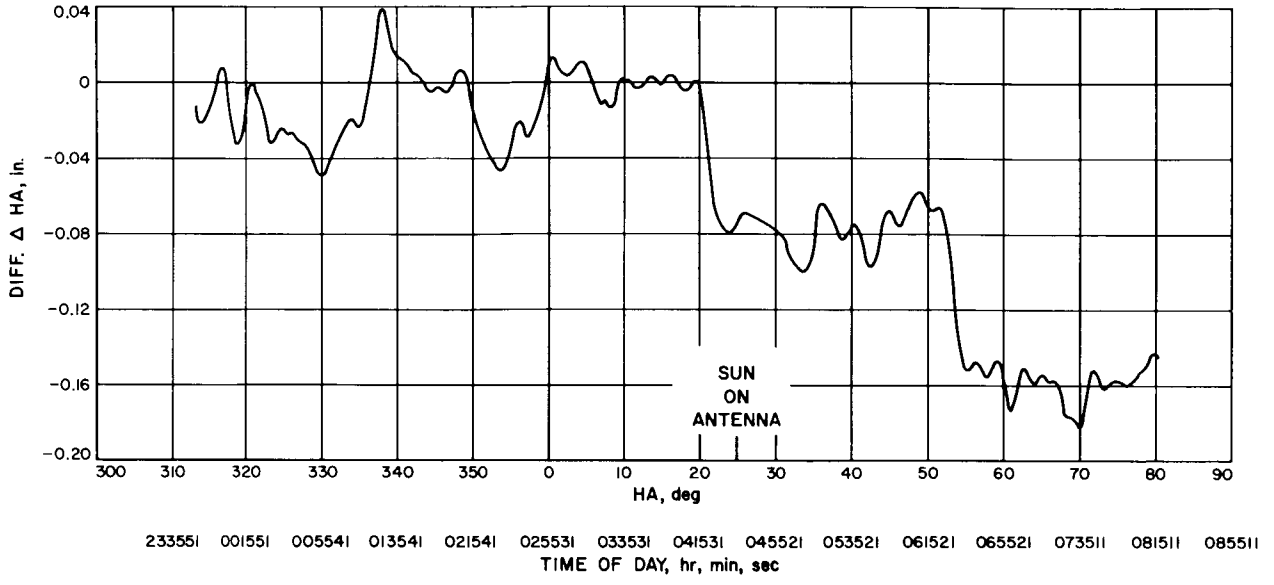

Fig. 39. ΔHA simulated RA-3 test No. 3, data referenced to nighttime only test, 17-18 March 1962 and 26-27 March 1962

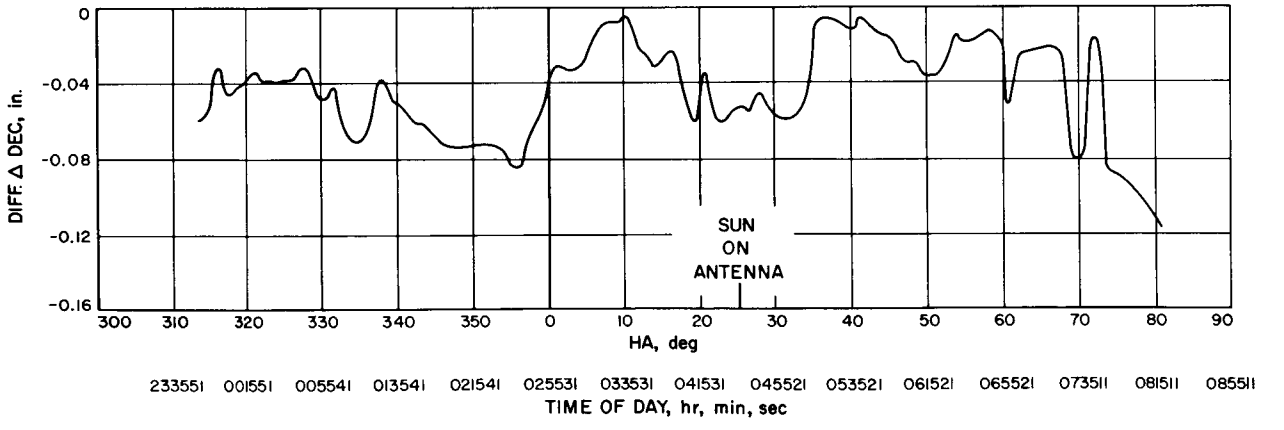

Fig. 40. ΔDEC simulated RA-3 test No. 3, data referenced to nighttime only test, 17-18 March 1962 and 26-27 March 1962

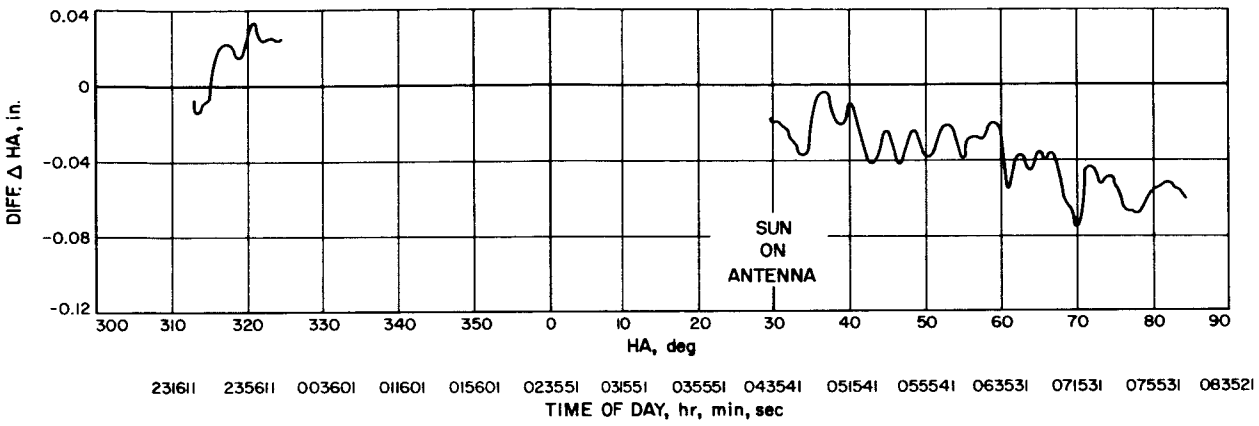

Fig. 41. ΔHA simulated RA-3 test No. 4, data referenced to nighttime only test, 22-23 March 1962 and 26-27 March 1962

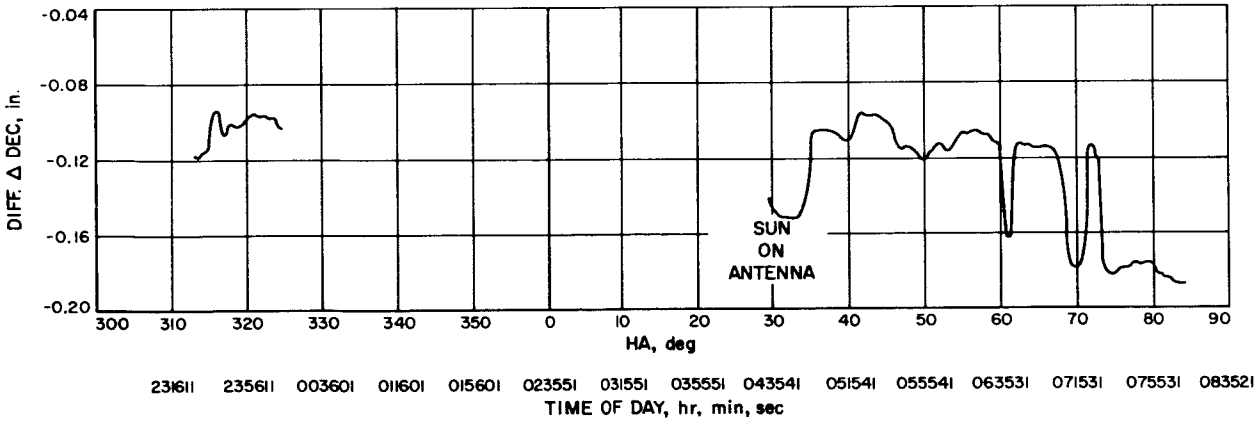

Fig. 42. ΔDEC simulated RA-3 test No. 4, data referenced to nighttime only test, 22-23 March 1962 and 26-27 March 1962

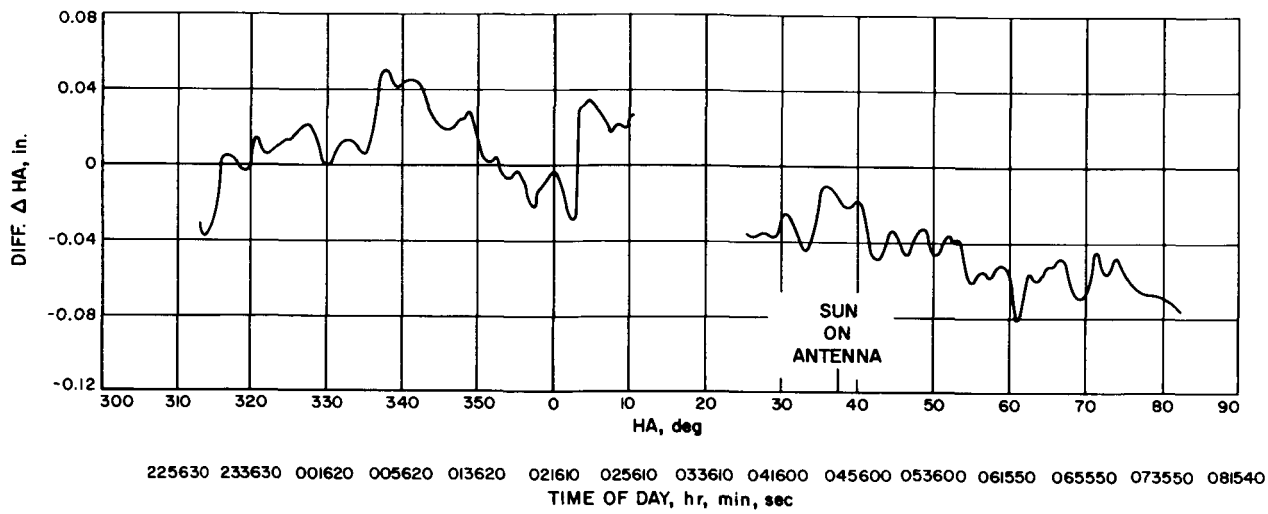

Fig. 43. ΔHA simulated RA-3 test No. 6, data referenced to nighttime only test, 27-28 March 1962 and 26-27 March 1962

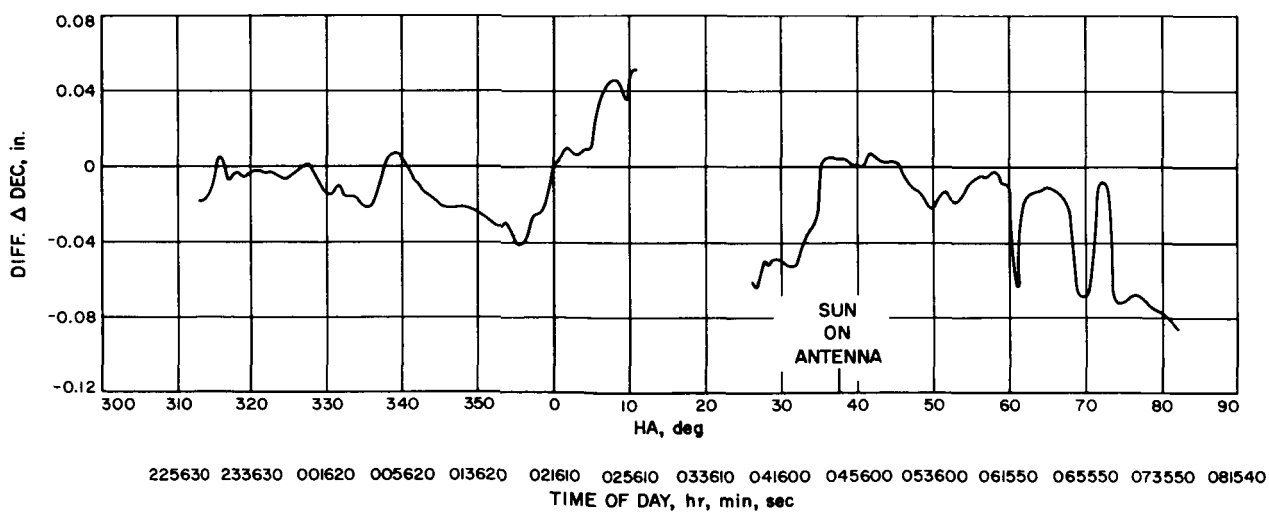

Fig. 44. ΔDEC simulated RA-3 test No. 6, data referenced to nighttime only test, 27-28 March 1962 and 26-27 March 1962

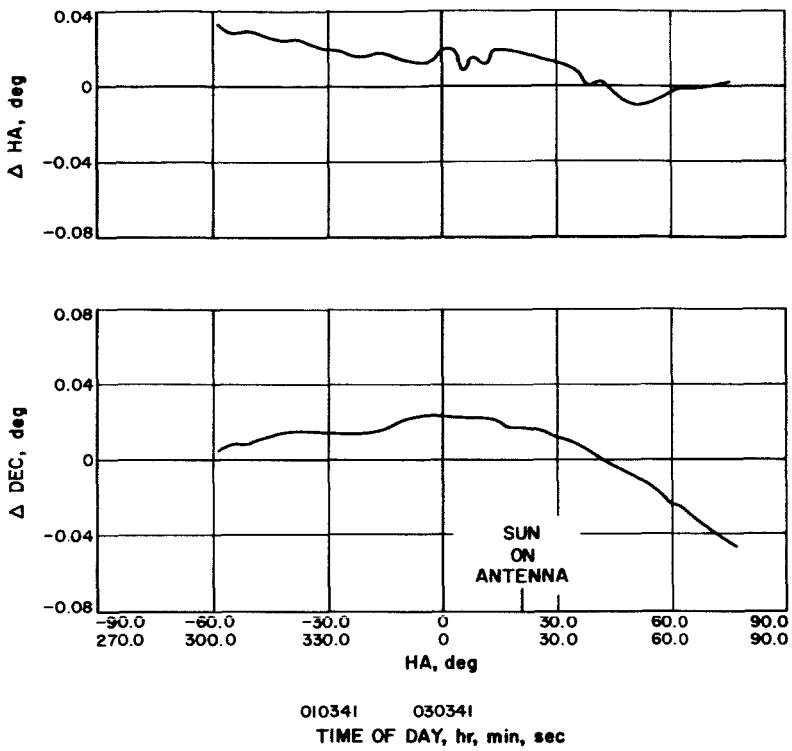

Fig. 45. Test No. 1—night into day optical startrack (Antares, SHA = 113.230, DEC = 333.652), Station 5, South Africa, 15 March 1962

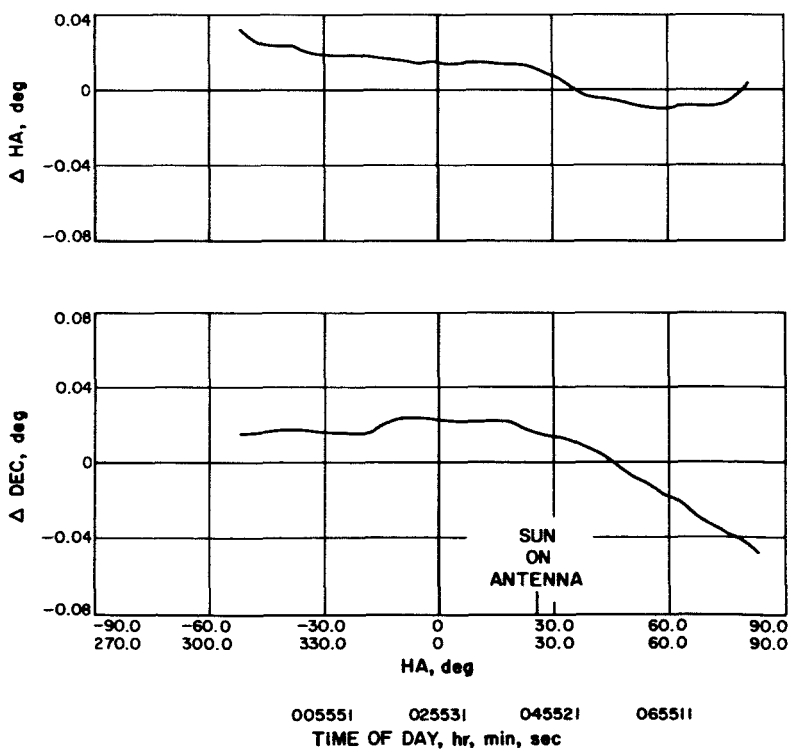

Fig. 46. Test No. 3—night into day optical startrack (Antares, SHA = 113.230, DEC = 333.652), Station 5, South Africa, 17 March 1962

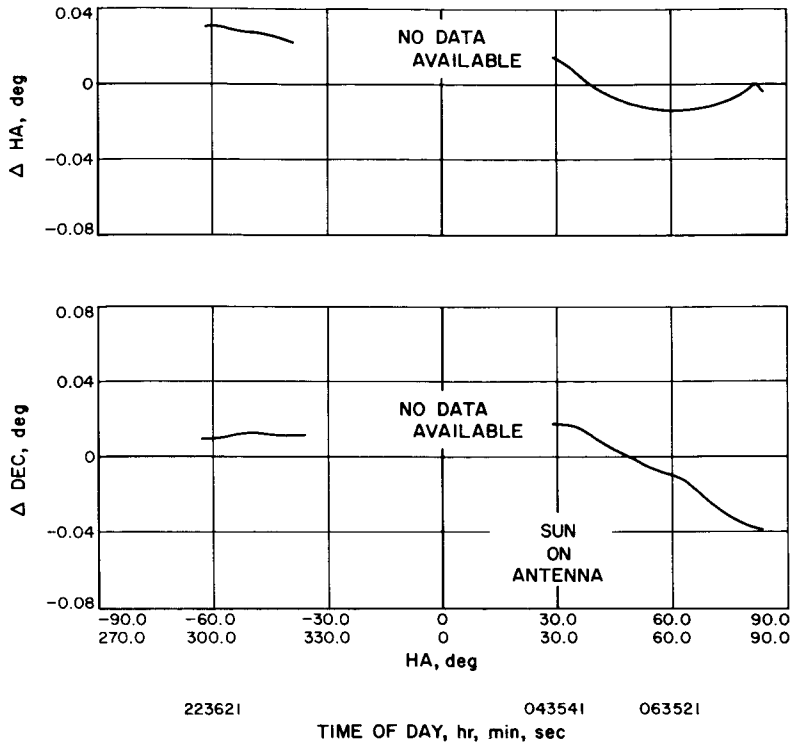

Fig. 47. Test No. 4—night into day optical startrack (Antares, SHA = 113.230, DEC = 333.652), Station 5, South Africa, 22 March 1962

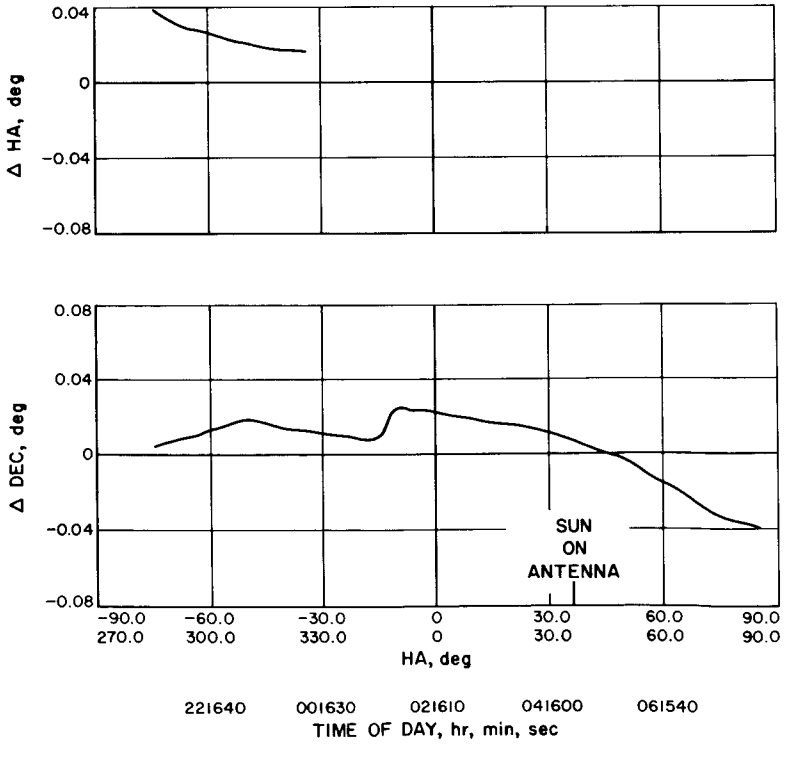

Fig. 48. Test No. 6—night into day optical startrack (Antares, SHA = 113.230, DEC = 333.652) Station 5, South Africa, 27 March 1962

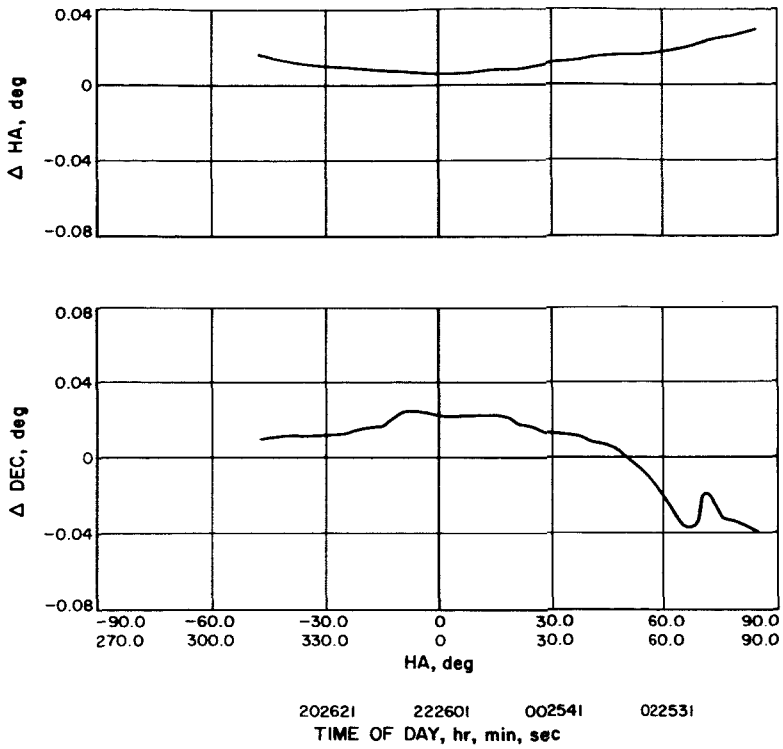

Fig. 49. Nighttime only optical startrack, (Beta Corvi, SHA = 171.898, DEC = 336.812), Station 5, South Africa, 26 March 1962

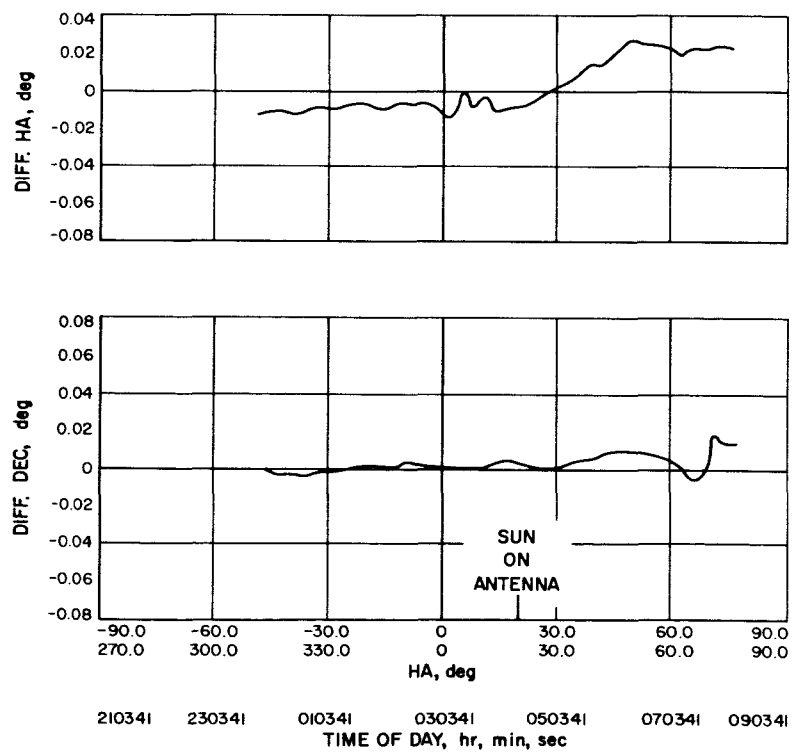

Fig. 50. Transition startrack test No. 1 compared with nighttime startrack, 15 March 1962 with 26 March 1962

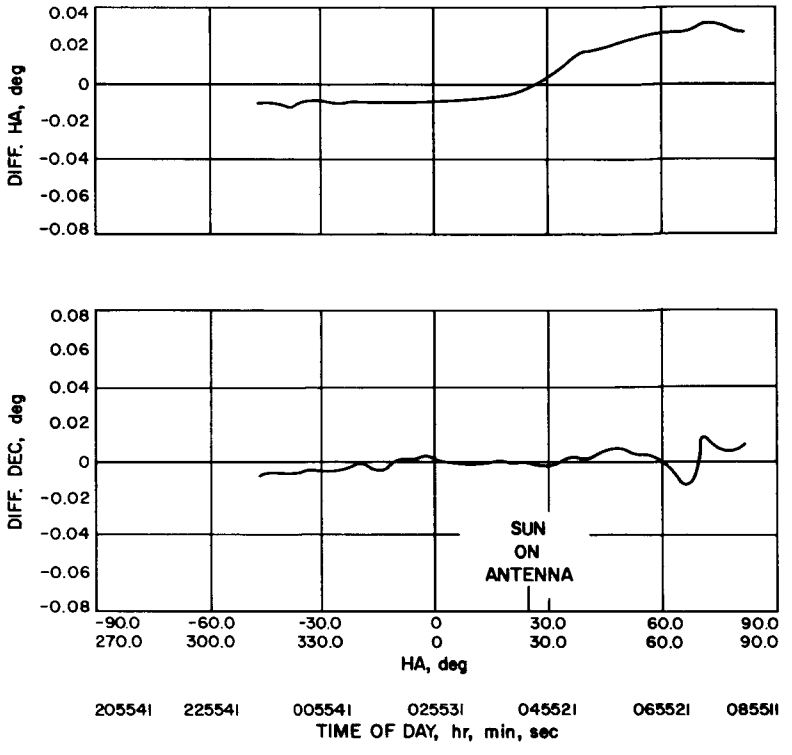

Fig. 51. Transition startrack test No. 3 compared with nighttime startrack, 17 March 1962 with 26 March 1962

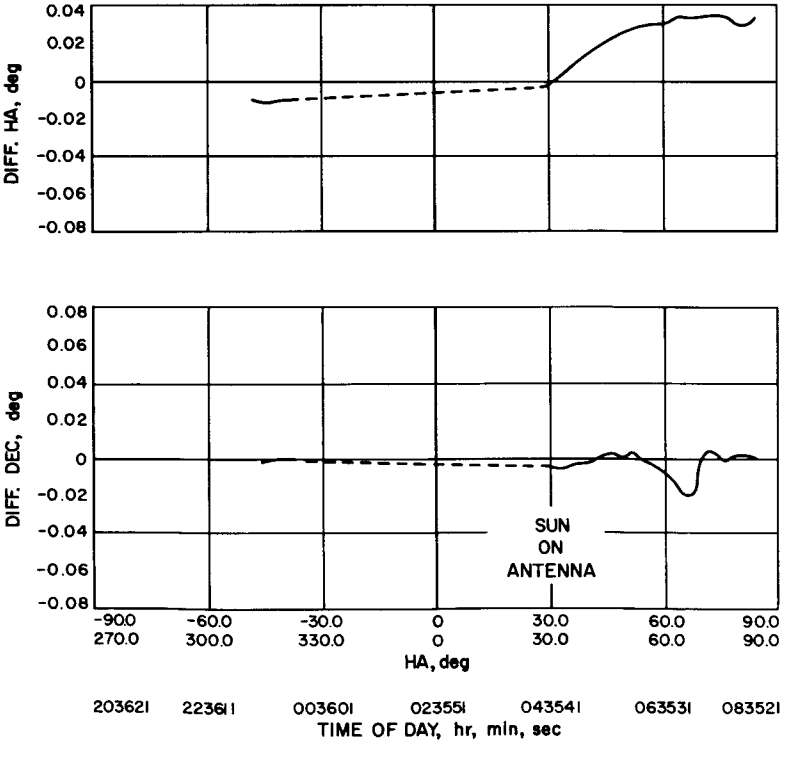

Fig. 52. Transition startrack test No. 4 compared with nighttime startrack, 22 March 1962 with 26 March 1962

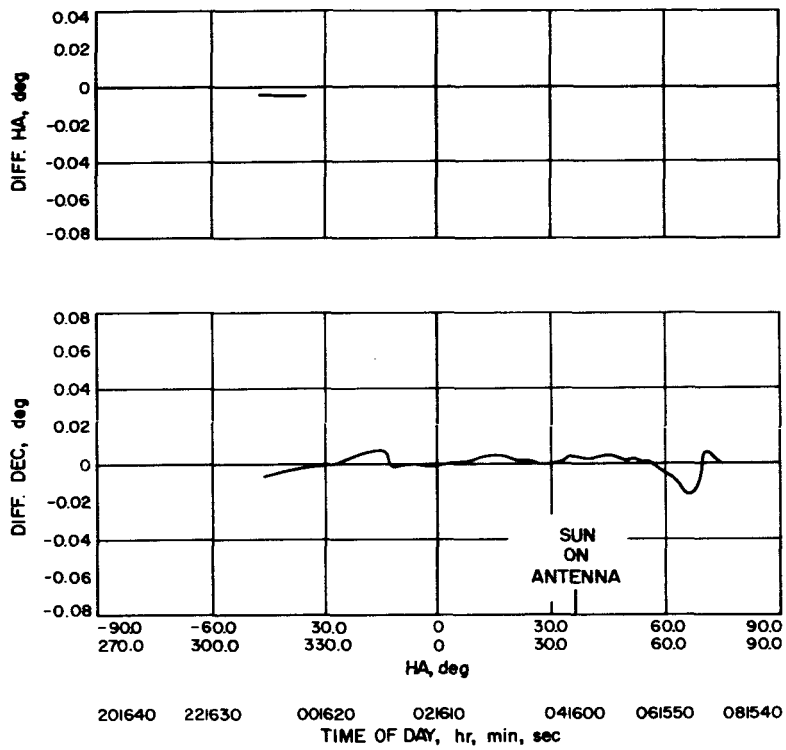

Fig. 53. Transition startrack test No. 6 compared with nighttime startrack, 27 March 1962 with 26 March 1962

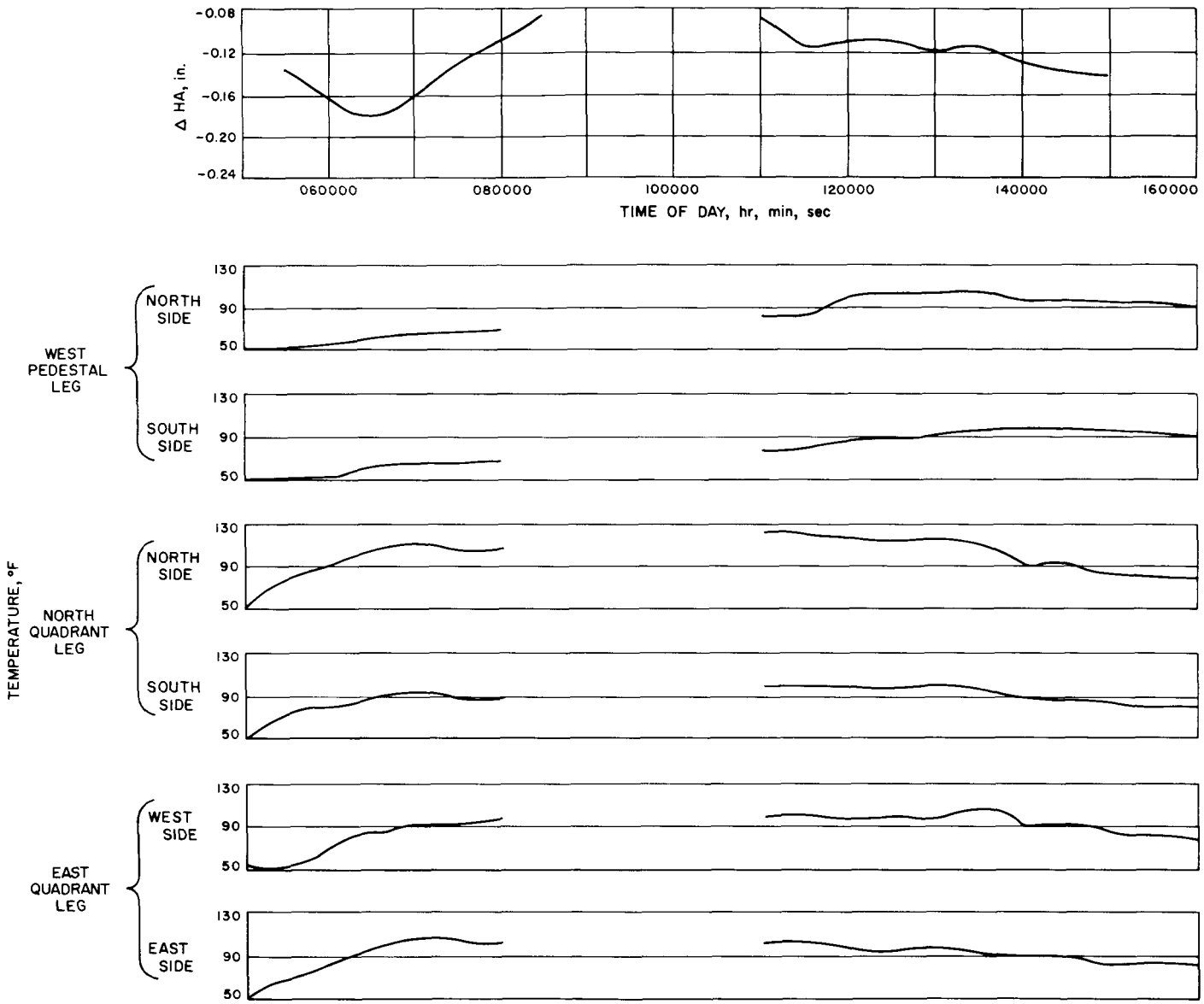

Fig. 54. Quad. ΔHA deflection vs. temperature measurement during Sun transit, 25 March 1962

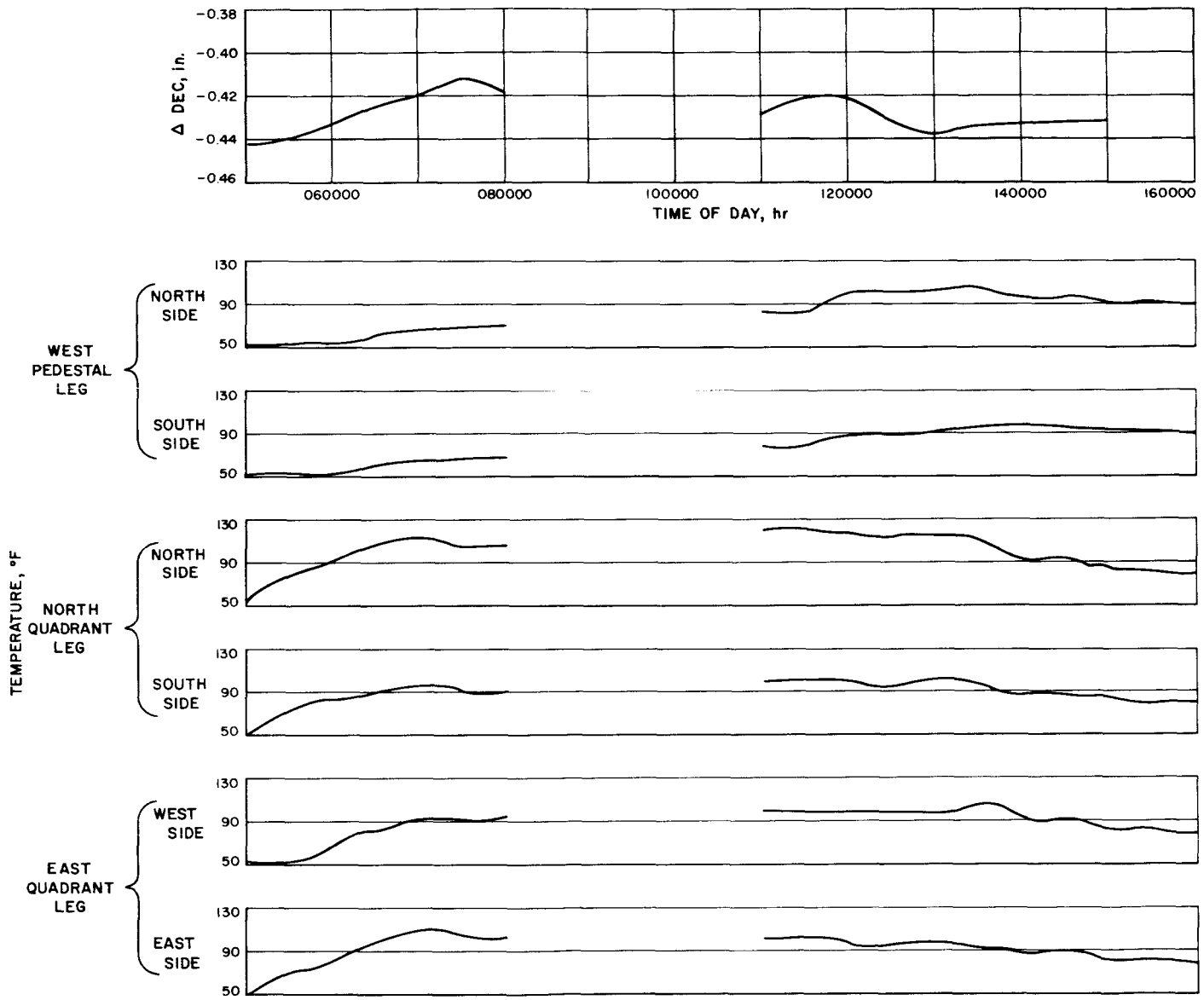

Fig. 55. Quad. ΔDEC deflection vs. temperature measurement during Sun transit, 25 March 1962

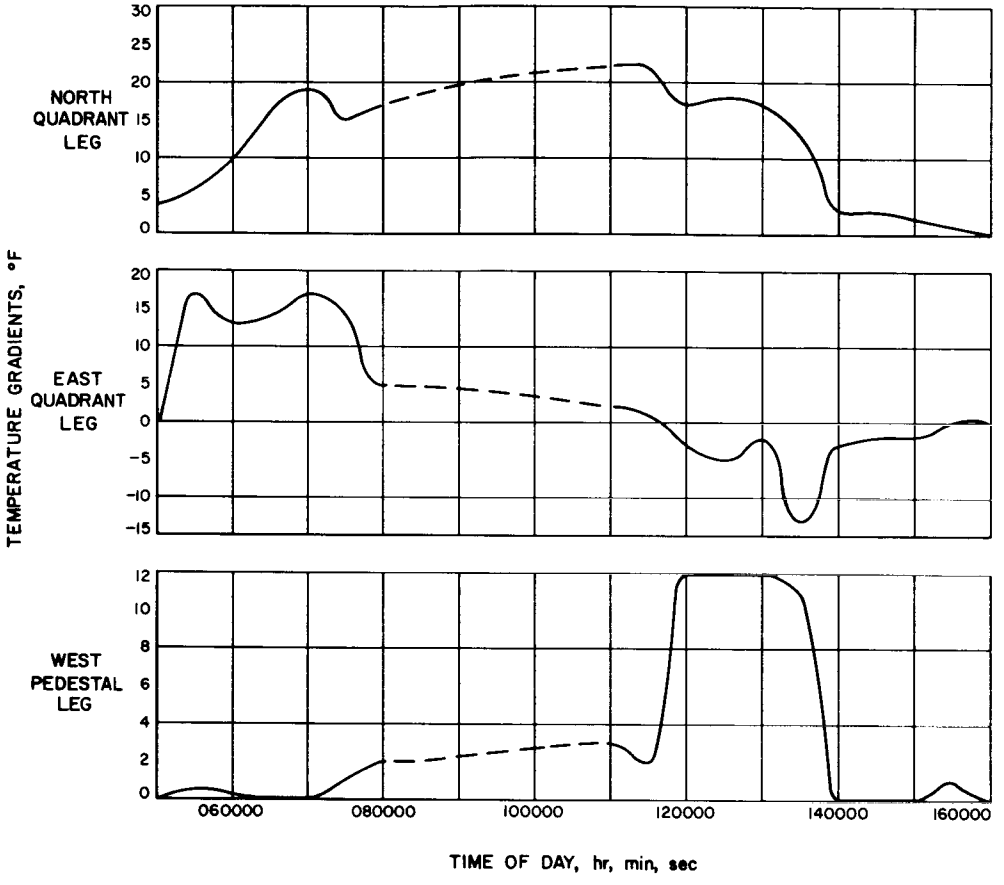

Fig. 56. Quad. temperature gradient measurements during Sun transit, 25 March 1962

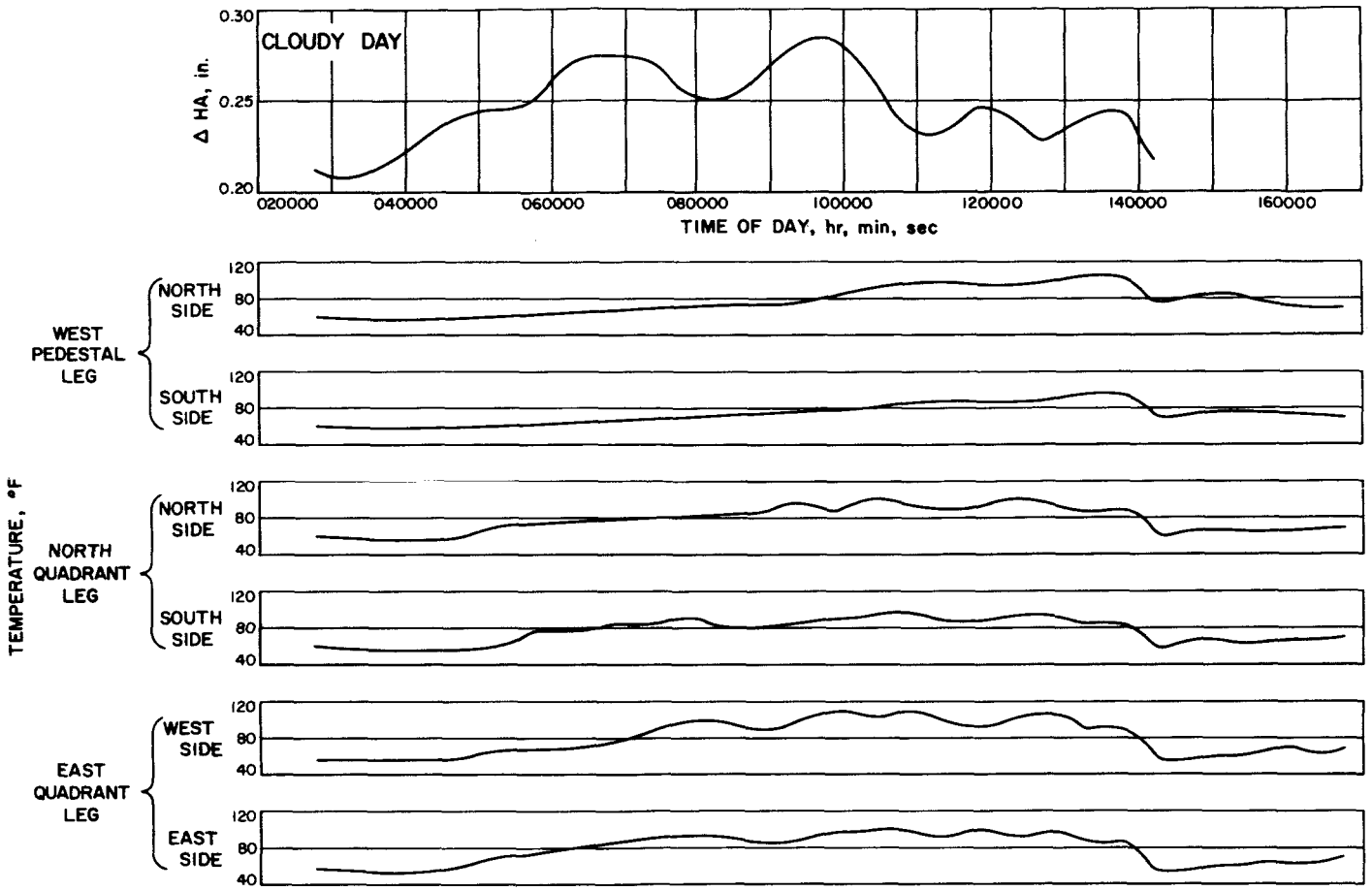

Fig. 57. Collimation-tower ΔHA deflection temperature test No. 1, 26 March 1962

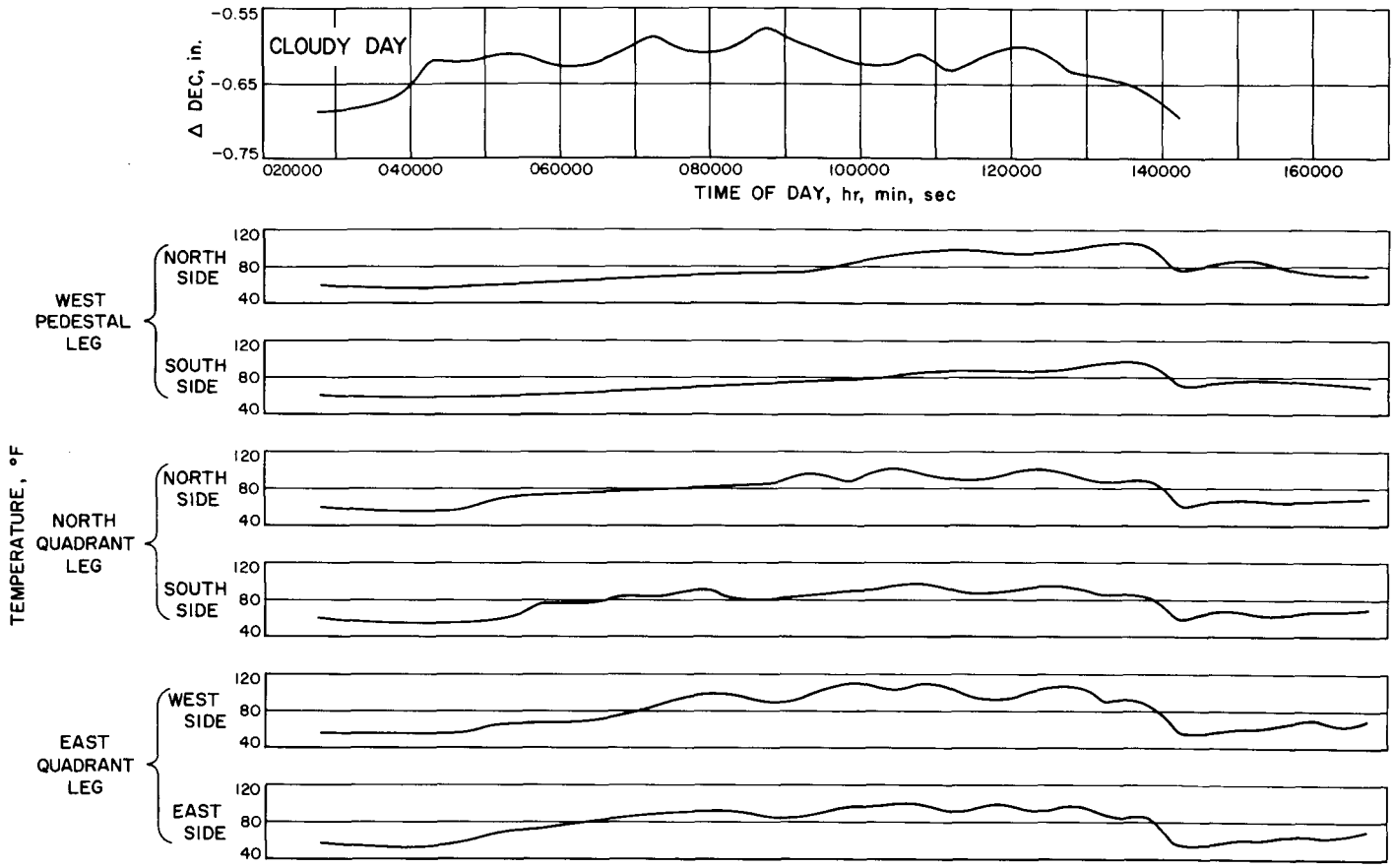

Fig. 58. Collimation-tower ΔDEC deflection temperature test No. 1, 26 March 1962

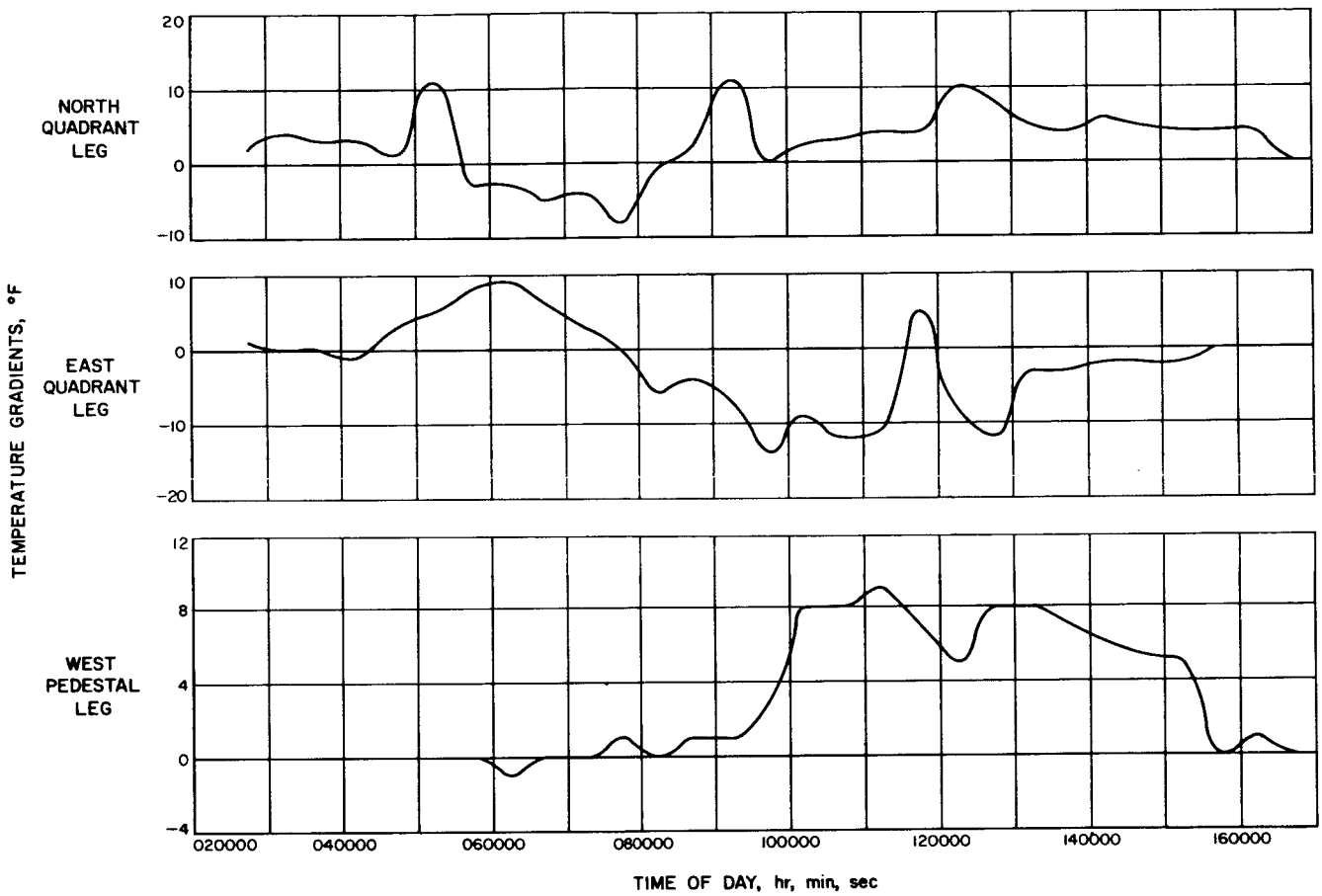

Fig. 59. Collimation-tower temperature gradient measurements, test No. 1, 26 March 1962

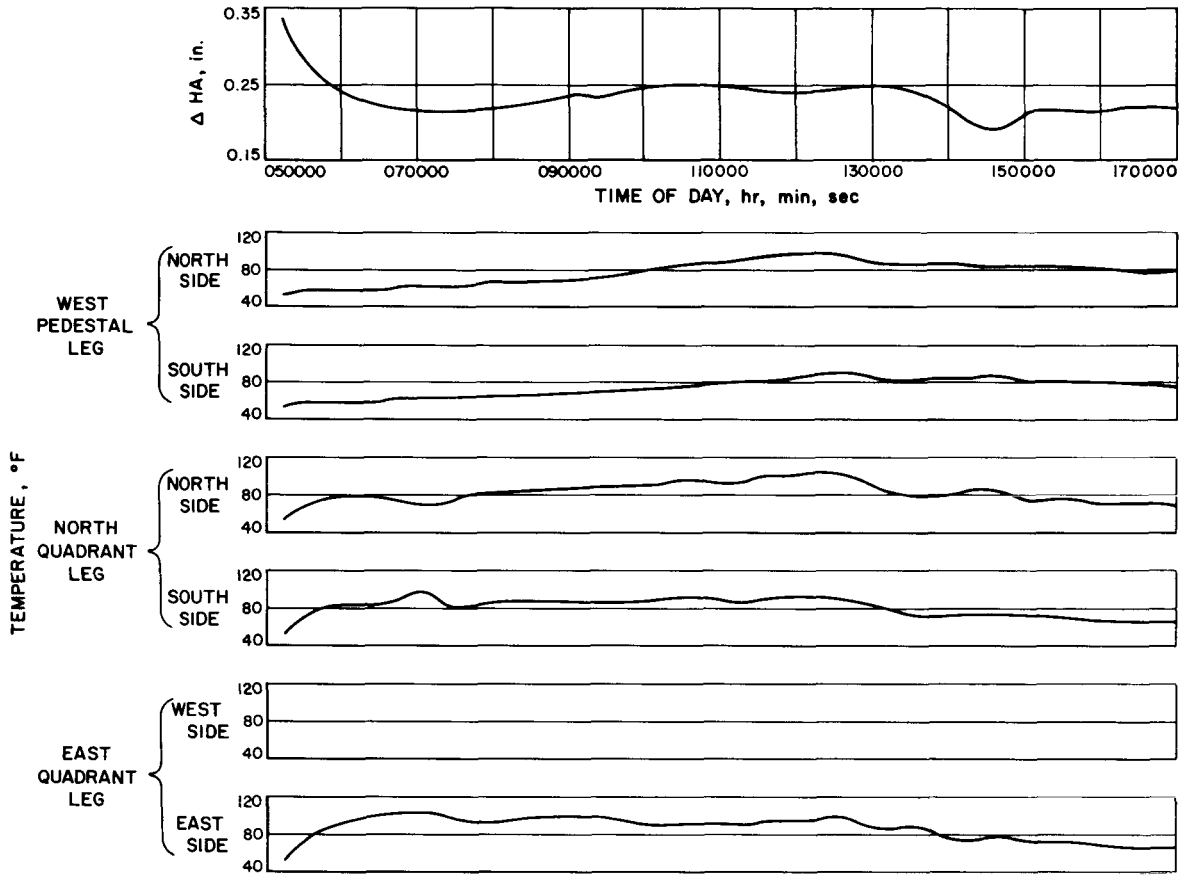

Fig. 60. Collimation-tower ΔHA deflection temperature test No. 2, 29 March 1962

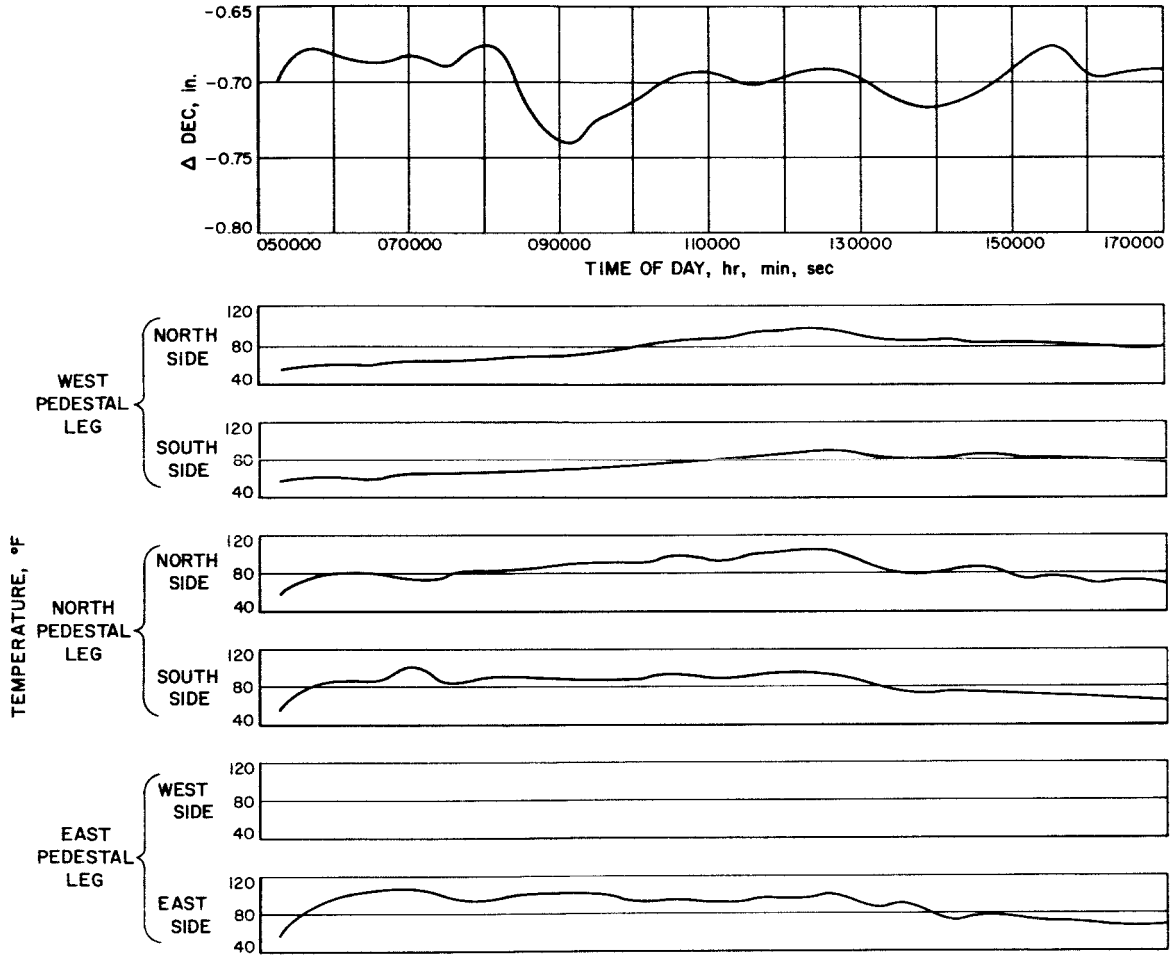

Fig. 61. Collimation-tower ΔDEC deflection temperature test No. 2, 29 March 1962

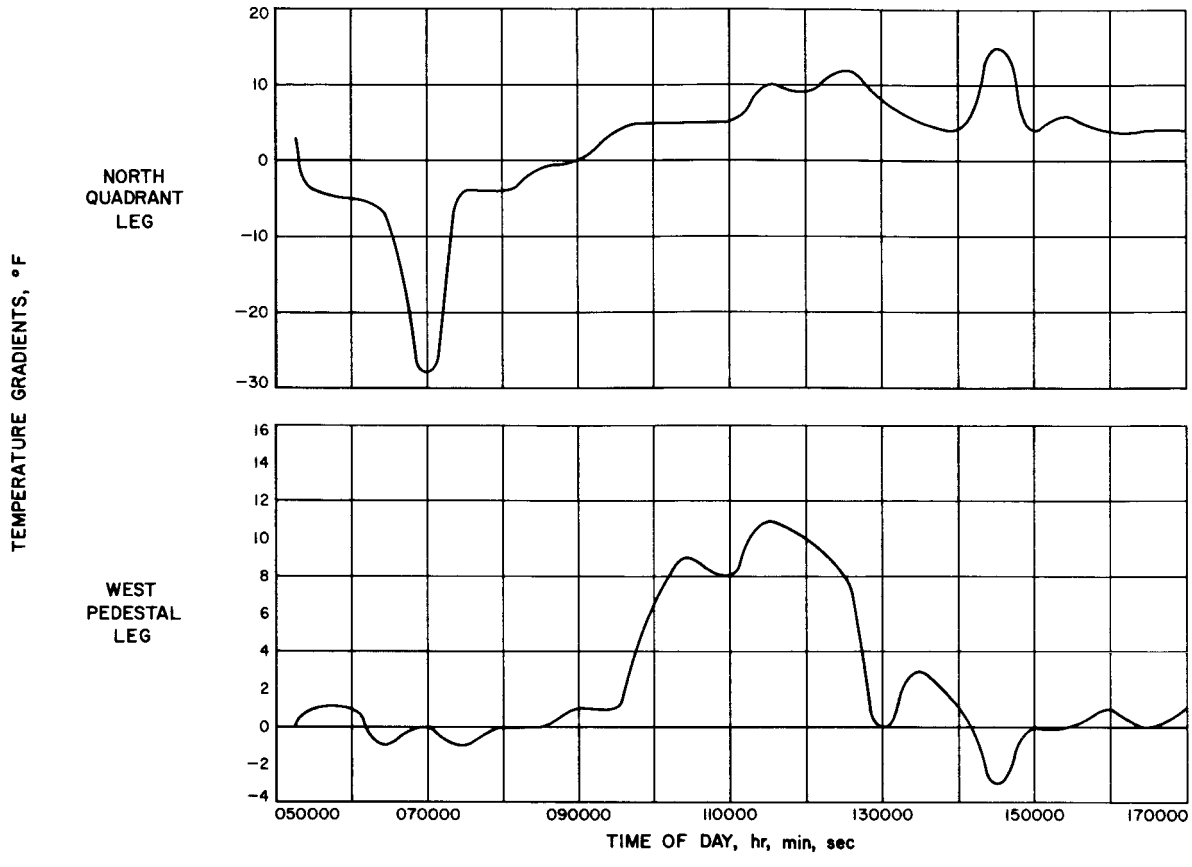

Fig. 62. Collimation-tower temperature gradient measurements, test No. 2, 29 March 1962

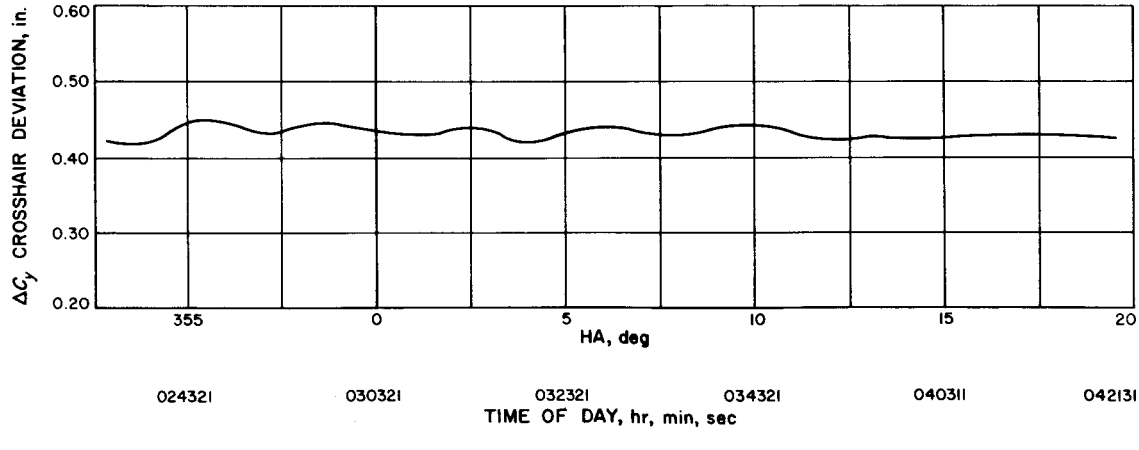

Fig. 63. ΔC_y deviation for simulated RA-3 test No. 1, 15-16 March 1962

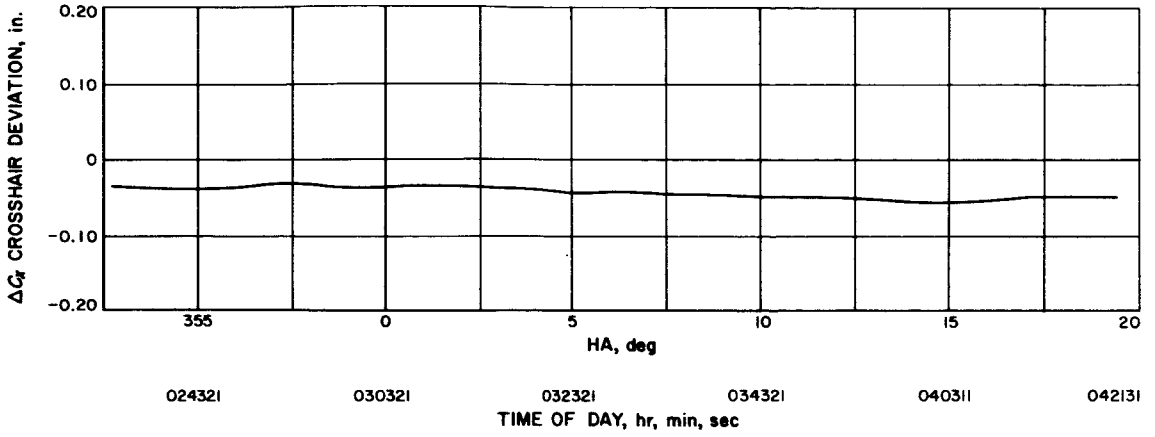

Fig. 64. ΔC_x deviation for simulated RA-3 test No. 1, 15-16 March 1962

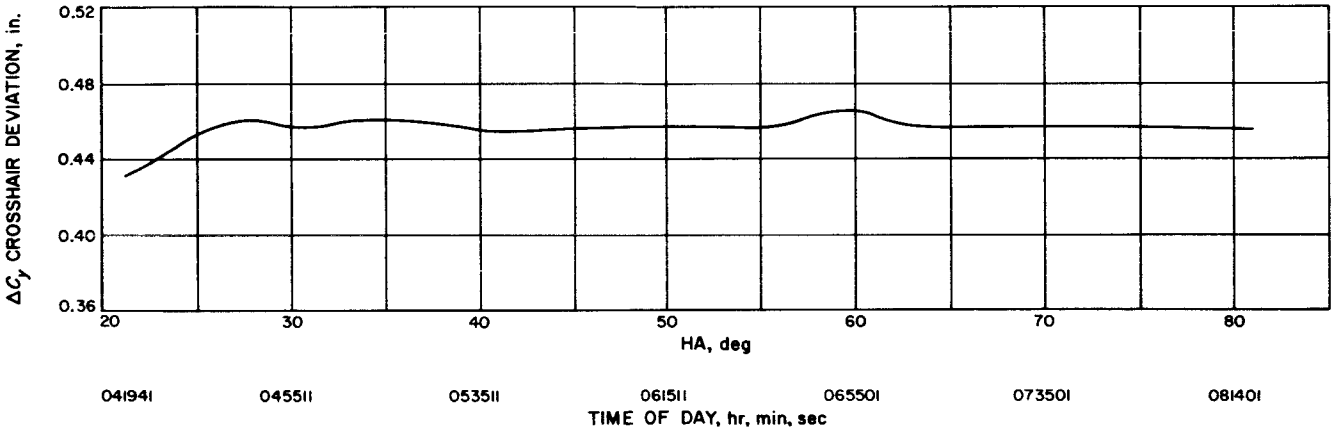

Fig. 65. ΔC_y deviation for simulated RA-3 test No. 3, 17-18 March 1962

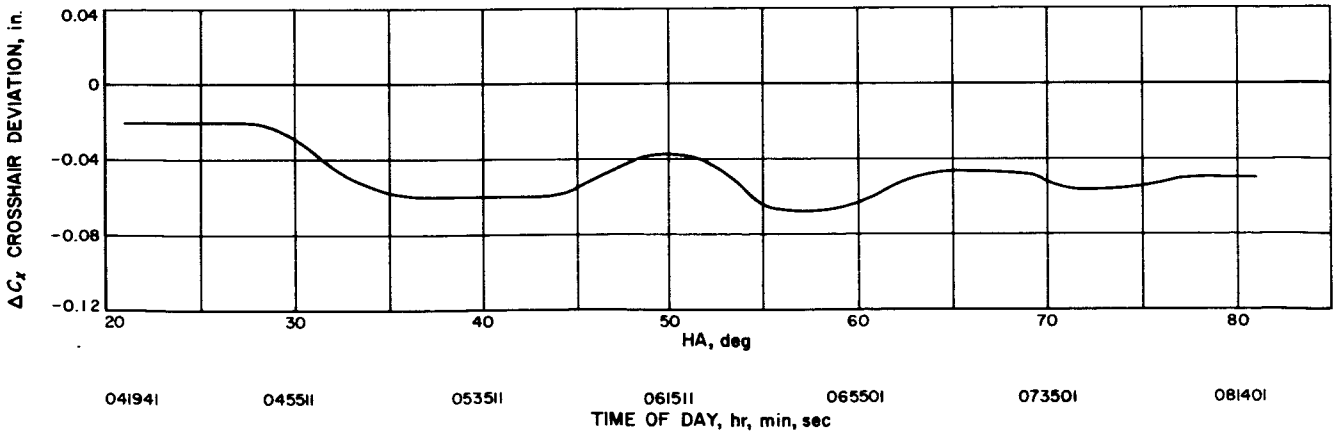

Fig. 66. ΔC_x deviation for simulated RA-3 test No. 3, 17-18 March 1962

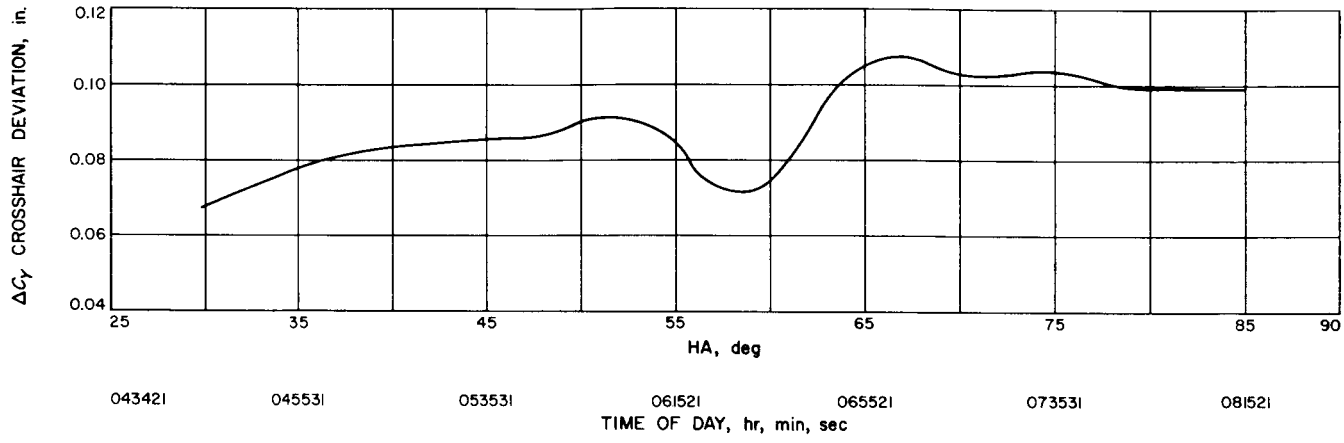

Fig. 67. ΔC_y deviation for simulated RA-3 test No. 4, 22-23 March 1962

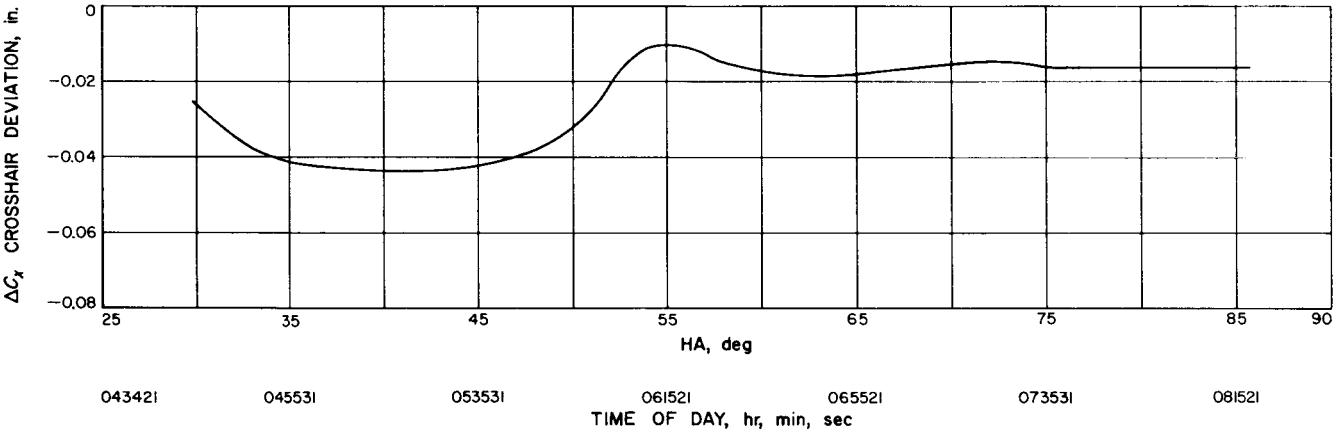

Fig. 68. ΔC_x deviation for simulated RA-3 test No. 4, 22-23 March 1962

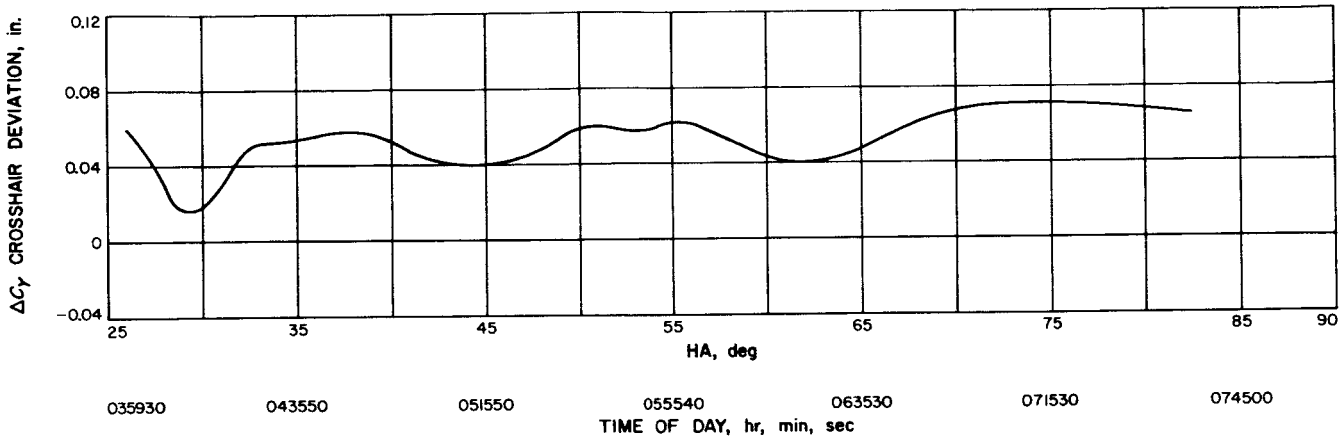

Fig. 69. ΔC_y deviation for simulated RA-3 test No. 6, 27-28 March 1962

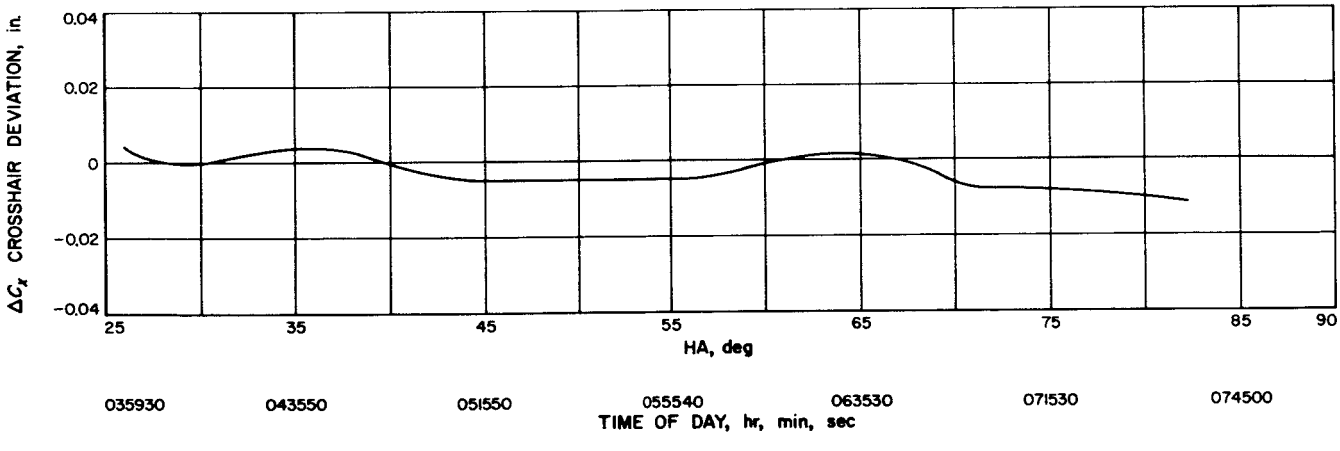

Fig. 70. ΔC_x deviation for simulated RA-3 test No. 6, 27-28 March 1962

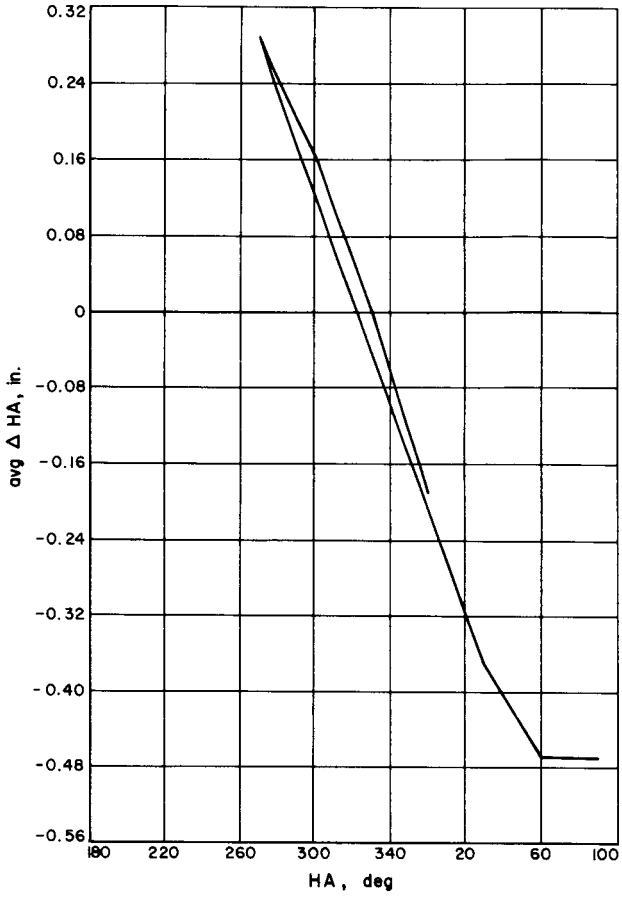

Fig. 71. Chaining deflection test, F. P. to boxgirder corner, film data for DEC = 289.100 deg, 21-22 March 1962

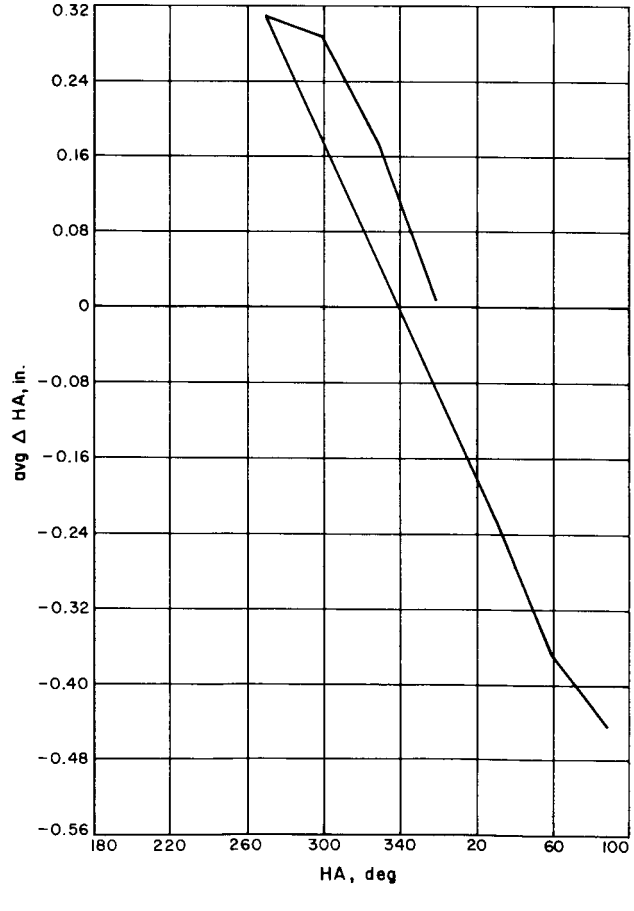

Fig. 72. Chaining deflection test, F. P. to boxgirder corner, film data for DEC = 334.000 deg, 21-22 March 1962

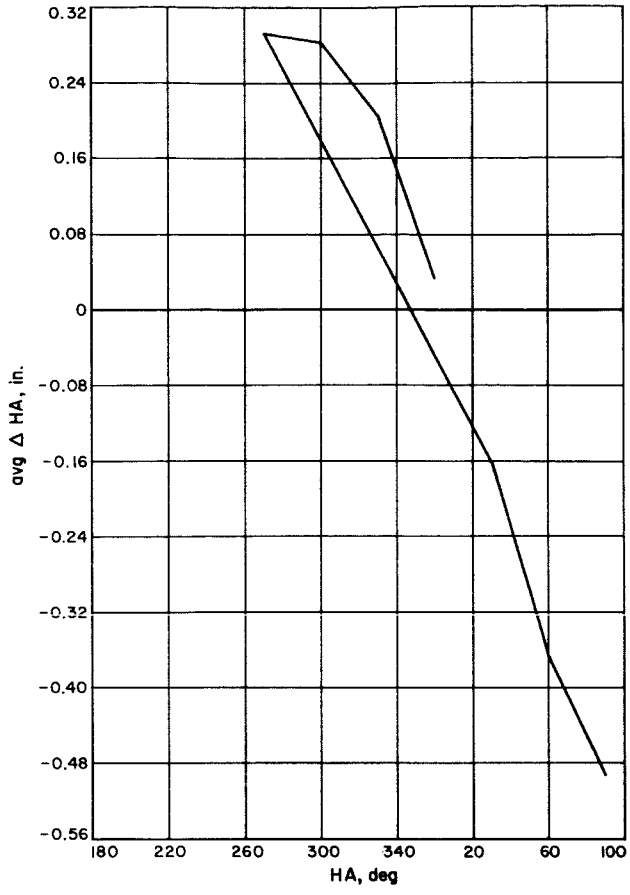

Fig. 73. Chaining deflection test, F. P. to boxgirder corner, film data for DEC = 18.900 deg, 21-22 March 1962

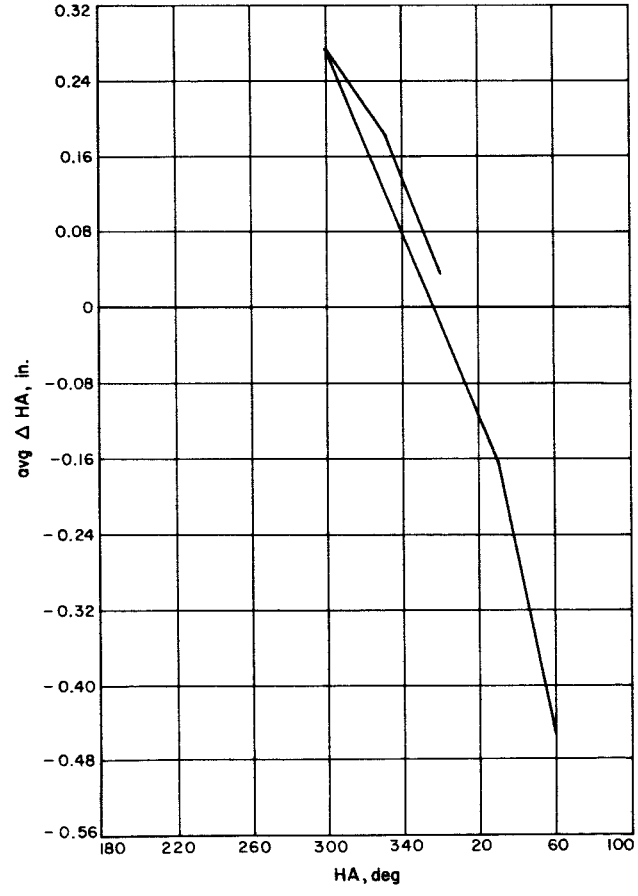

Fig. 74. Chaining deflection test, F. P. to boxgirder corner, film data for DEC = 47.700 deg, 21-22 March 1962

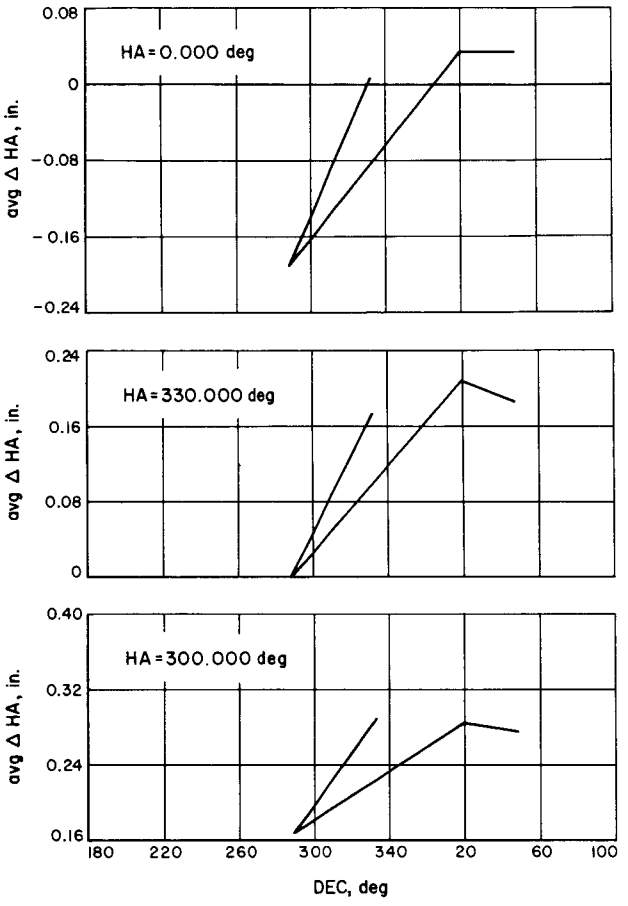

Fig. 75. Chaining deflection test, F. P. to boxgirder corner, film data for HA = 0.000 deg, 330.000 deg, 300.000 deg vs. avg. ΔHA, 21-22 March 1962

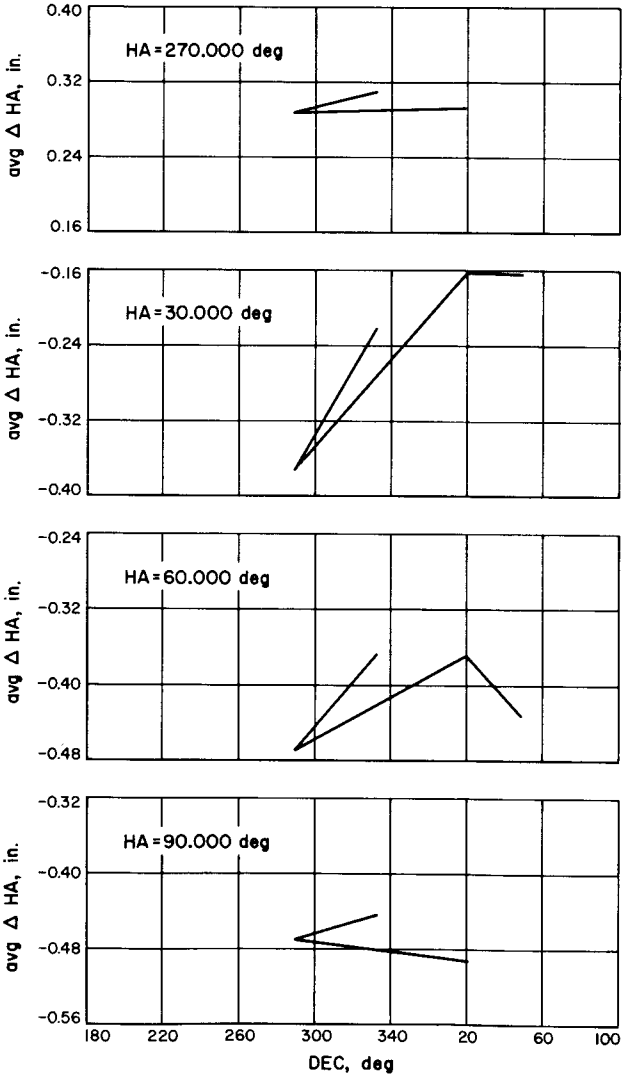

Fig. 76. Chaining deflection test, F. P. to boxgirder corner, film data for HA = 270.000 deg, 30.000 deg, 60.000 deg, and 90.000 deg, 21-22 March 1962

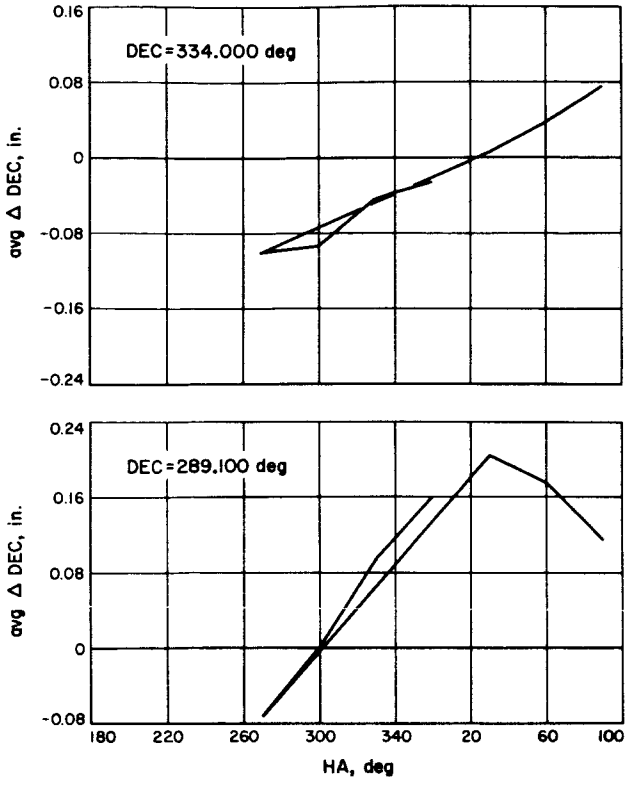

Fig. 77. Chaining deflection test, F. P. to boxgirder corner, film data for DEC = 334.000 deg and 289.100 deg, 21-22 March 1962

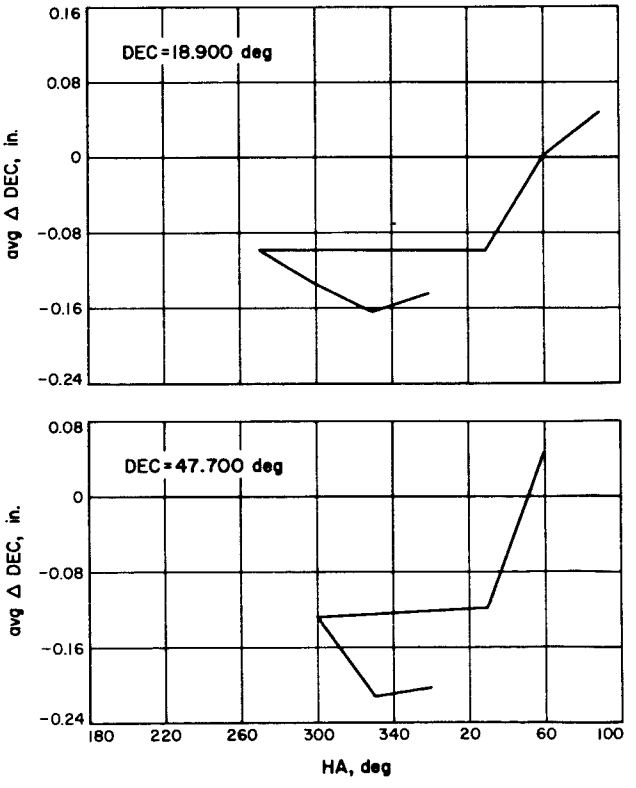

Fig. 78. Chaining deflection test, F. P. to boxgirder corner, film data for DEC = 18.900 deg and 47.700 deg, 21-22 March 1962

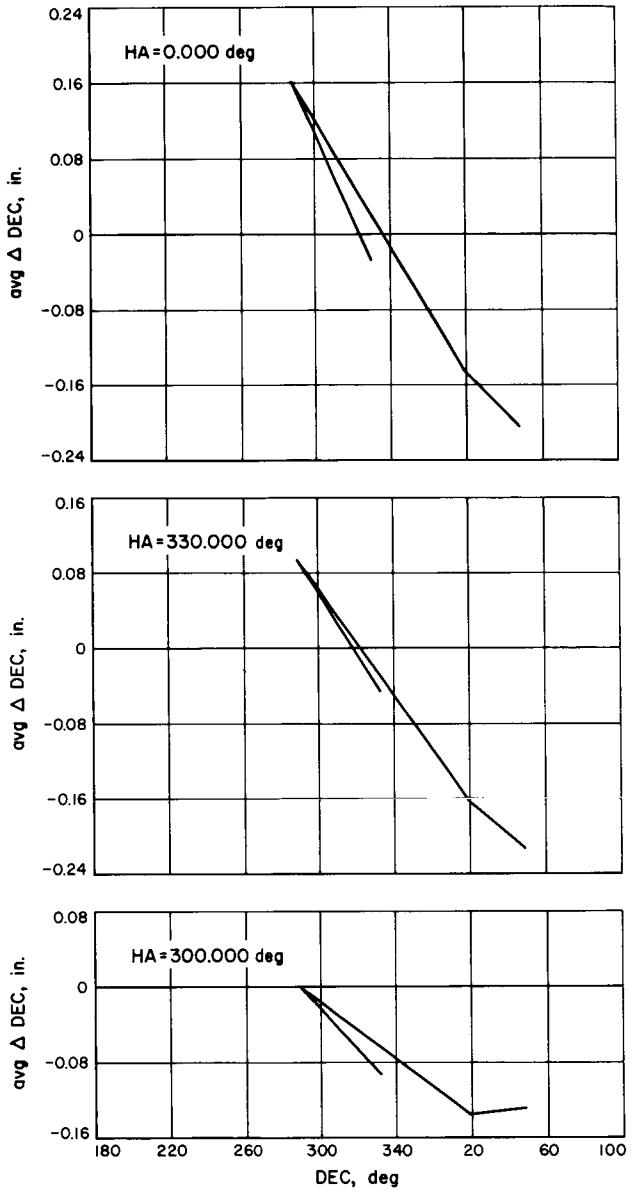

Fig. 79. Chaining deflection test, F. P. to boxgirder corner, film data for HA = 0.000 deg, 330.000 deg, and 300.000 deg vs. avg. ΔDEC, 21-22 March 1962

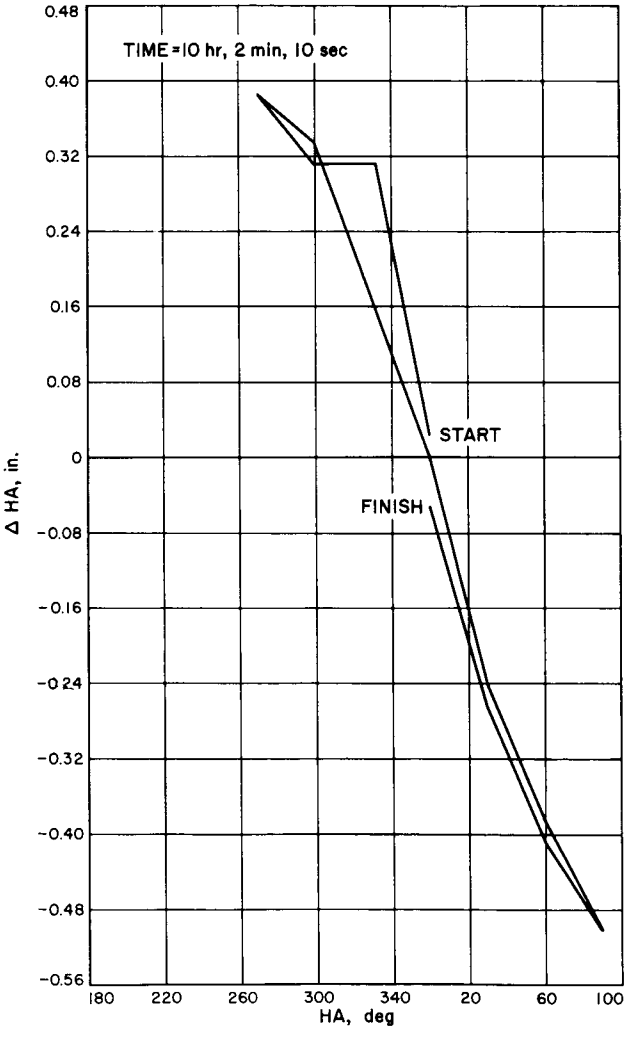

Fig. 80. Chaining deflection test, F. P. to boxgirder corner, tab data for DEC = 289.01 deg vs. ΔHA, 21-22 March 1962

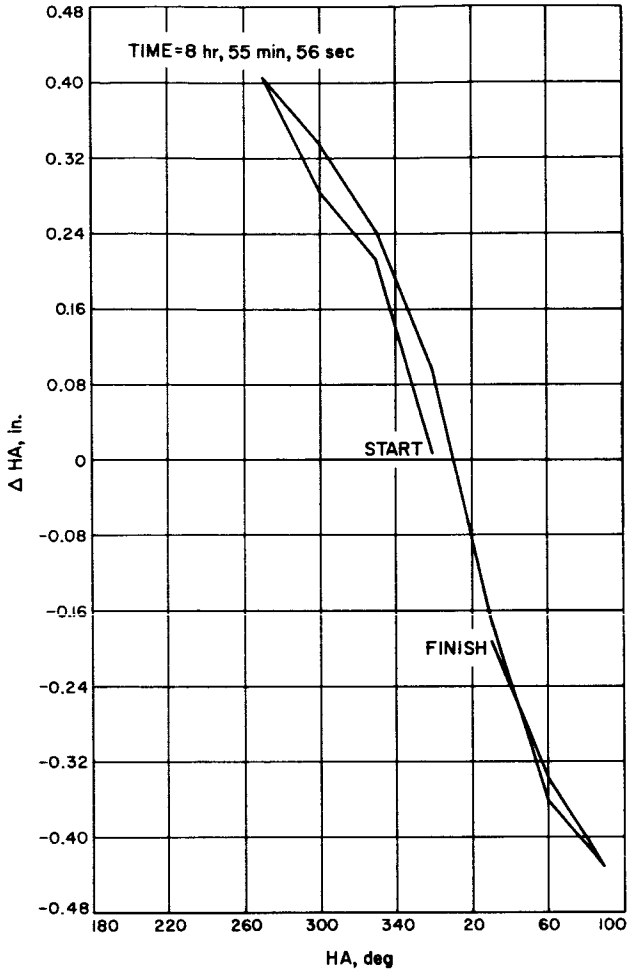

Fig. 81. Chaining deflection test, F. P. to boxgirder corner, tab data for DEC = 333.99 deg vs. ΔHA, 21-22 March 1962

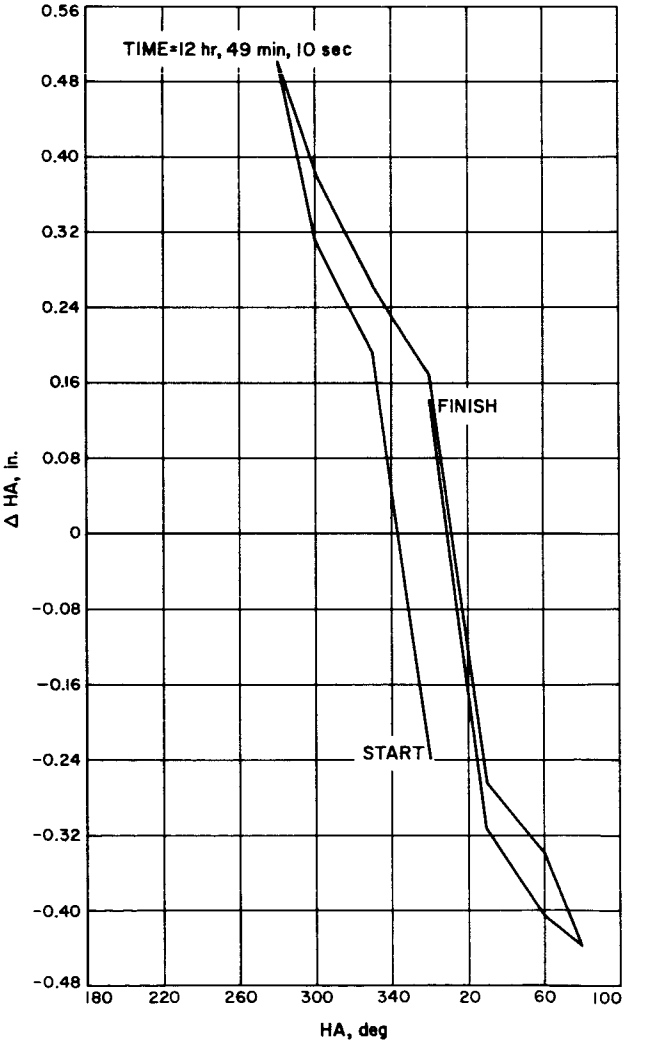

Fig. 82. Chaining deflection test, F. P. to boxgirder corner, tab data for DEC = 19.03 deg vs. ΔHA, 21-22 March 1962

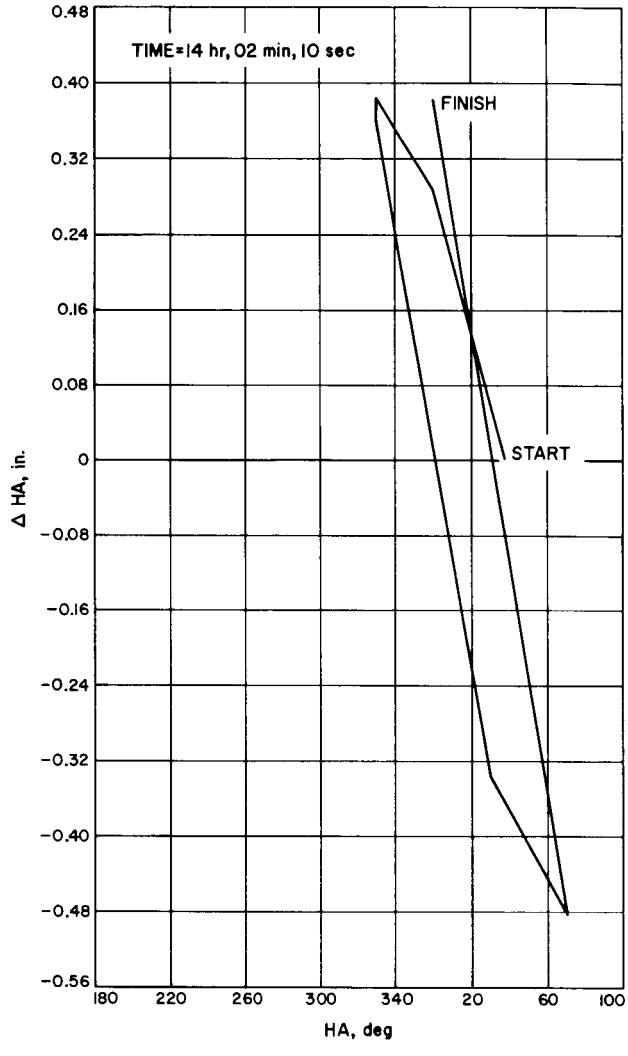

Fig. 83. Chaining deflection test, F. P. to boxgirder corner, tab data for DEC = 47.87 deg vs. ΔHA, 21-22 March 1962

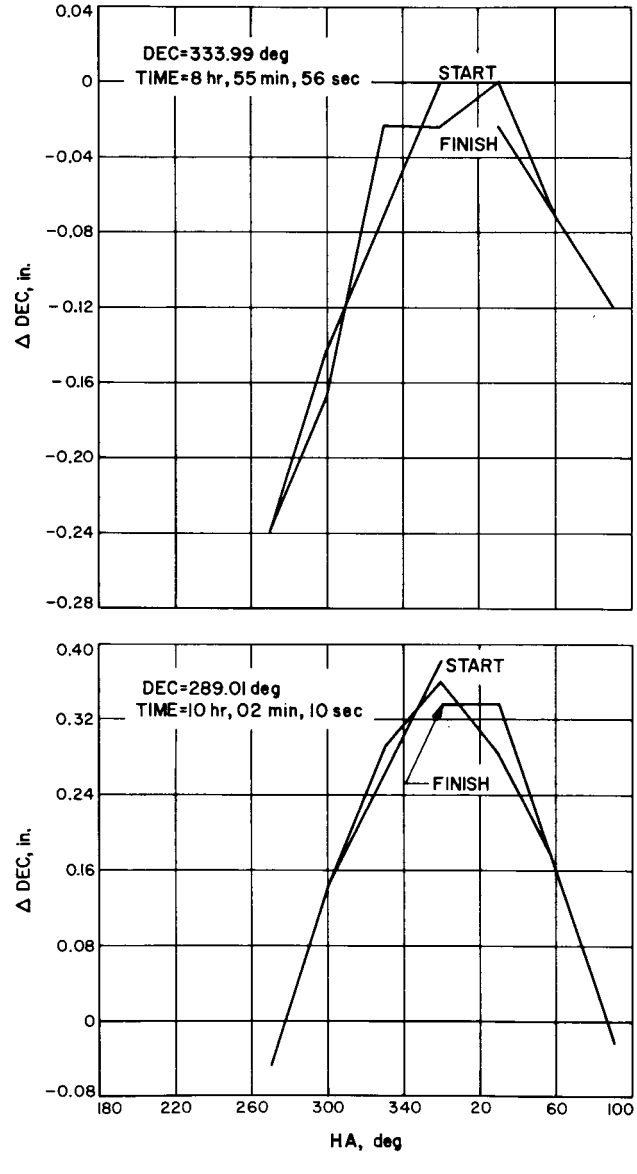

Fig. 84. Chaining deflection test, F. P. to boxgirder corner, tab data for DEC = 333.99 deg and 289.01 deg vs. ΔDEC, 21-22 March 1962

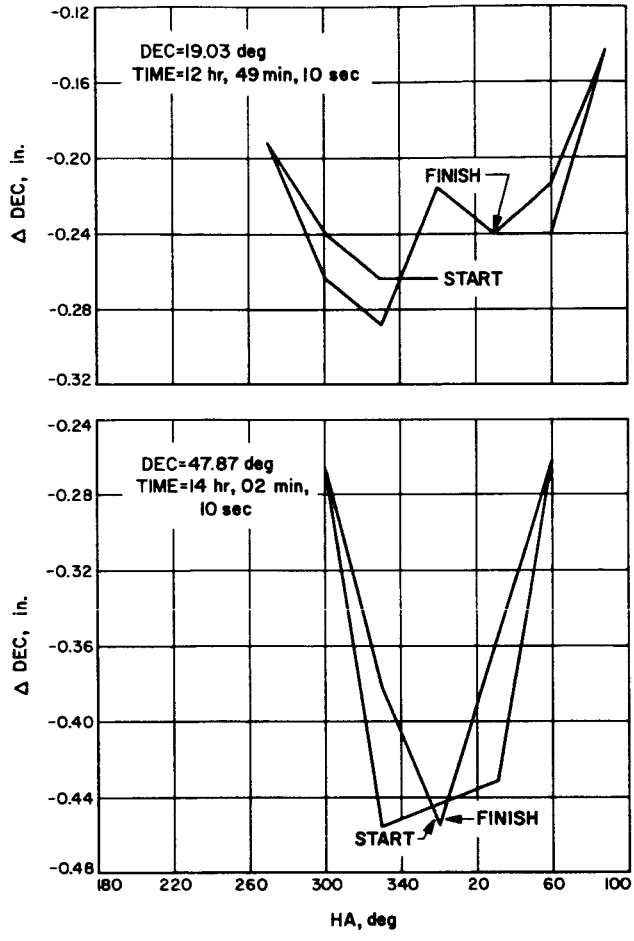

Fig. 85. Chaining deflection test, F. P. to boxgirder corner, tab data for DEC = 19.03 deg and 47.87 deg vs. ΔDEC, 21-22 March 1962

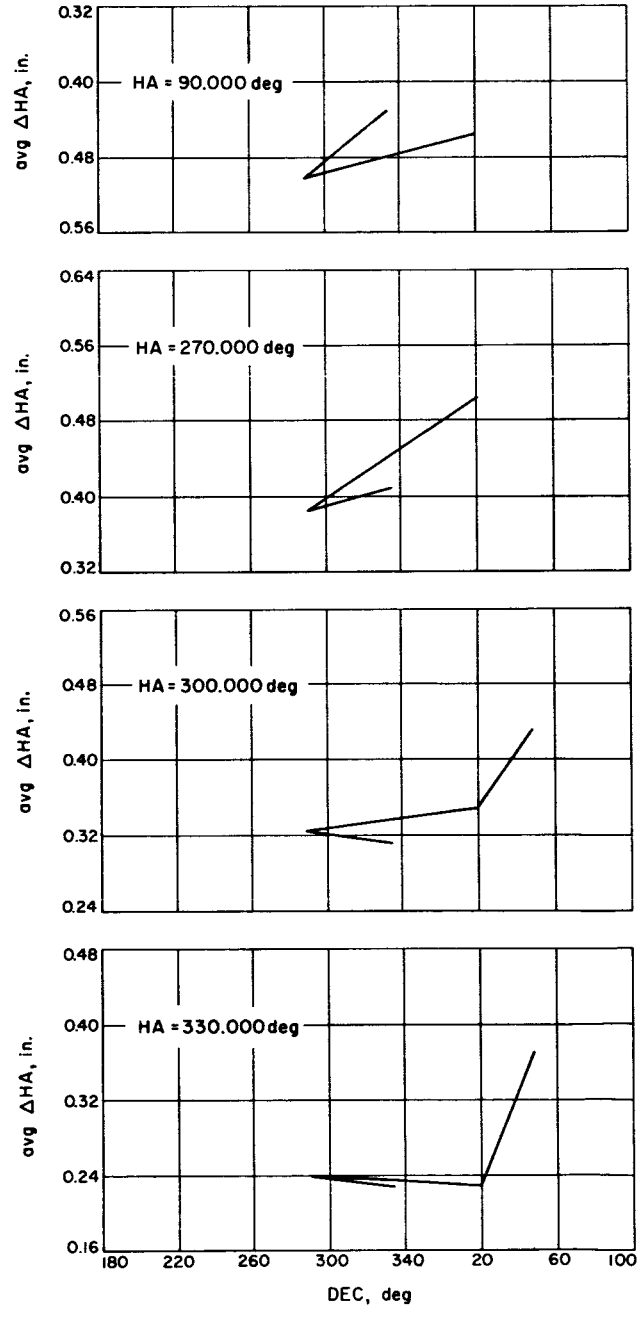

Fig. 86. Chaining deflection test, F. P. to boxgirder corner, tab data for HA = 90.000 deg, 270.000 deg, 300.000 deg, and 330.000 deg vs. avg. ΔHA, 21-22 March 1962

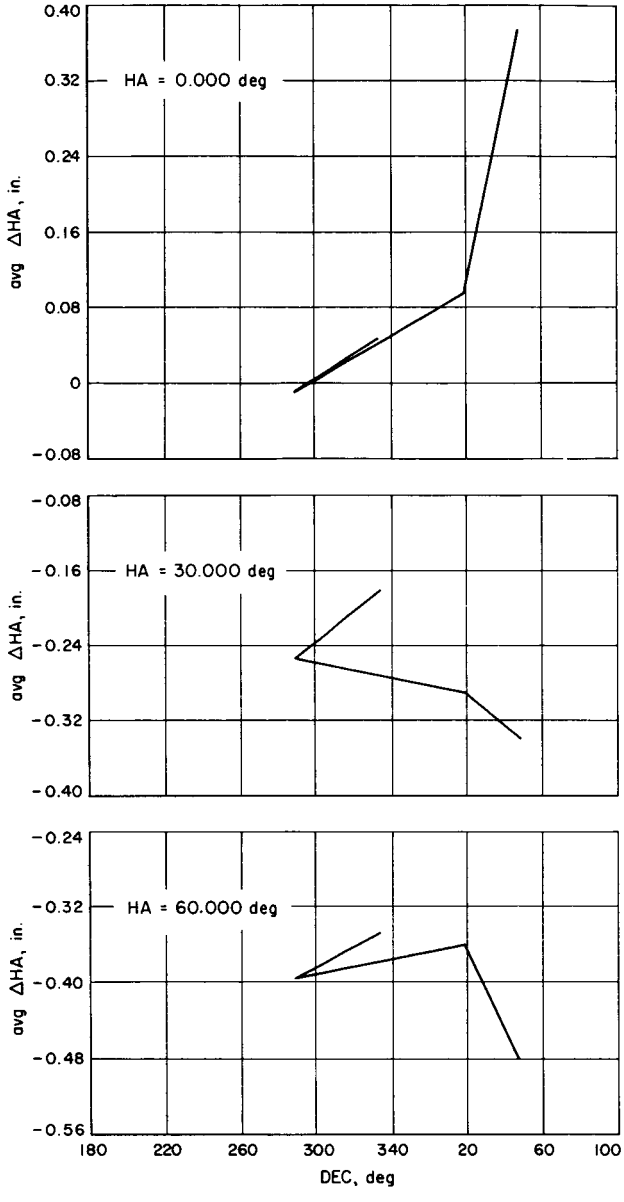

Fig. 87. Chaining deflection test, F. P. to boxgirder corner, tab data for HA = 0.000 deg, 30.000 deg, and 60.000 deg vs. avg. ΔHA, 21-22 March 1962

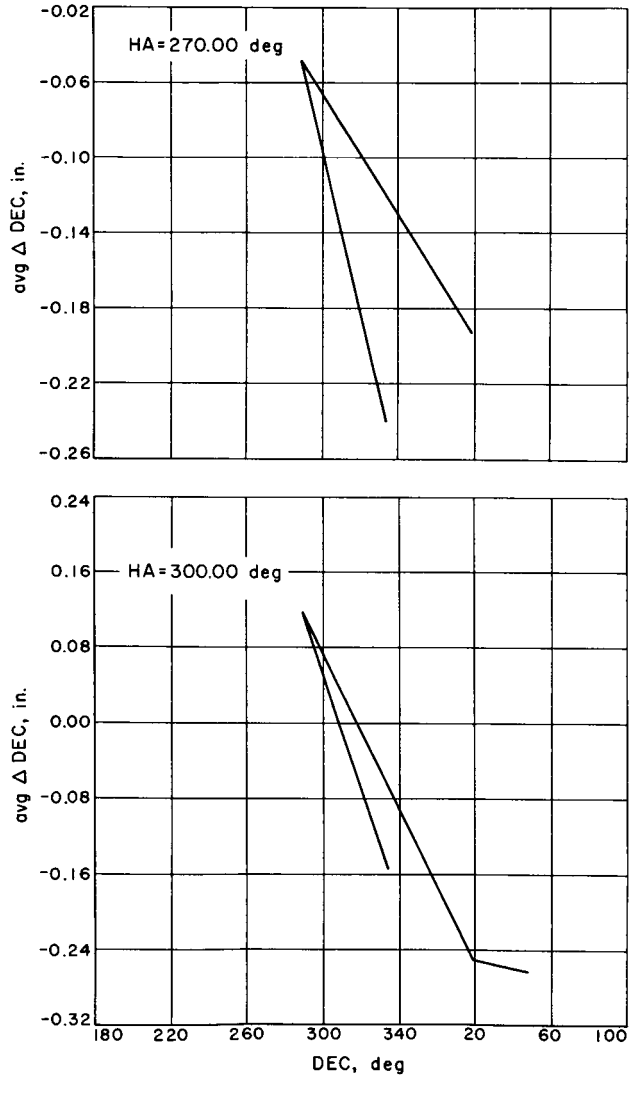

Fig. 88. Chaining deflection test, F. P. to boxgirder corner, tab data for HA = 270.00 deg and 300.00 deg vs. avg. ΔDEC, 21-22 March 1962

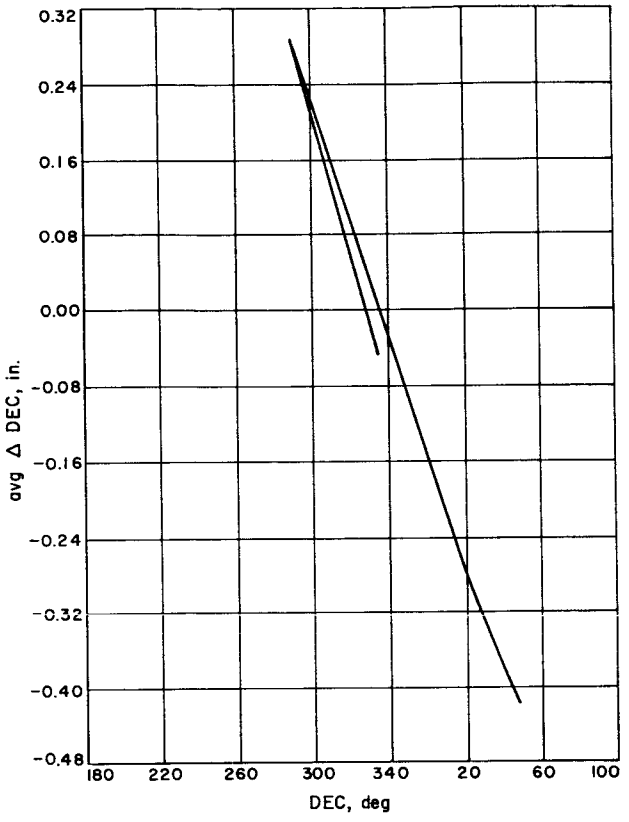

Fig. 89. Chaining deflection test, F. P. to boxgirder corner, tab data for HA = 330.00 deg vs. avg. ΔDEC, 21-22 March 1962

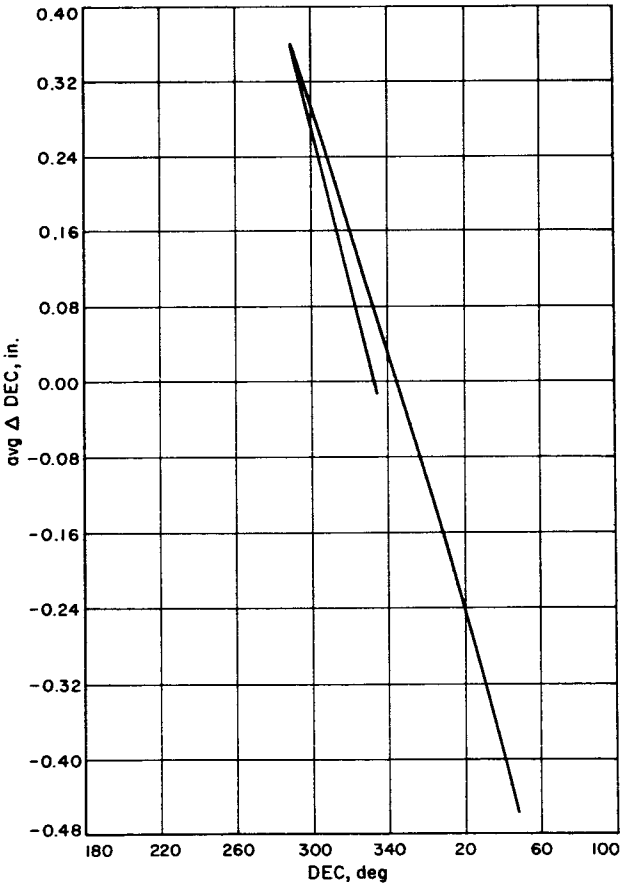

Fig. 90. Chaining deflection test, F. P. to boxgirder corner, tab data for HA = 0.00 deg vs. avg. ΔDEC, 21-22 March 1962

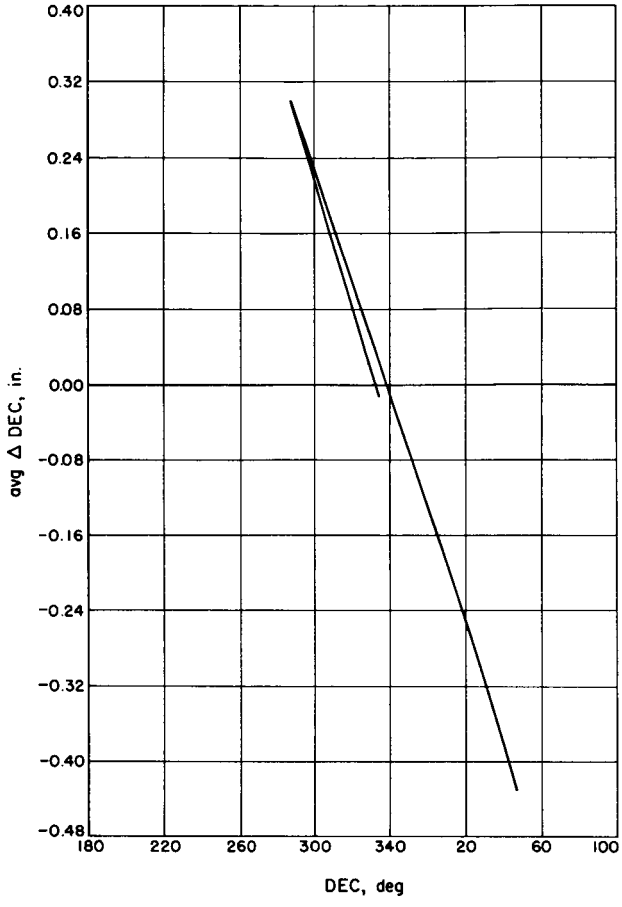

Fig. 91. Chaining deflection test, F. P. to boxgirder corner, tab data for HA = 30.00 deg vs. avg. ΔDEC, 21-22 March 1962

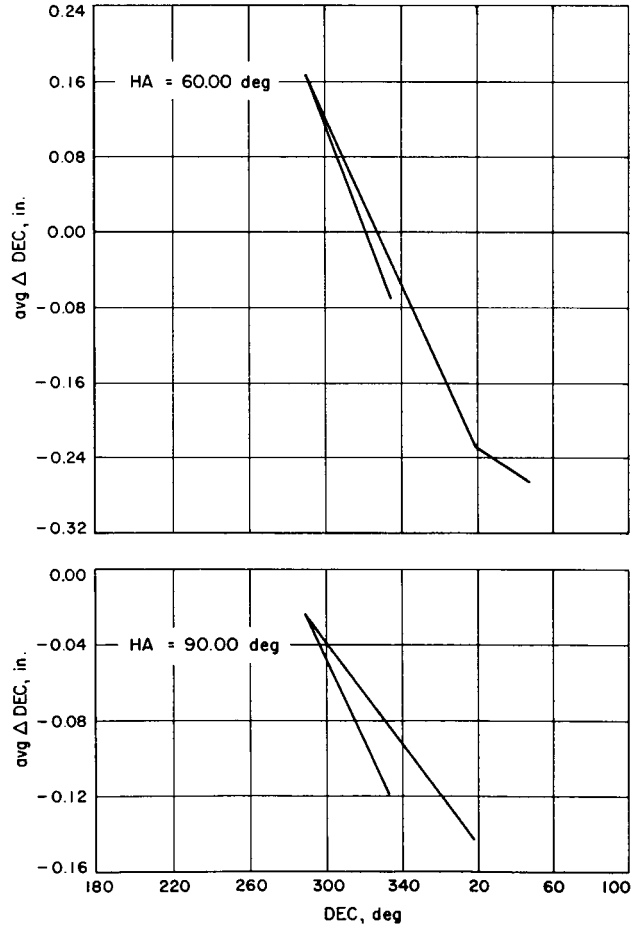

Fig. 92. Chaining deflection test, F. P. to boxgirder corner, tab data for HA = 60.00 and 90.00 deg vs. avg. ΔDEC, 21-22 March 1962

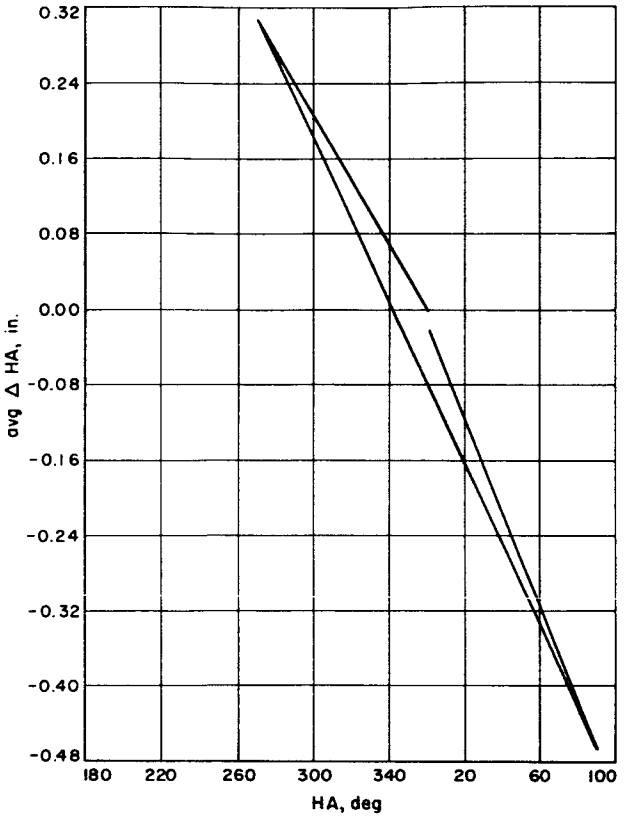

Fig. 93. Chaining deflection test, F. P. to dish edges, film data for DEC = 334.070 deg vs. avg. ΔHA, 23 March 1962

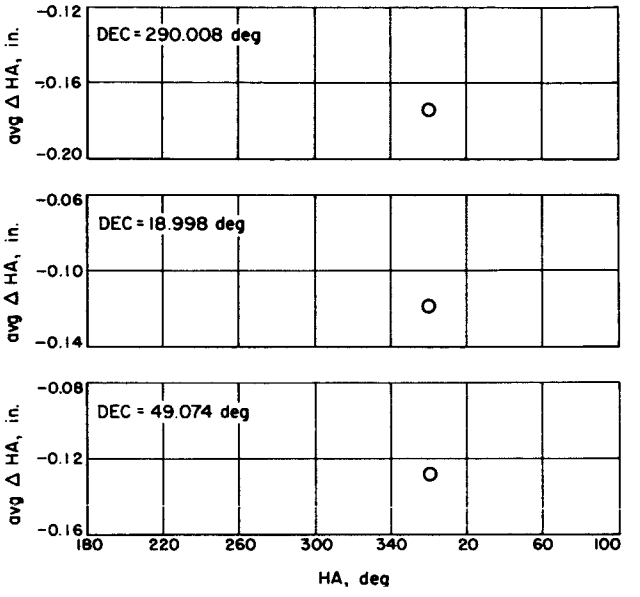

Fig. 94. Chaining deflection test, F. P. to dish edges, film data for DEC = 290.008 deg, 18.998 deg, and 49.074 deg vs. avg. ΔHA, 23 March 1962

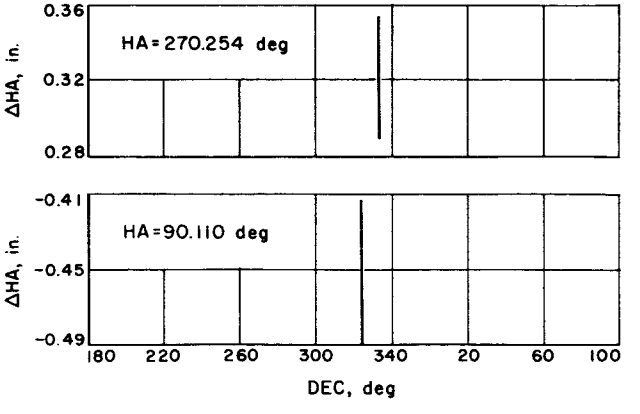

Fig. 95. Chaining deflection test, F. P. to dish edges, film data for HA = 270.254 deg and 90.110 deg vs. ΔHA, 23 March 1962

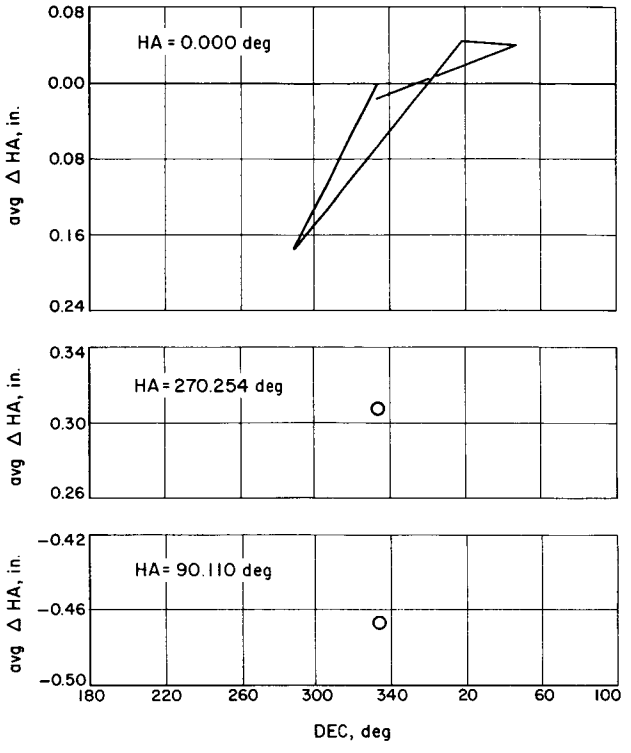

Fig. 96. Chaining deflection test, F. P. to dish edges, film data for HA = 0.000 deg, 270.254 deg, and 90.110 deg vs. avg. ΔHA, 23 March 1962

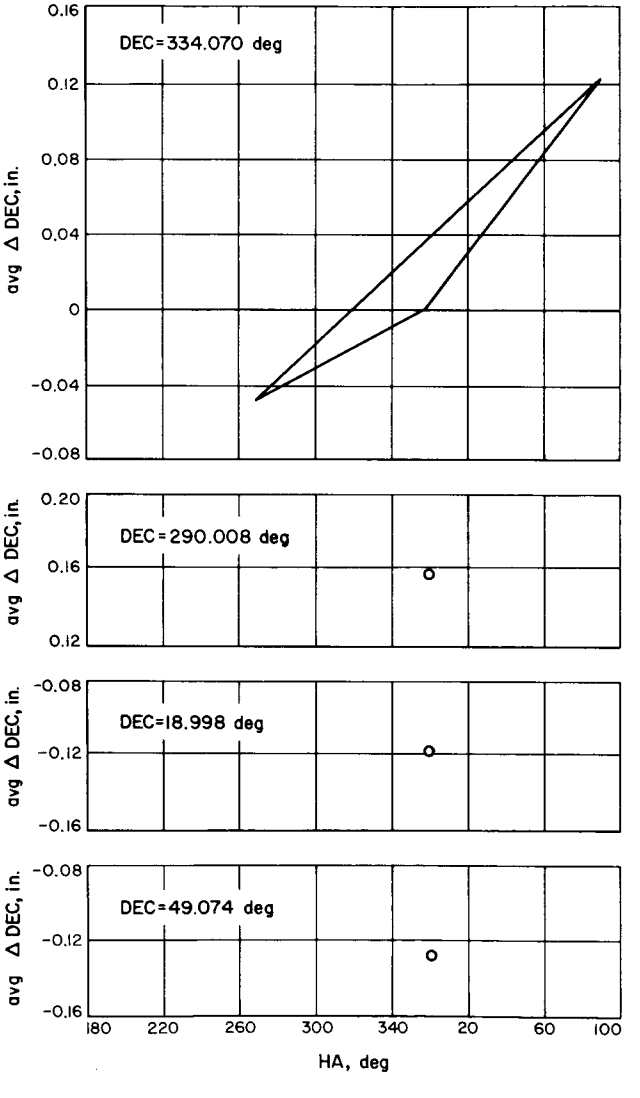

Fig. 97. Chaining deflection test, F. P. to dish edges, film data for DEC = 334.070 deg, 290.008 deg, 18.998 deg, and 49.074 deg vs. avg. ΔDEC, 23 March 1962

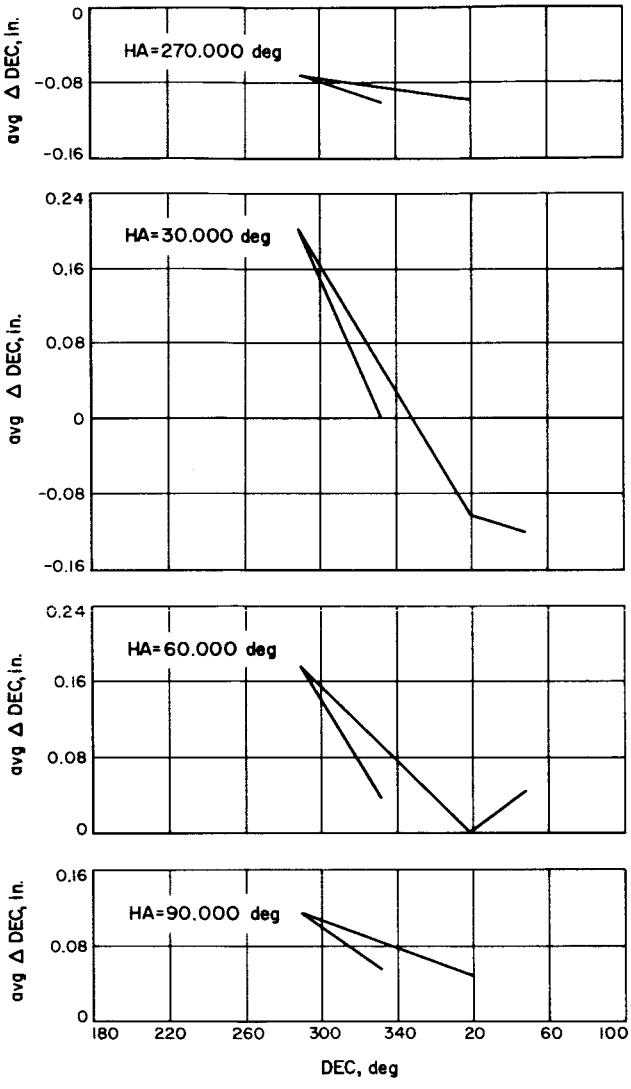

Fig. 98. Chaining deflection test, F. P. to boxgirder corner, film data for HA = 270.000 deg, 30.000 deg, 60.000 deg, and 90.000 deg, 21-22 March 1962

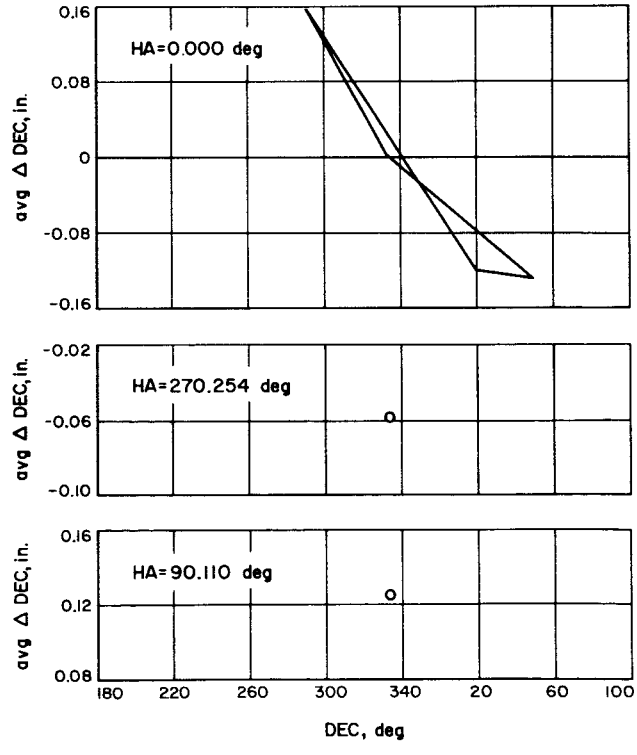

Fig. 99. Chaining deflection test, F. P. to dish edges, film data for HA = 0.000 deg, 270.254 deg, and 90.110 deg, 23 March 1962

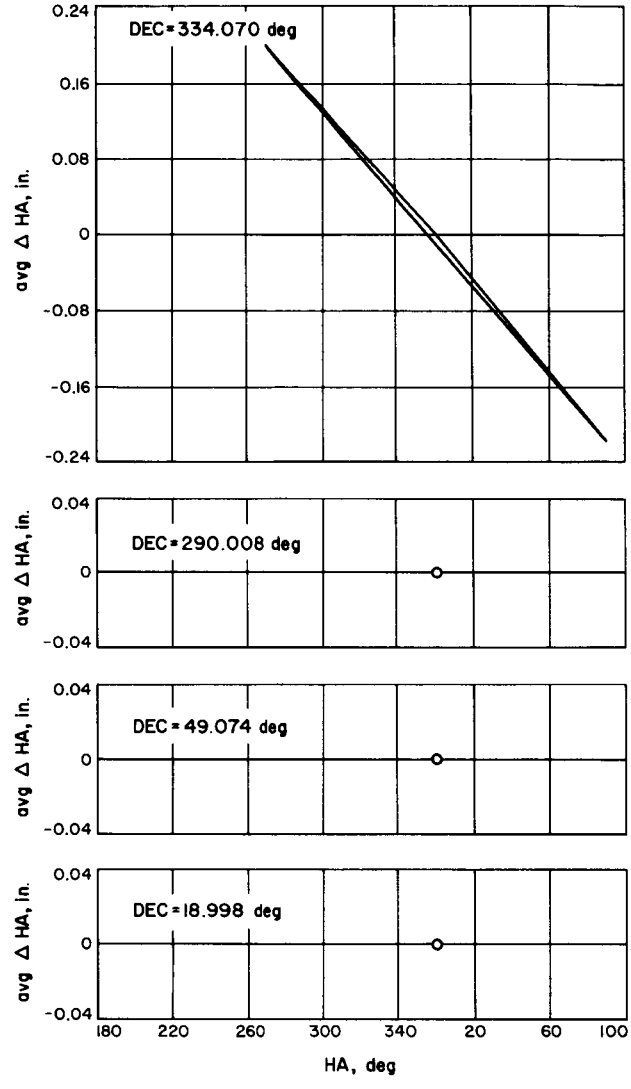

Fig. 100. Chaining deflection test, F. P. to dish edges, tab data for DEC = 334.070 deg, 290.008 deg, 49.074 deg, and 18.998 deg vs. avg. ΔHA, 23 March 1962

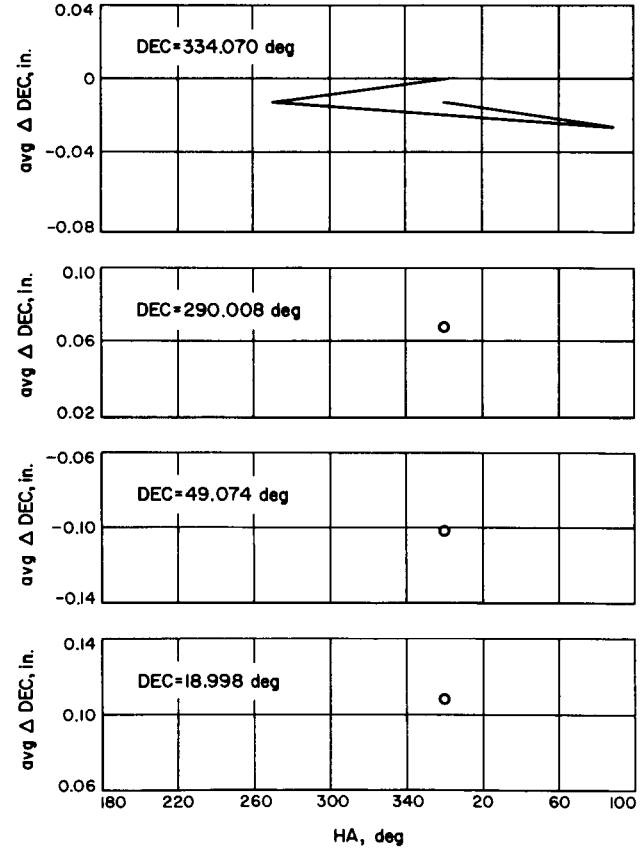

Fig. 101. Chaining deflection test, F. P. to dish edges, tab data for DEC = 334.070 deg, 290.008 deg, 49.074 deg, and 18.998 deg vs. avg. ΔDEC, 23 March 1962

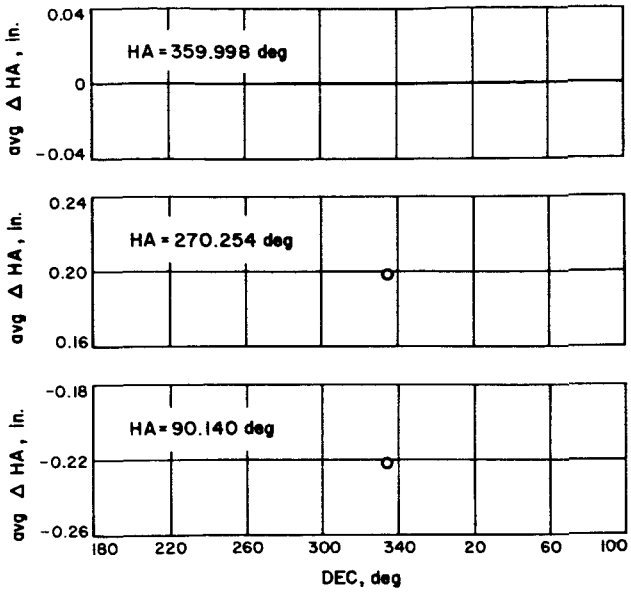

Fig. 102. Chaining deflection test, F. P. to dish edges, tab data for HA = 359.998 deg, 270.254 deg, and 90.140 deg vs. avg. ΔHA, 23 March 1962

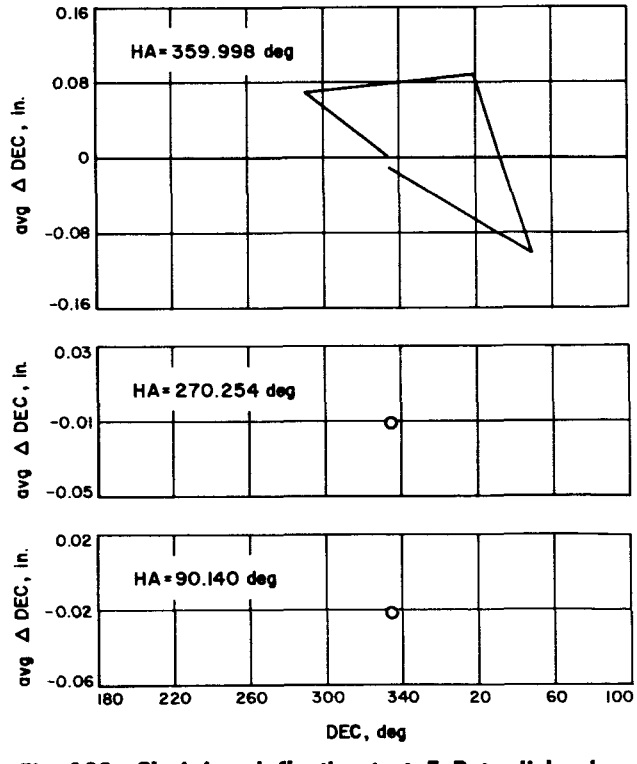

Fig. 103. Chaining deflection test, F. P. to dish edges, tab data for HA = 359.998 deg, 270.254 deg, and 90.140 deg vs. avg. ΔDEC, 23 March 1962

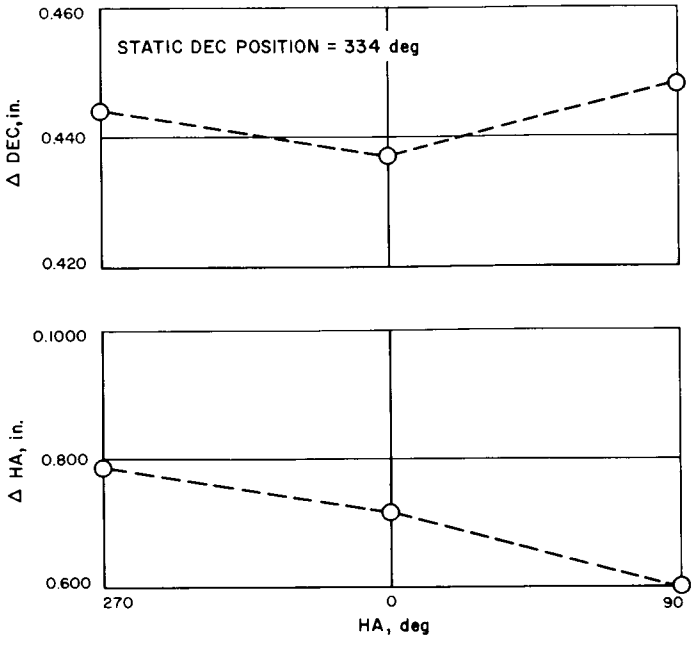

Fig. 104. Feed F. P. movement relative to local quadripod structure, for constant DEC

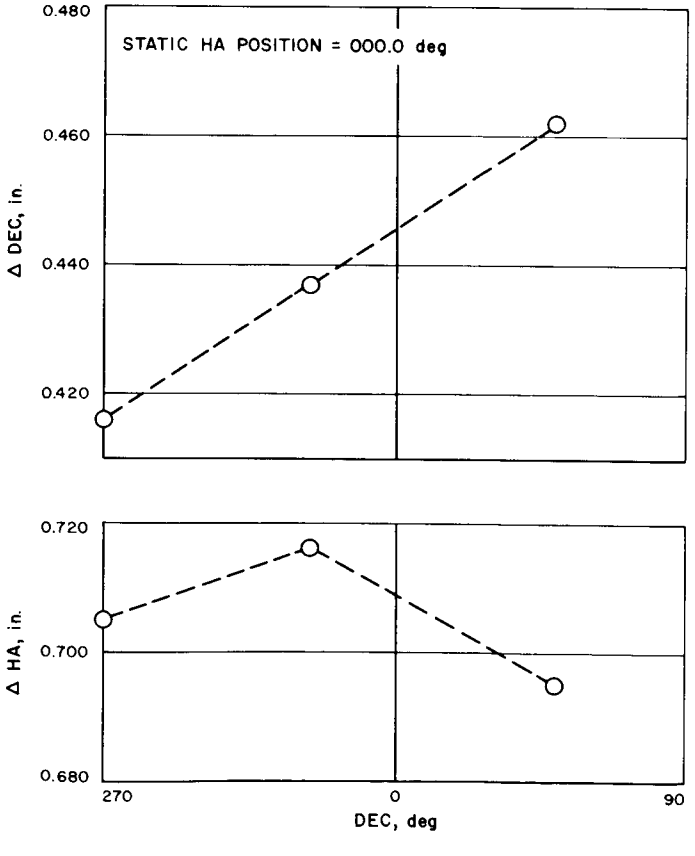

Fig. 105. Feed F. P. movement relative to local quadripod structure, for constant HA

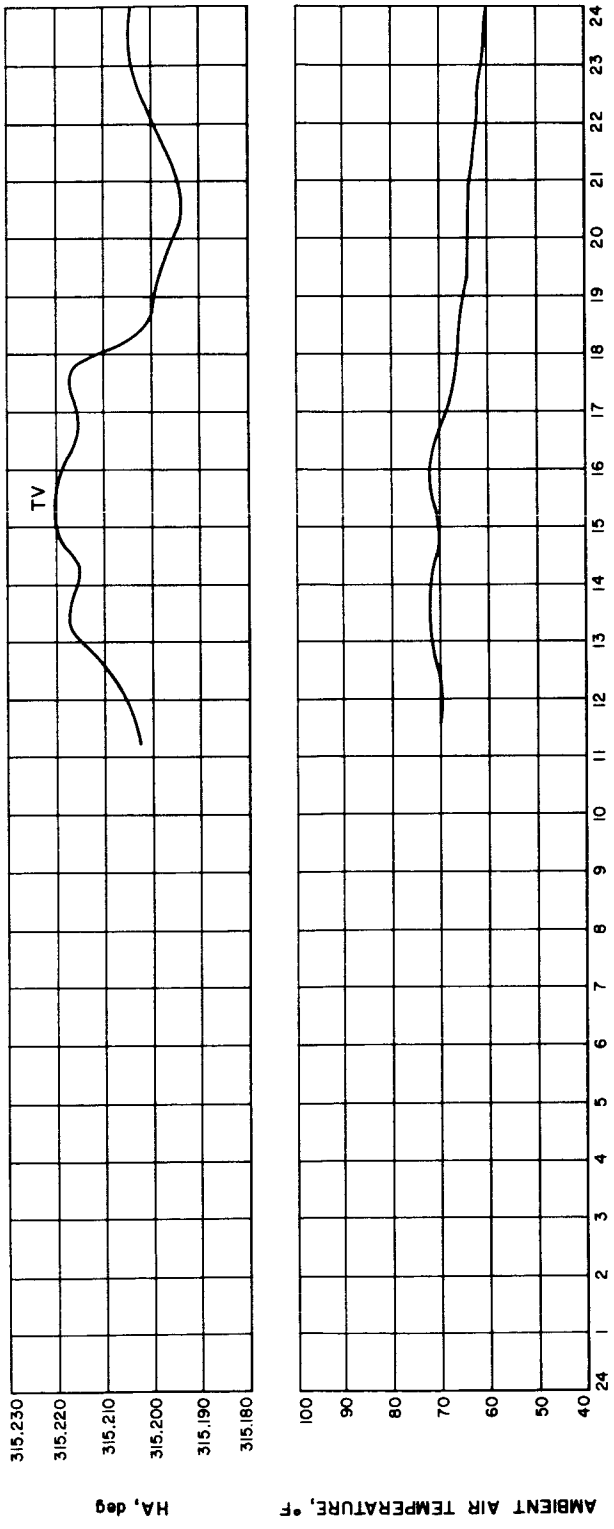

Fig. 106. RF–TV boresight vs. temperature, HA, 27 November 1961

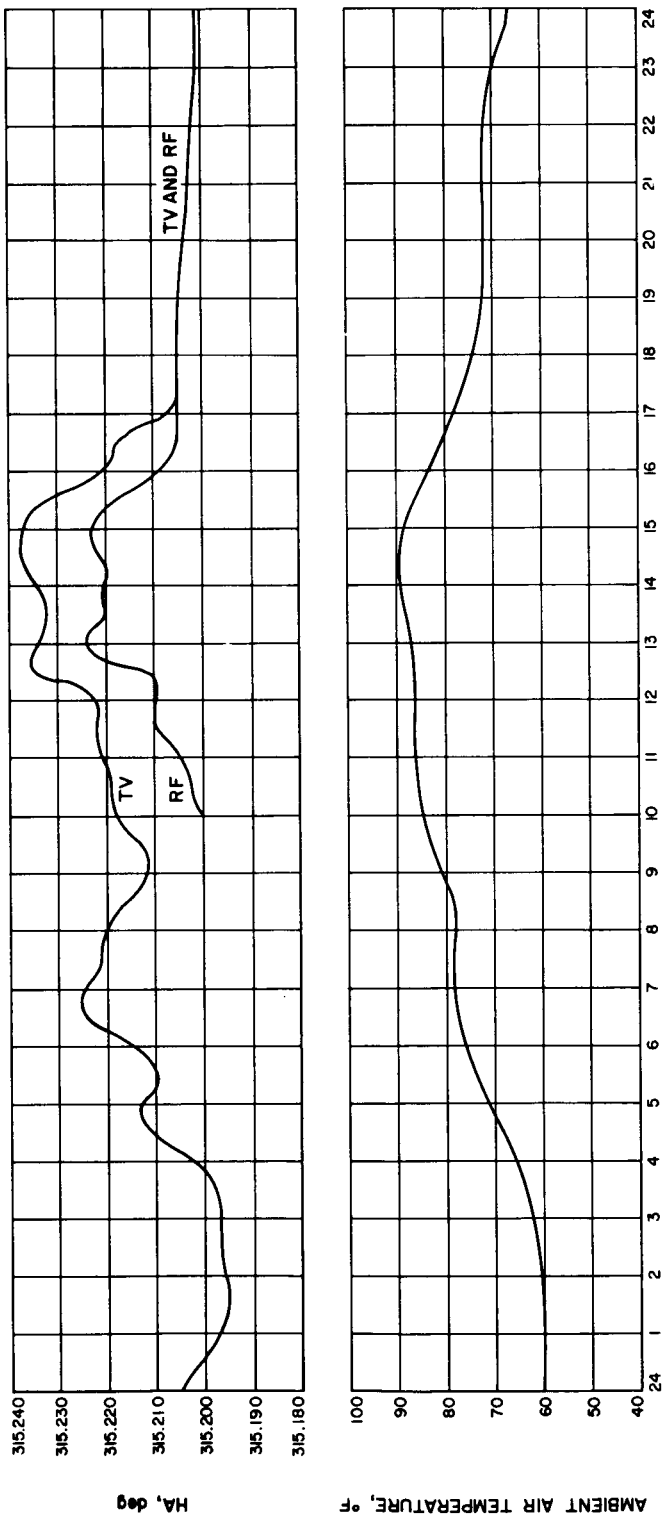

Fig. 107. RF–TV boresight vs. temperature, HA, 28 November 1961

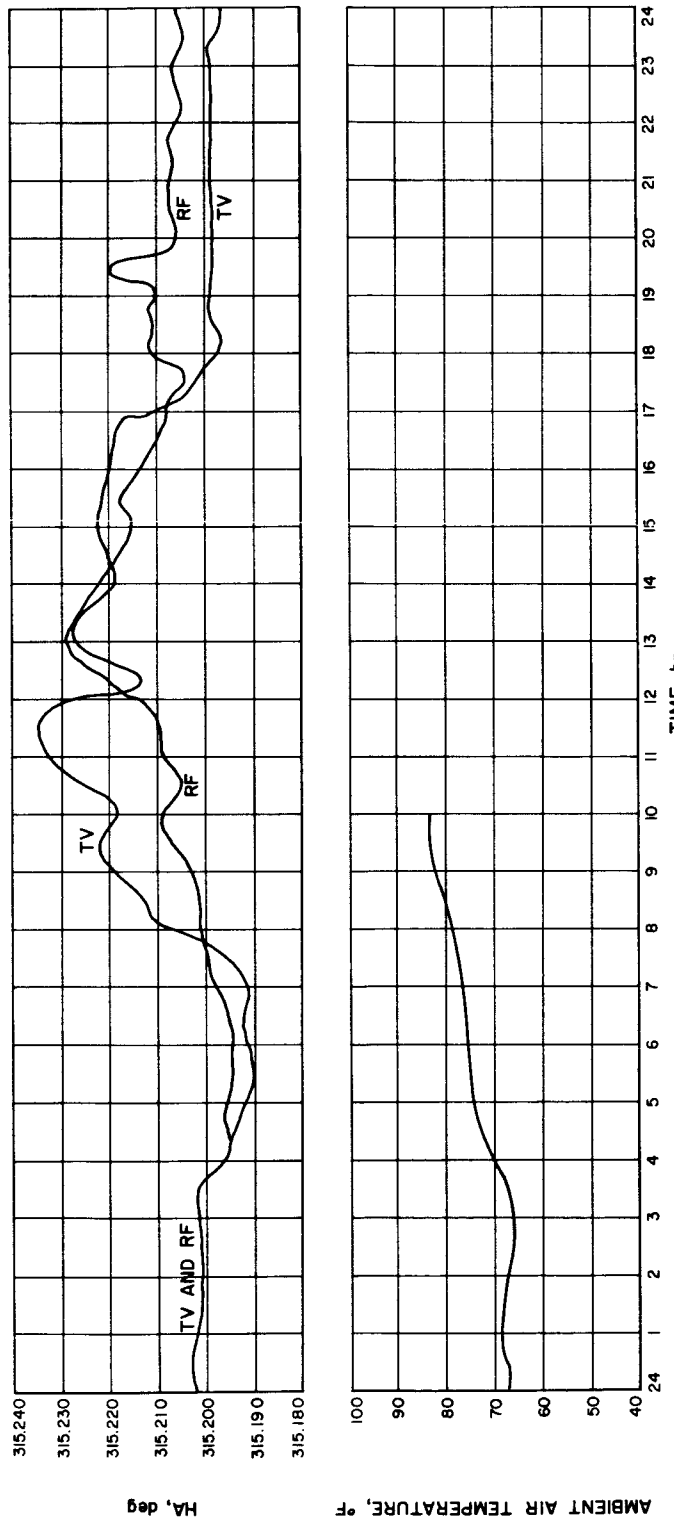

Fig. 108. RF–TV boresight vs. temperature, HA, 29 November 1961

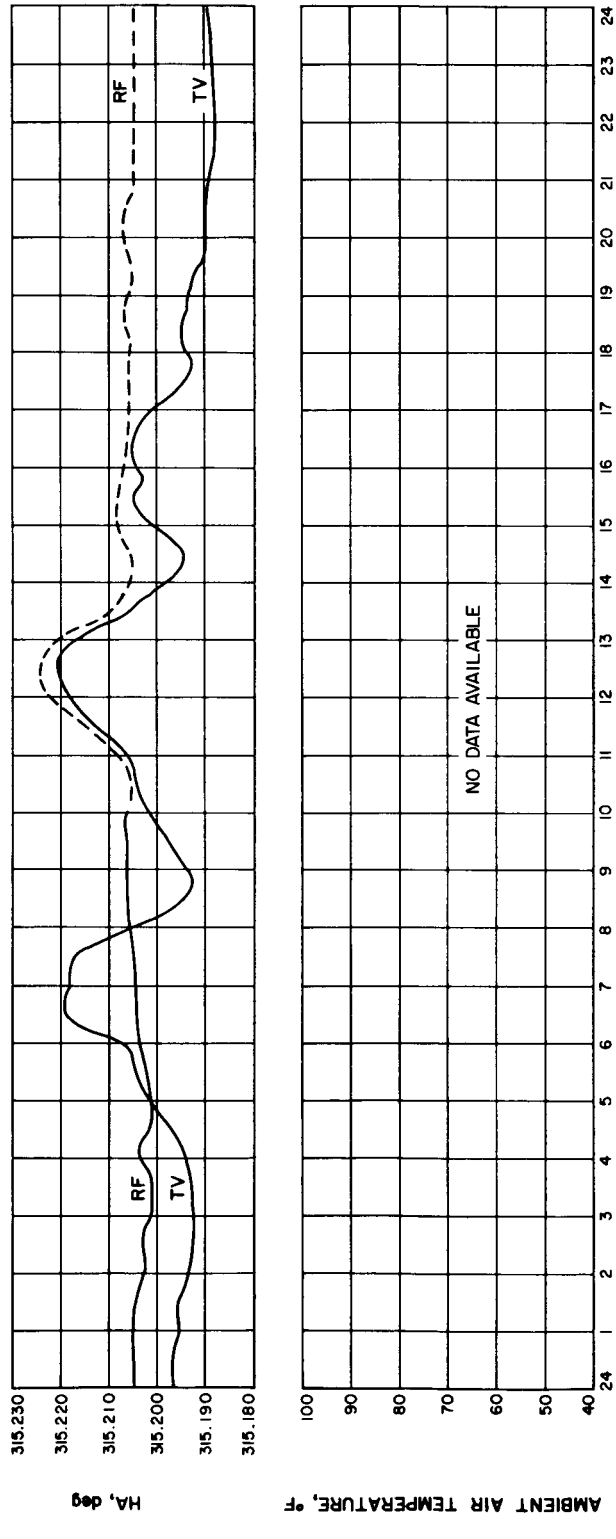

Fig. 109. RF–TV boresight vs. temperature, HA, 30 November 1961

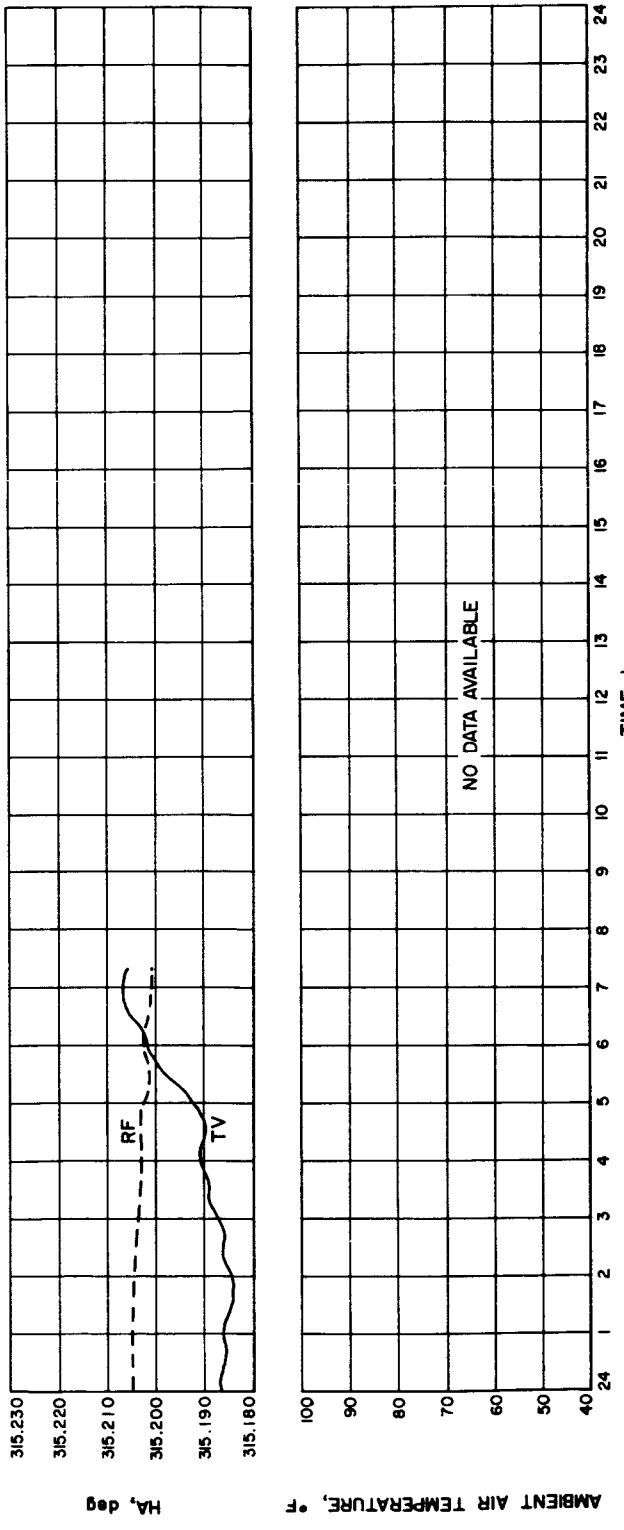

Fig. 110. RF–TV boresight vs. temperature, HA, 1 December 1961

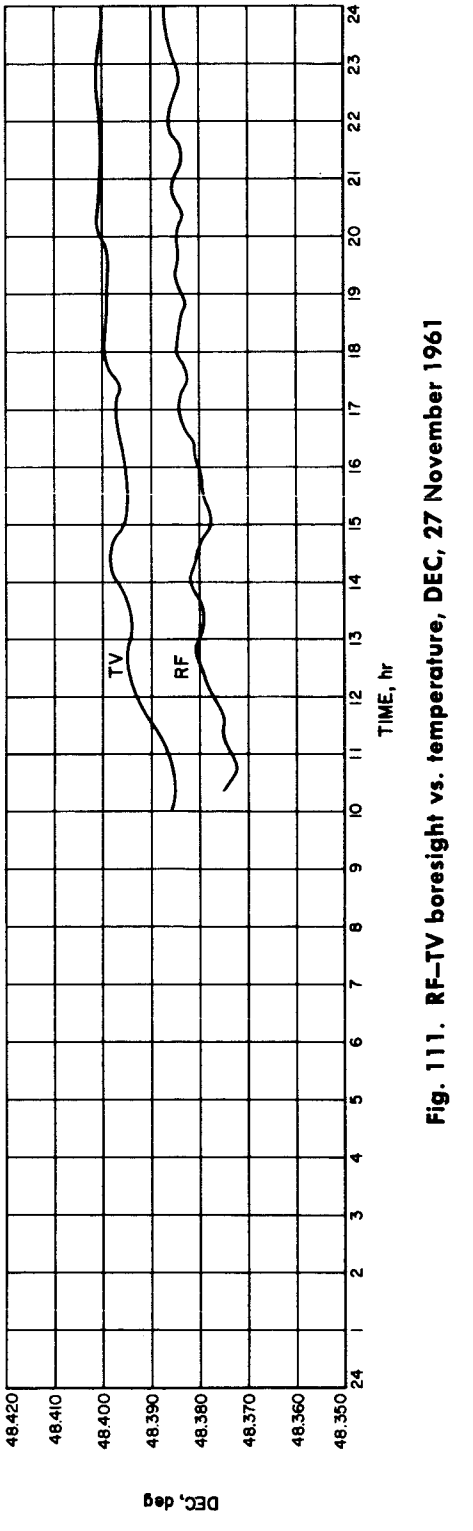

Fig. 111. RF–TV boresight vs. temperature, DEC, 27 November 1961

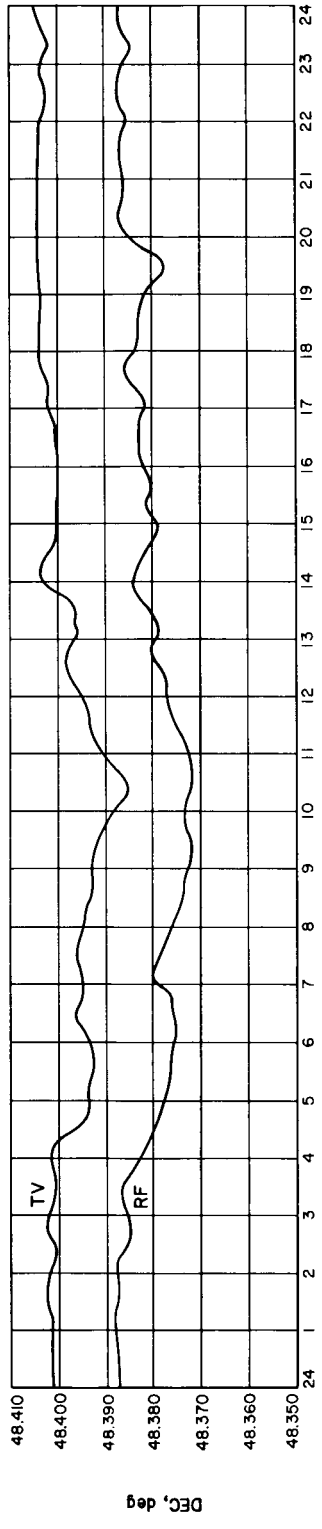

Fig. 112. RF–TV boresight vs. temperature, DEC, 28 November 1961

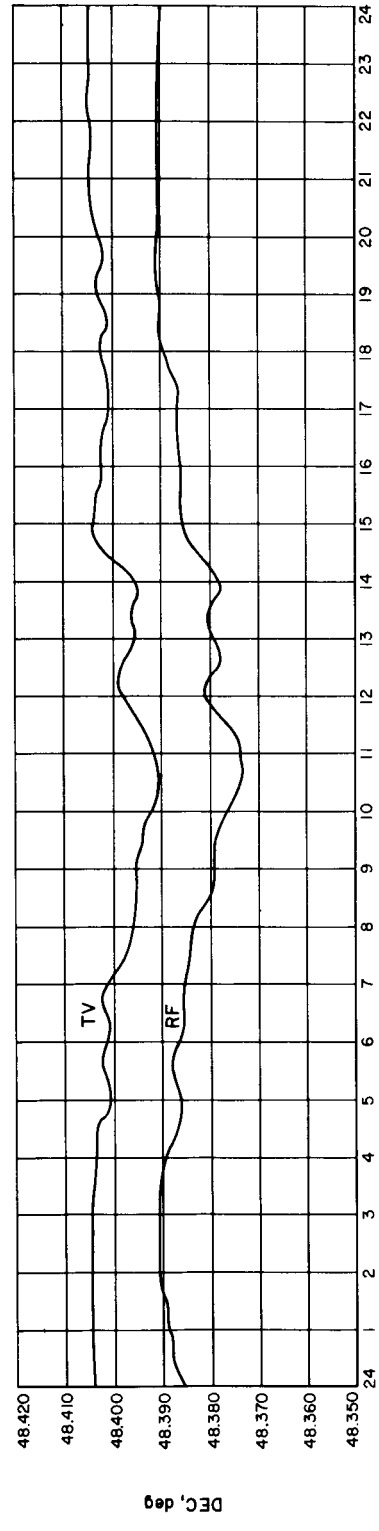

Fig. 113. RF–TV boresight vs. temperature, DEC, 29 November 1961

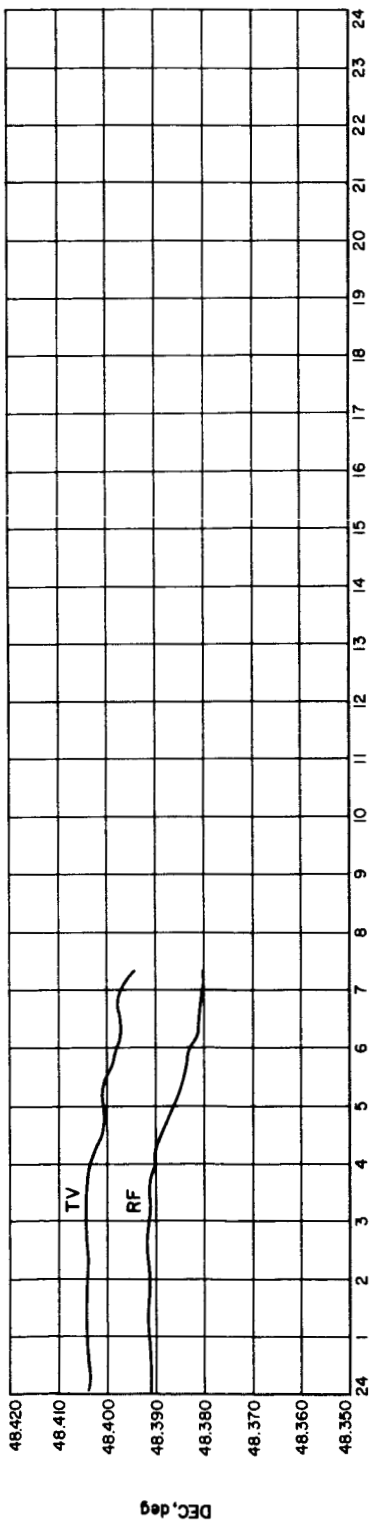

Fig. 114. RF–TV boresight vs. temperature, DEC, 30 November 1961

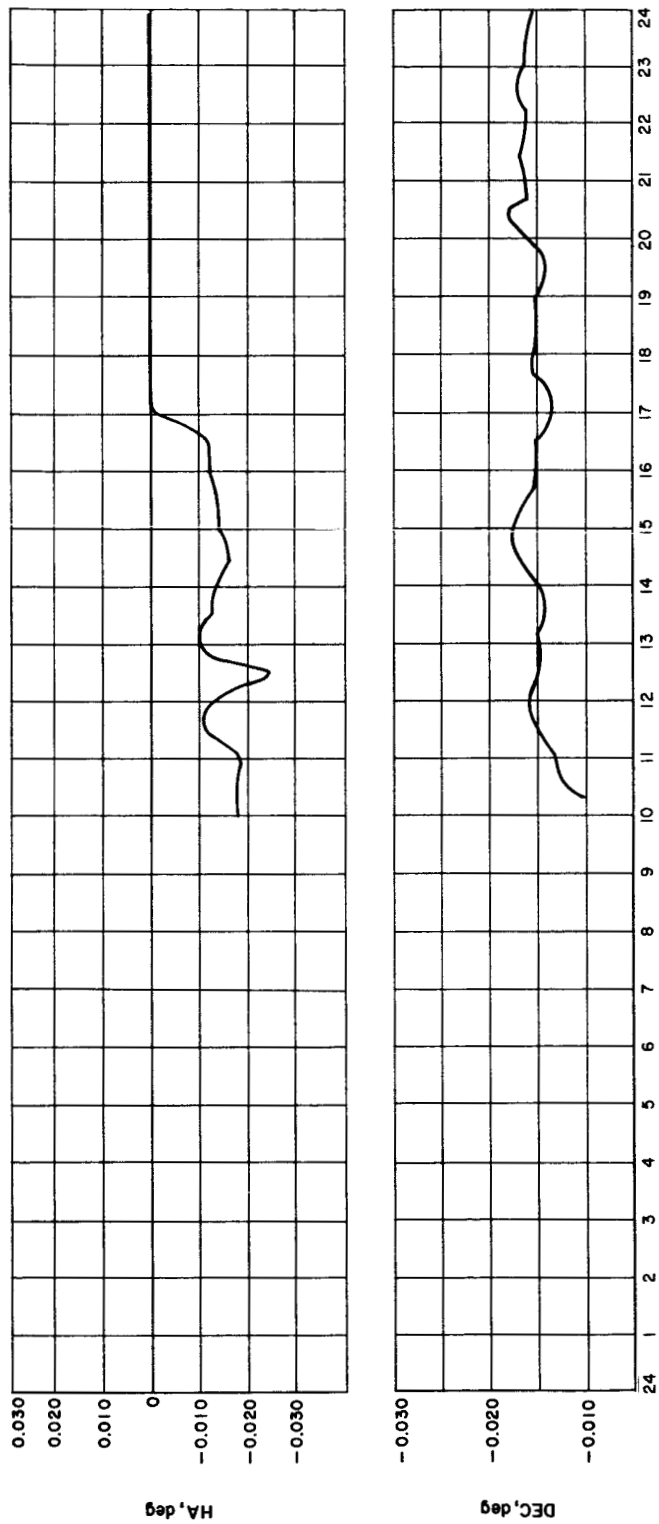

Fig. 115. RF — TV boresight differences vs. time of day, 27 November 1961

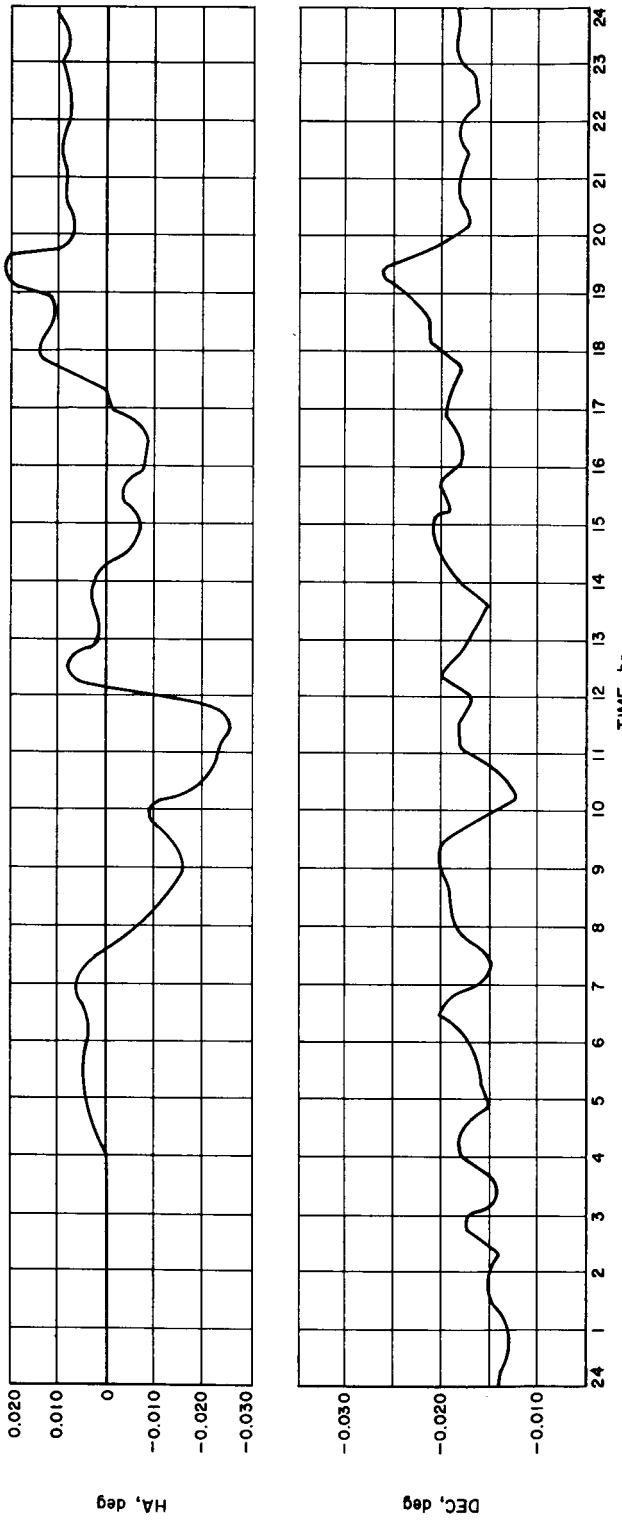

Fig. 116. RF — TV boresight differences vs. time of day, 28 November 1961

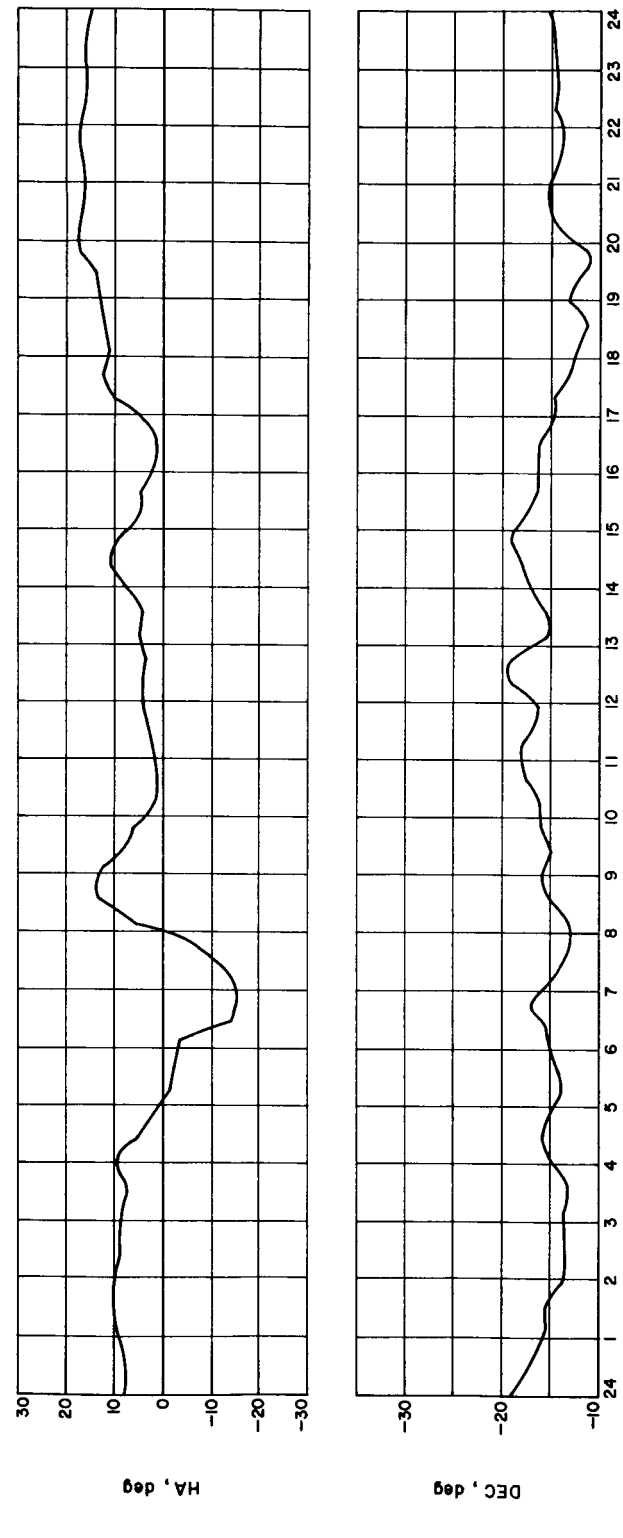

Fig. 117. RF — TV boresight differences vs. time of day, 29 November 1961

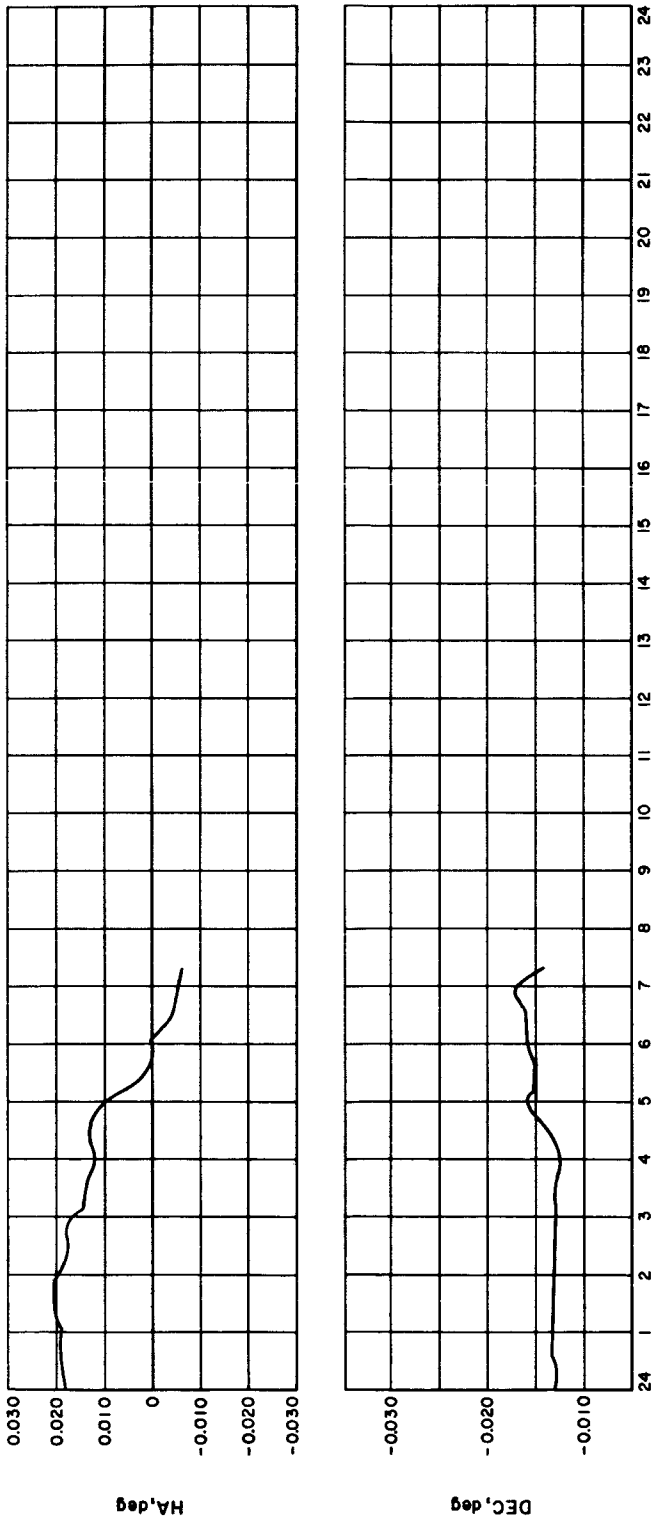

Fig. 118. RF — TV boresight differences vs. time of day, 30 November 1961

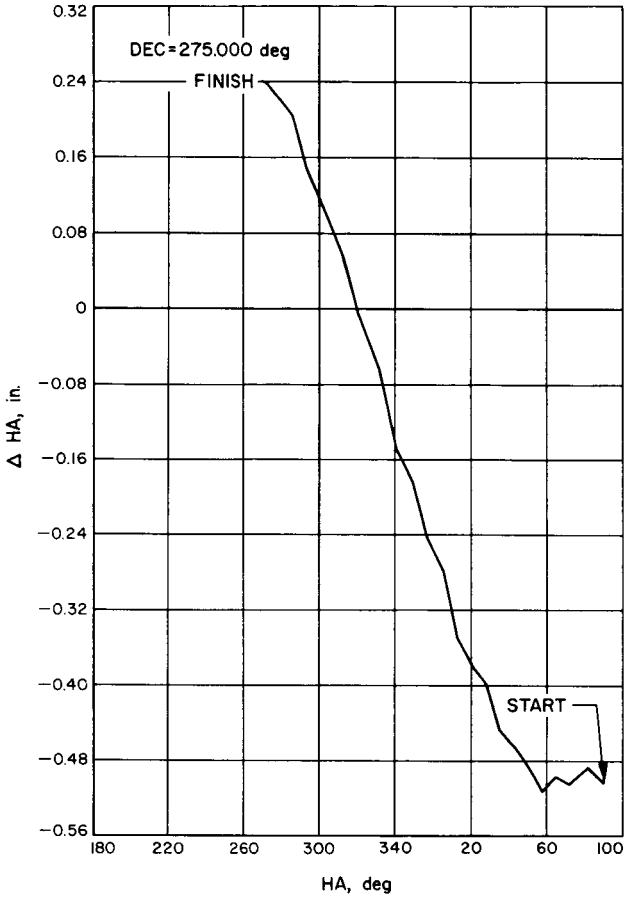

Fig. 119. Multiple DEC deflection test, film data for DEC = 275.000 deg, 28 March 1962

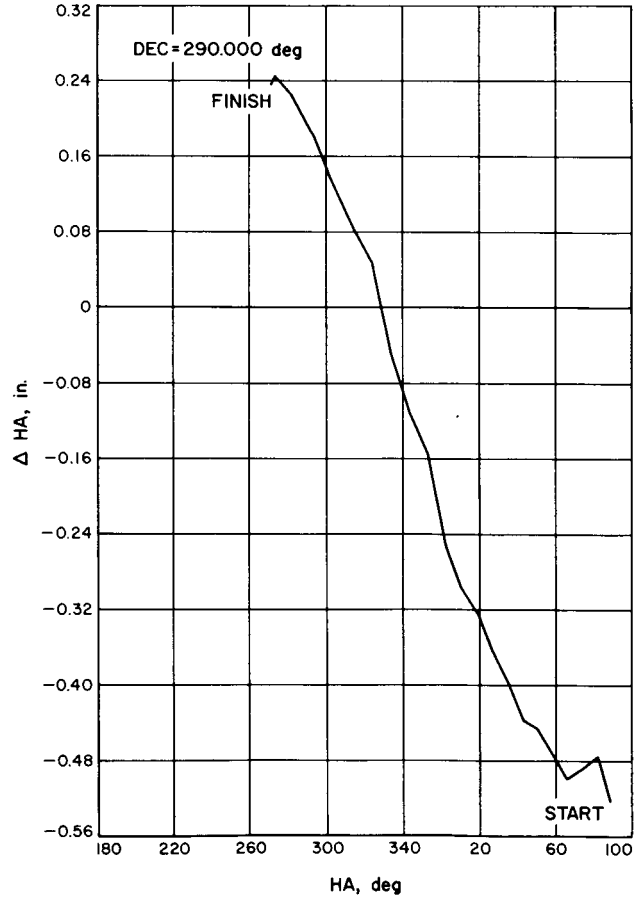

Fig. 120. Multiple DEC deflection test, film data for DEC = 290.000 deg vs. ΔHA, 28 March 1962

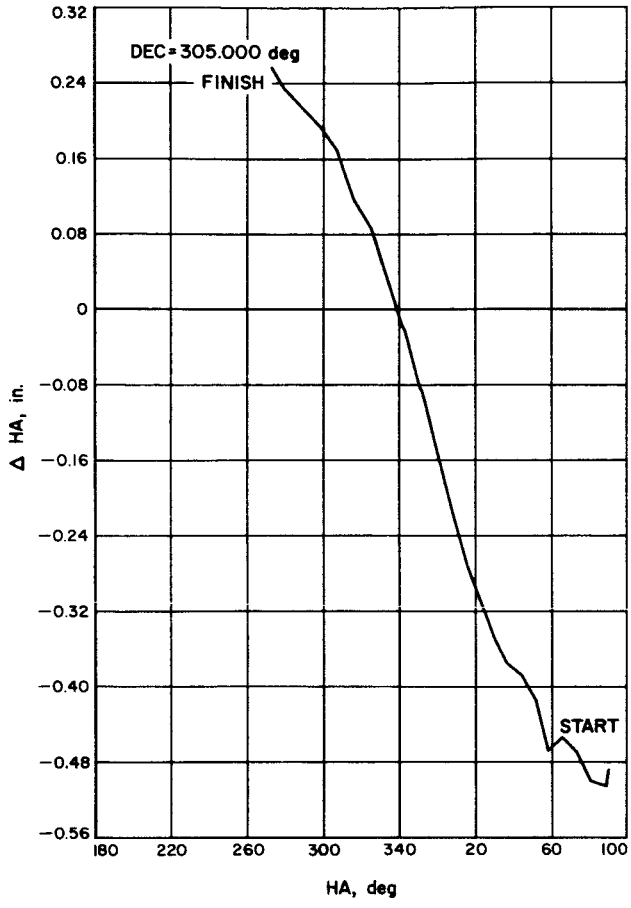

Fig. 121. Multiple DEC deflection test, film data for DEC = 305.000 deg vs. ΔHA, 28 March 1962

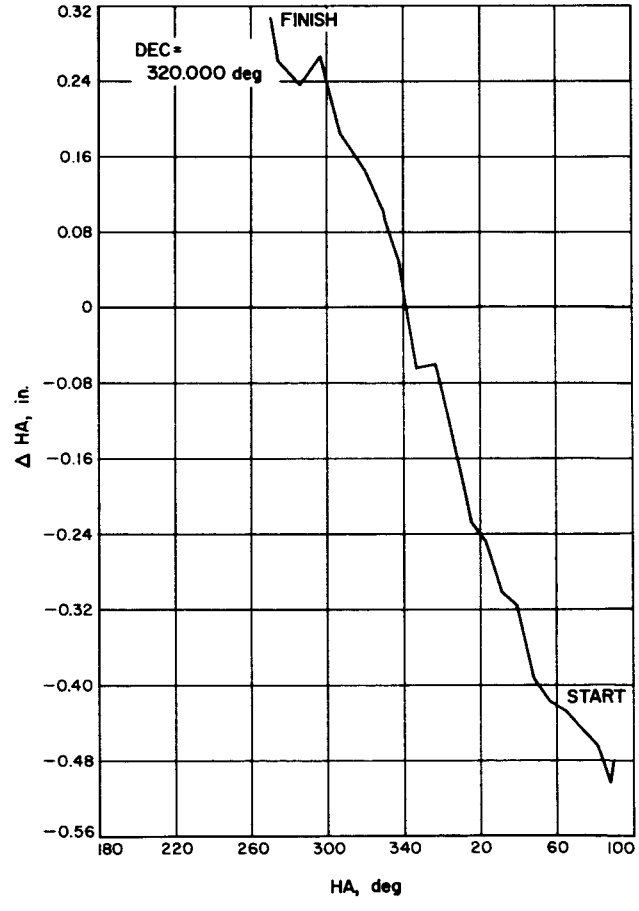

Fig. 122. Multiple DEC deflection test, film data for DEC = 320.000 deg vs. ΔHA, 28 March 1962

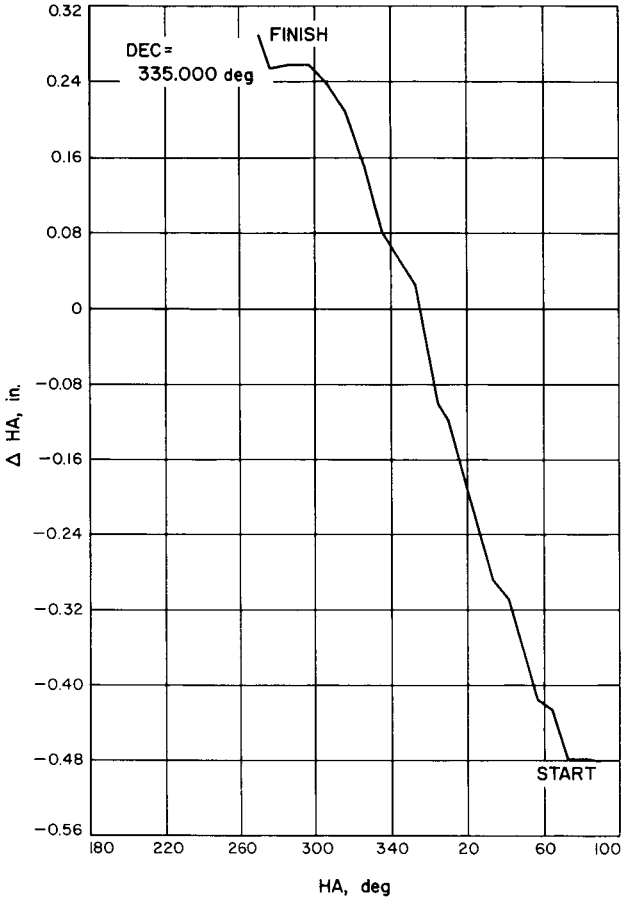

Fig. 123. Multiple DEC deflection test, film data for DEC = 335.000 deg vs. ΔHA, 28 March 1962

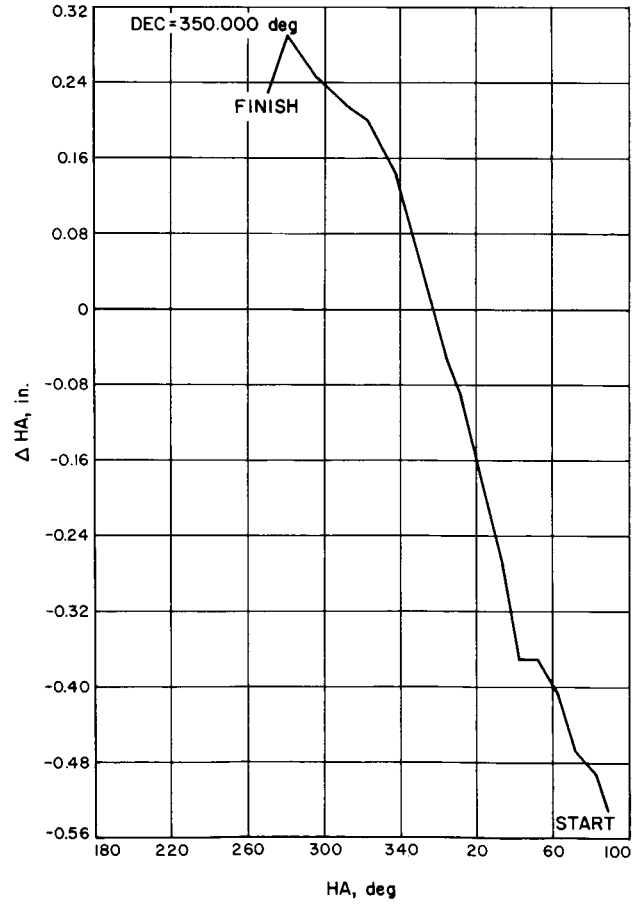

Fig. 124. Multiple DEC deflection test, film data for DEC = 350.000 deg vs. ΔHA, 28 March 1962

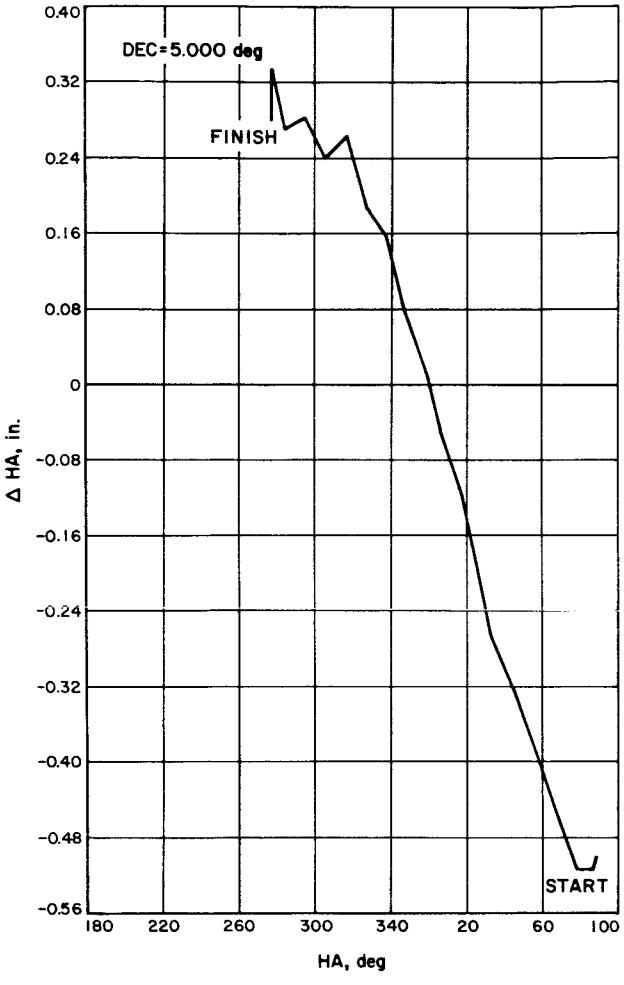

Fig. 125. Multiple DEC deflection test, film data for DEC = 5.000 deg vs. ΔHA, 28 March 1962

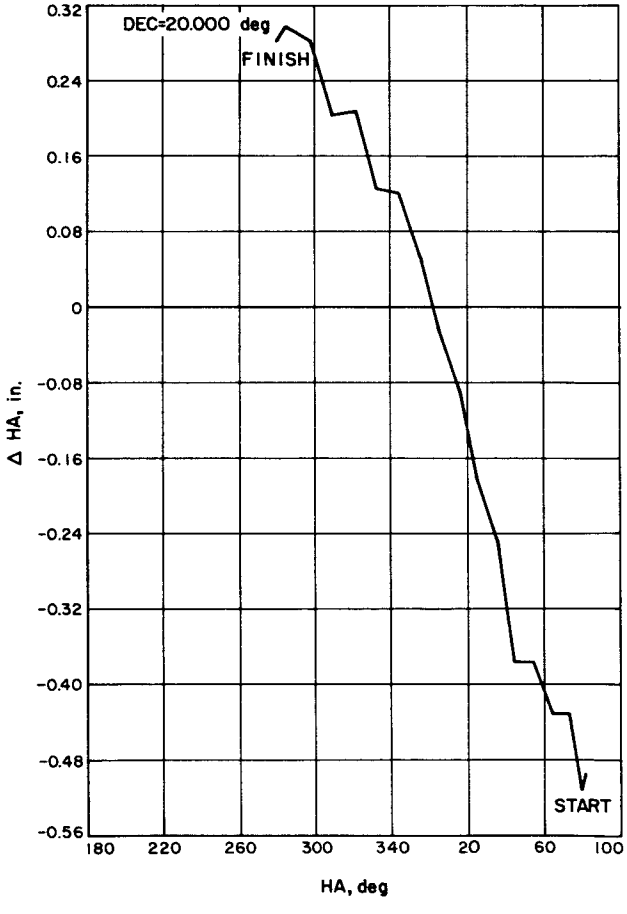

Fig. 126. Multiple DEC deflection test, film data for DEC = 20.000 deg vs. ΔHA, 28 March 1962

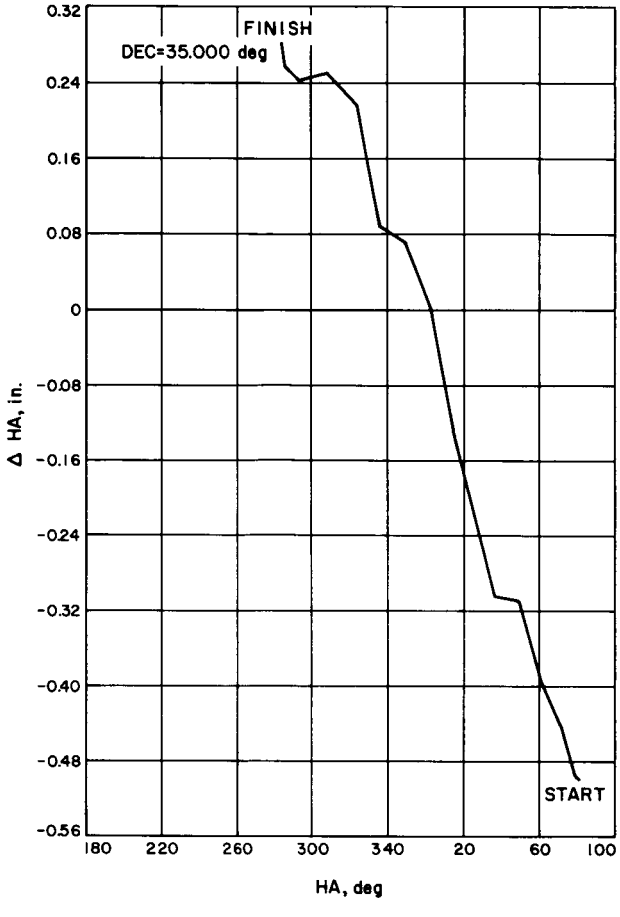

Fig. 127. Multiple DEC deflection test, film data for DEC = 35.000 deg vs. ΔHA, 28 March 1962

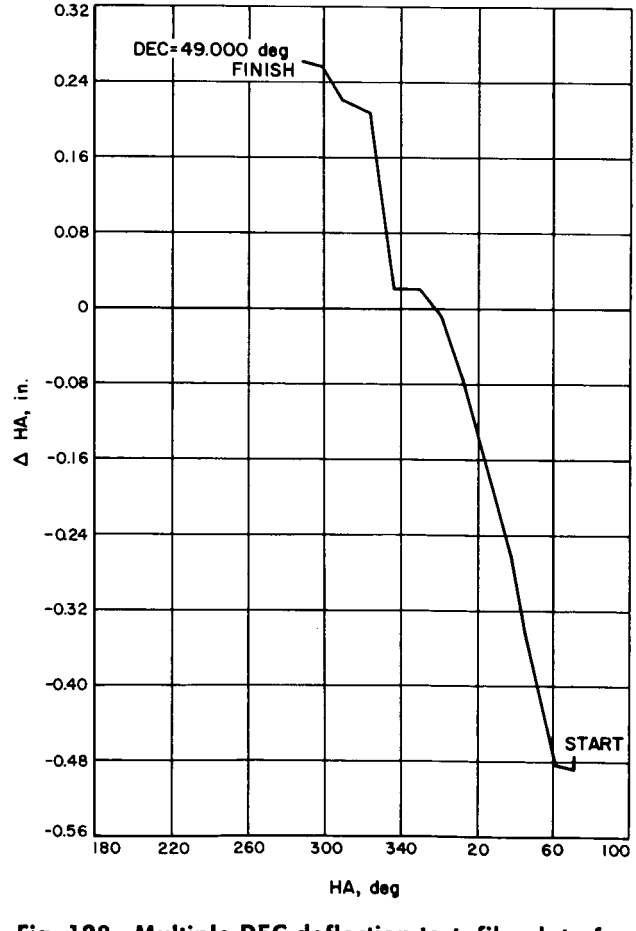

Fig. 128. Multiple DEC deflection test, film data for DEC = 49.000 deg vs. ΔHA, 28 March 1962

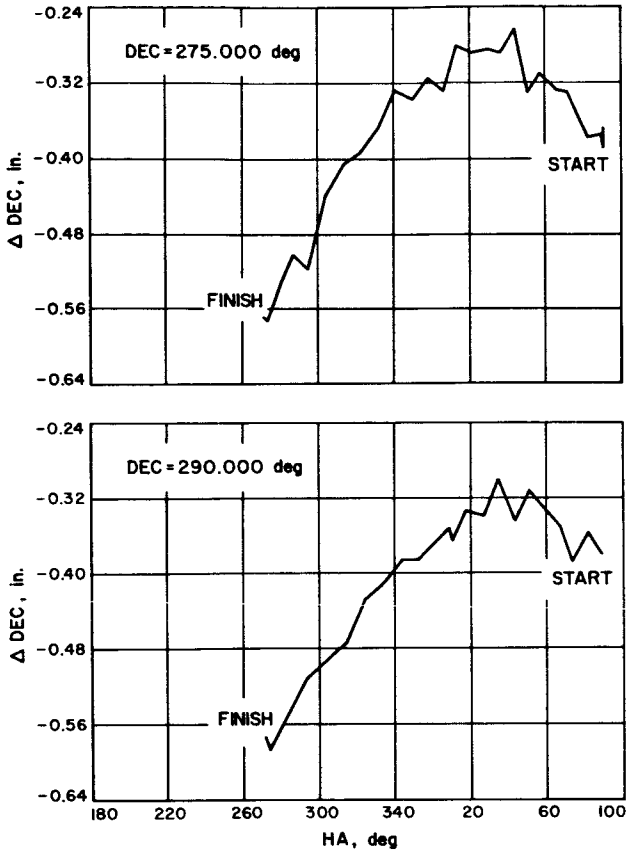

Fig. 129. Multiple DEC deflection test, film data for DEC = 275.000 deg and 290.000 deg vs. ΔDEC, 28 March 1962

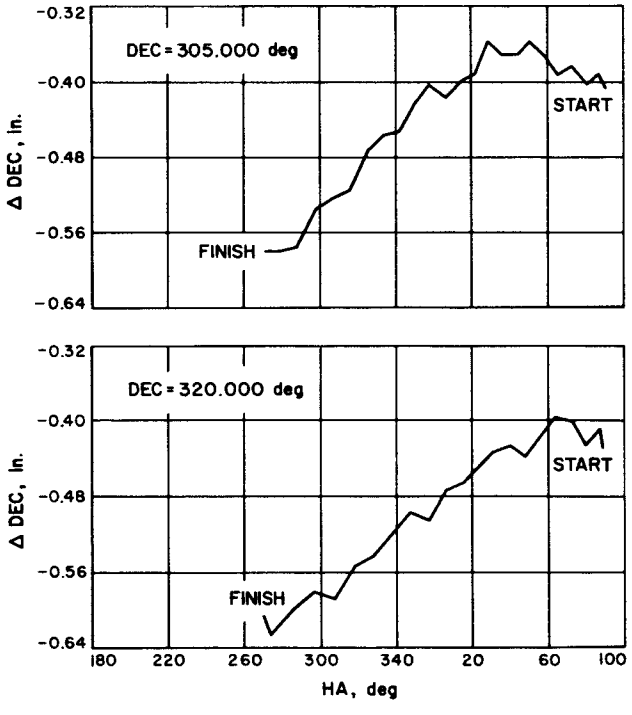

Fig. 130. Multiple DEC deflection test, film data for DEC = 305.000 deg and 320.000 deg vs. ΔDEC, 28 March 1962

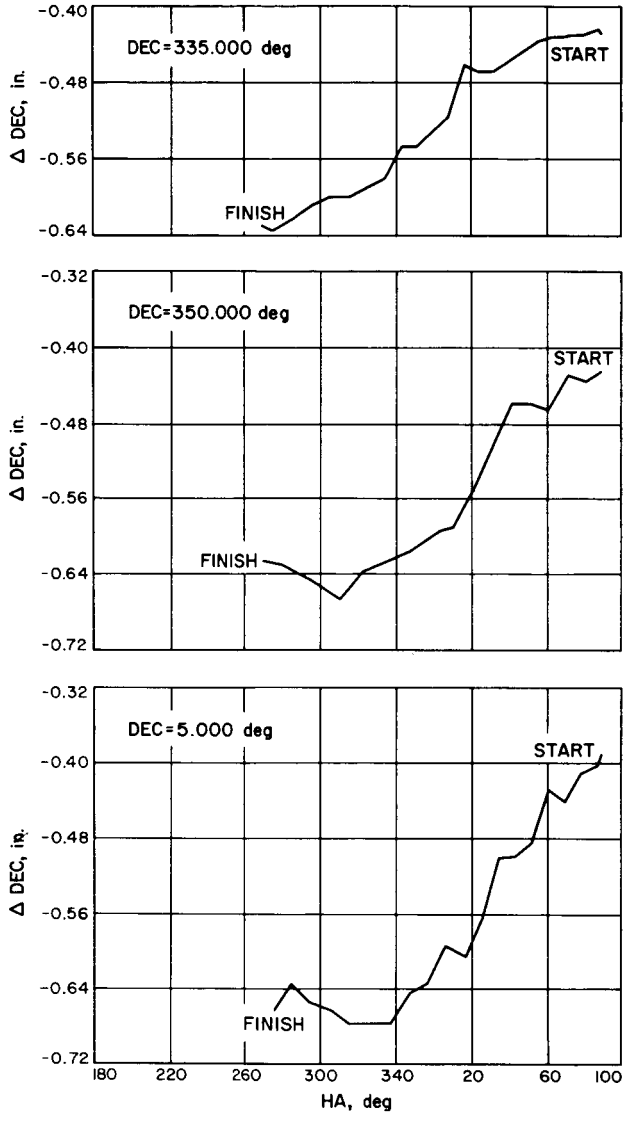

Fig. 131. Multiple DEC deflection test, film data for DEC = 335.000 deg, 350.000 deg, and 5.000 deg vs. ΔDEC, 28 March 1962

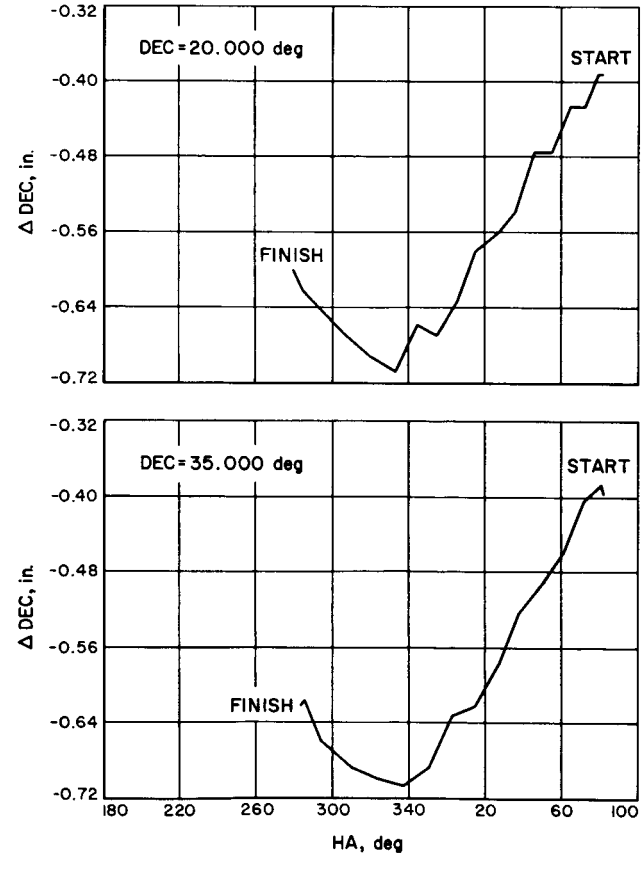

Fig. 132. Multiple DEC deflection test, film data for DEC = 20.000 deg and 35.000 deg vs. ΔDEC, 28 March 1962

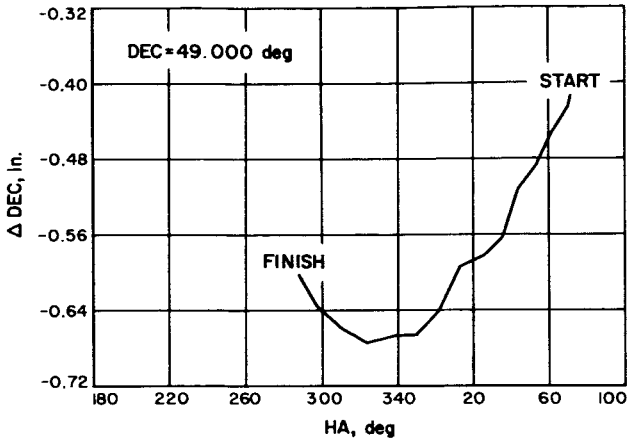

Fig. 133. Multiple DEC deflection test, film data for DEC = 49.000 deg vs. ΔDEC, 28 March 1962

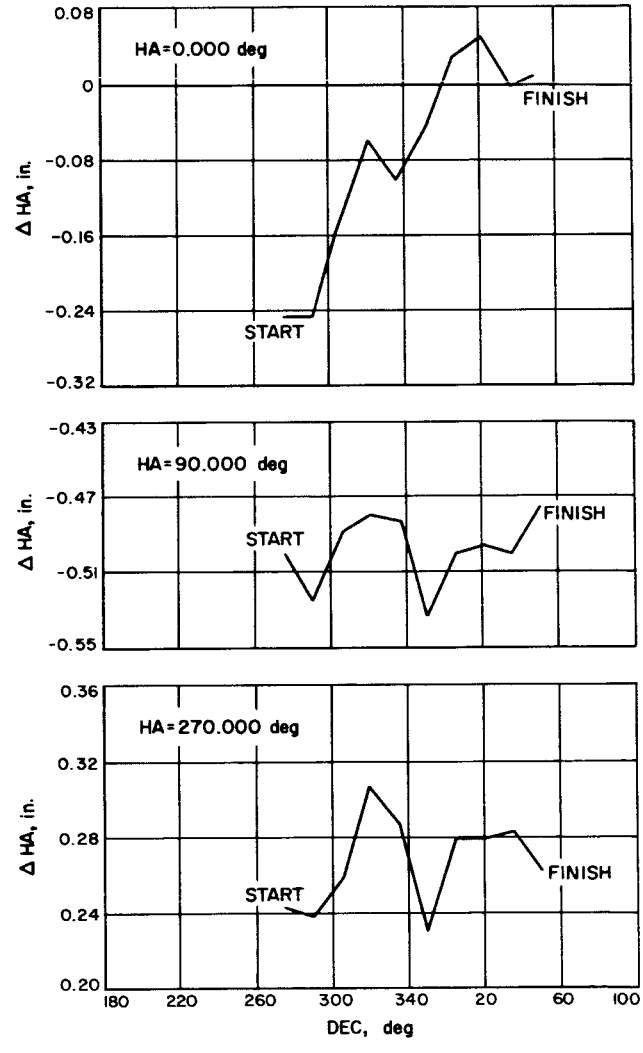

Fig. 134. Multiple DEC deflection test, film data for HA = 0.000 deg, 90.000 deg, and 270.000 deg vs. ΔHA, 28 March 1962

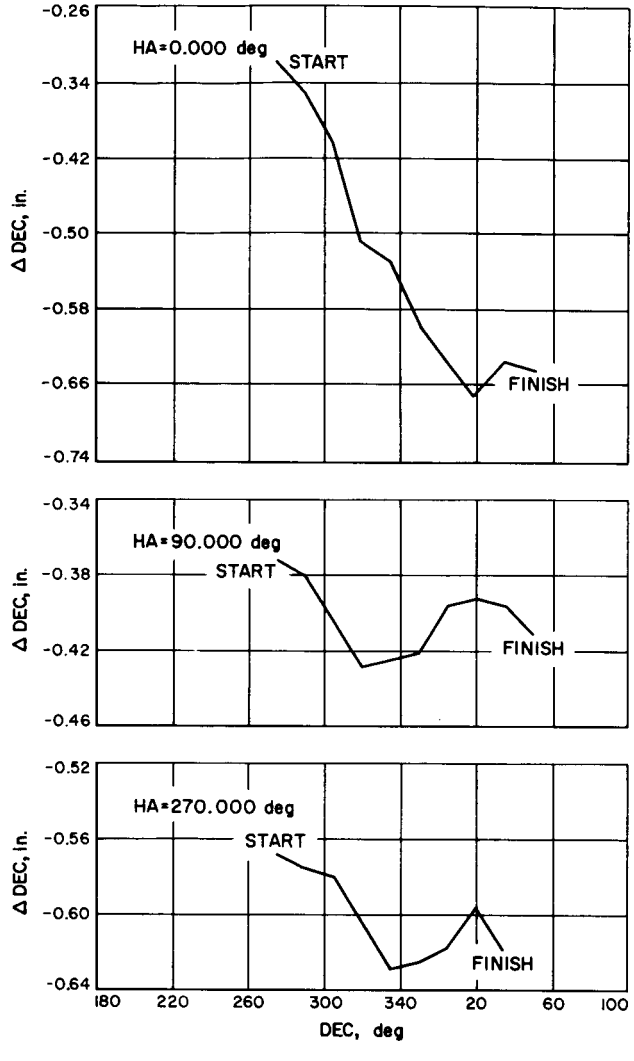

Fig. 135. Multiple DEC deflection test, film data for HA = 0.000 deg, 90.000 deg, and 270.000 deg vs. ΔDEC, 28 March 1962

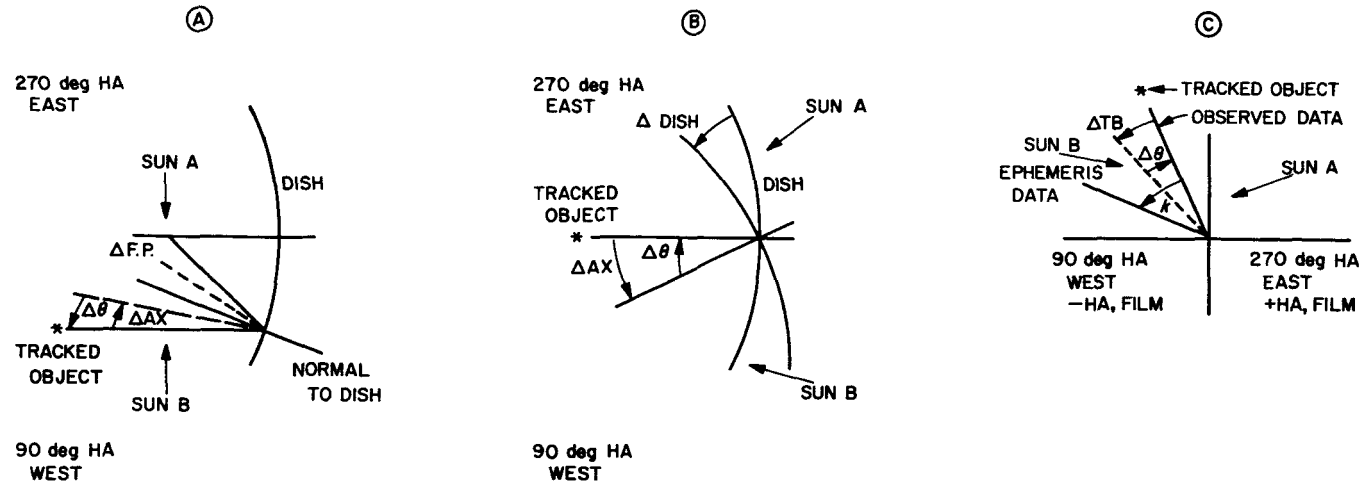

Δθ POSITIVE FOR SUN A

Δθ NEGATIVE FOR SUN B

Δθ NEGATIVE FOR SUN A

Δθ POSITIVE FOR SUN B

Δθ NEGATIVE FOR SUN A

Δθ POSITIVE FOR SUN B

Fig. 136. Polarity significance of deflection data; HA plane

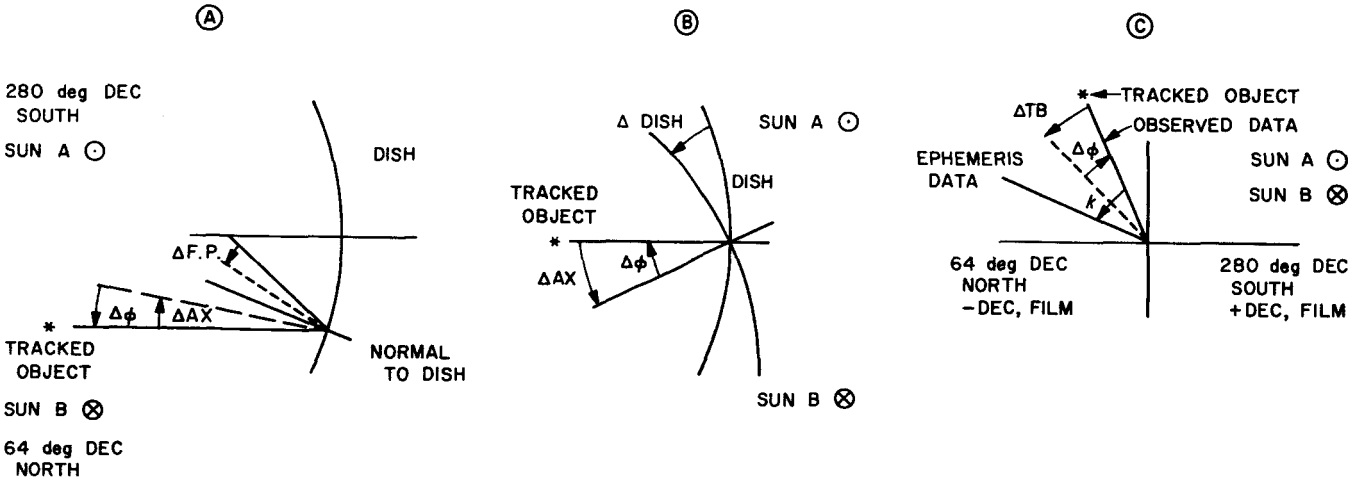

Δϕ ONLY MINOR EFFECT DUE TO SUN A OR SUN B SAME POLARITY

Δϕ ONLY MINOR EFFECT DUE TO SUN A OR SUN B SAME POLARITY

Δϕ ONLY MINOR EFFECT DUE TO SUN A OR SUN B SAME POLARITY

Fig. 137. Polarity significance of deflection data; DEC plane